AD-A107 114 BUNDESWEHR MUNICH UNIV (GERMANY F R) INST FOR HIGH-F--ETC F/G 9/5
CROSS CORRELATION IN A SPACE-DIVERSITY SYSTEM ON A MILITARY VEH--ETC(U)
AUG 81 G FLACHENECKER, L TSCHIMPKE DAJA37-80-C-0347

UNCLASSIFIED NL

1 + 2

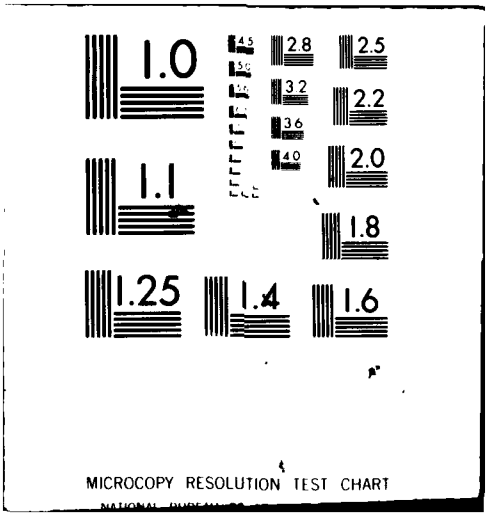
1.0
1.1
1.25
1.4
1.6
1.8
2.0
2.2
2.5
2.8
3.2
3.6
4.0
MICROCOPY RESOLUTION TEST CHART

1. Summary

Mobile reception in built-up areas is disturbed by interference-fading effects due to multiple incident waves caused from reflecting and scattering objects in the vicinity. The fading can be reduced with the help of space-diversity systems, i.e. with more than one antenna on the car.

The fade-reduction factor or the diversity gain of such a system strongly depends on the cross correlation of the antenna-output voltages. The related correlation factor is a function of frequency, is influenced by the car's surface, and depends on the mounting locations of the antennas. If a space-diversity system shall be established proper antenna locations on the car in mind have to be determined.

This report records the results of determining the cross correlation between antennas for various antenna-mounting configurations for a US Army 1/4-ton truck, M151 A2. The antenna receiving patterns are measured for the various configurations. These signal strength measurements are converted to correlation factors of signal power by assuming a Rayleigh distribution of the multipath signal strengths. The Rayleigh distribution has been shown to accurately characterize multipath reception in the 30-80 MHz band in built-up areas. In this manner, the requirement for time-consuming test drives was eliminated, and a more thorough investigation of the cross correlation phenomena was made possible for the same resources.

The results show that for the stipulated frequency range, there are several possible antenna locations which have adequate fade reduction (or diversity gain) in a space diversity system.

2. List of content

Keywords:

MOBA (Military Operation in Built-up Areas)

mobile reception

diversity system

space diversity

diversity gain

fade-reduction factor

correlation factor

covariance function

receiving patterns

List of Illustrations

Fig. 1: Example of a spatial field distribution and locally received voltages of two car antennas.

Fig. 2: Block diagrams of four basic diversity-combining systems.

Fig. 3: Mounting locations of the different antennas to be measured. Not all antennas shown here are always mounted simultaneously. (Ref. to Fig. 10, 23, 36, 59).

Fig. 4: Basic representation of N incident waves.

Fig. 5: Distribution of the magnitude of the electrical field strength in a field built up from N = 5 and N = 20 randomly distributed waves, respectively, compared to the Rayleigh distribution (100 calculated cases, each case represented by 1000 independent samples). The representation for N = 20 is completed with the probability function of a selection-diversity system exposed to the different calculated fields.

Fig. 6a): Truck on the turntable
b): Measuring area.

Fig. 7: Measuring equipment on the truck during function tests.

Fig. 8: Block diagram of the measuring equipment.

Fig. 9: Magnitude and phase angle of the receiving patterns $\underline{C}_2$ and $\underline{C}_6$ of antenna 2 and antenna 6, respectively. f = 50 MHz.

Fig. 10: Antenna configuration for Fig. 11 through 22.

Fig. 11: Receiving pattern of antenna 1 for f = 30/35/40/45 MHz. Roof not mounted. (Antenna configuration as in Fig. 10)

Fig. 12: Receiving pattern of antenna 1 for f = 50/55/60/65 MHz. Roof not mounted. (Antenna configuration as in Fig. 10)

Fig. 13: Receiving pattern of antenna 1 for f = 70/75/80 MHz. Roof not mounted. (Antenna configuration as in Fig. 10)

Fig. 14: Receiving pattern of antenna 1 for f = 30/35/40/45 MHz. Roof mounted. (Antenna configuration as in Fig. 10)

Fig. 15: Receiving pattern of antenna 1 for f = 50/55/60/65 MHz. Roof mounted. (Antenna configuration as in Fig. 10)

Fig. 16: Receiving pattern of antenna 1 for f = 70/75/80 MHz. Roof mounted. (Antenna configuration as in Fig. 10)

Fig. 17: Receiving pattern of antenna 2 for f = 30/35/40/45 MHz. Roof not mounted. (Antenna configuration as in Fig. 10)

Fig. 18: Receiving pattern of antenna 2 for f = 50/55/60/65 MHz. Roof not mounted. (Antenna configuration as in Fig. 10)

Fig. 19: Receiving pattern of antenna 2 for
f = 70/75/80 MHz. Roof not mounted.
(Antenna configuration as in Fig. 10)

Fig. 20: Receiving pattern of antenna 6 for
f = 30/35/40/45 MHz. Roof not mounted.
(Antenna configuration as in Fig. 10)

Fig. 21: Receiving pattern of antenna 6 for
f = 50/55/60/65 MHz. Roof not mounted.
(Antenna configuration as in Fig. 10)

Fig. 22: Receiving pattern of antenna 6 for
f = 70/75/80 MHz. Roof not mounted.
(Antenna configuration as in Fig. 10)

Fig. 23: Antenna configuration for Fig. 24 through 35.

Fig. 24: Receiving pattern of antenna 1 for
f = 30/35/40/45 MHz. Roof not mounted.
(Antenna configuration as in Fig. 23)

Fig. 25: Receiving pattern of antenna 1 for
f = 50/55/60/65 MHz. Roof not mounted.
(Antenna configuration as in Fig. 23)

Fig. 26: Receiving pattern of antenna 1 for
f = 70/75/80 MHz. Roof not mounted.
(Antenna configuration as in Fig. 23)

Fig. 27: Receiving pattern of antenna 3 for
f = 30/35/40/45 MHz. Roof not mounted.
(Antenna configuration as in Fig. 23)

Fig. 36: Antenna configuration for Figs. 37 through 45.

Fig. 37: Receiving pattern of antenna 1 for f = 30/34/40/44 MHz. Roof not mounted. (Antenna configuration as in Fig. 36)

Fig. 38: Receiving pattern of antenna 1 for f = 50/54/60/64 MHz. Roof not mounted. (Antenna configuration as in Fig. 36)

Fig. 39: Receiving pattern of antenna 1 for f = 70/74/80 MHz. Roof not mounted. (Antenna configuration as in Fig. 36)

Fig. 40: Receiving pattern of antenna 4 for f = 30/34/40/44 MHz. Roof not mounted. (Antenna configuration as in Fig. 36)

Fig. 41: Receiving pattern of antenna 4 for f = 50/54/60/64 MHz. Roof not mounted. (Antenna configuration as in Fig. 36)

Fig. 42: Receiving pattern of antenna 4 for f = 70/74/80 MHz. Roof not mounted. (Antenna configuration as in Fig. 36)

Fig. 43: Receiving pattern of antenna 5 for f = 30/34/40/45 MHz. Roof not mounted. (Antenna configuration as in Fig. 36)

Fig. 44: Receiving pattern of antenna 5 for f = 50/54/60/64 MHz. Roof not mounted. (Antenna configuration as in Fig. 36)

Fig. 45: Receiving pattern of antenna 5 for f = 70/74/80 MHz. Roof not mounted. (Antenna configuration as in Fig. 36)

Fig. 46: Measured normalized covariance function (correlation factor) for various antenna combinations within the antenna configuration of Fig. 10. Roof not mounted.

Fig. 47: Measured normalized covariance function (correlation factor) for various antenna combinations within the antenna configuration of Fig. 10. Roof mounted.

Fig. 48: Measured normalized covariance function (correlation factor) for various antenna combinations within the antenna configuration of Fig. 23. Roof not mounted.

Fig. 49: Measured normalized covariance function (correlation factor) for various antenna combinations within the antenna configuration of Fig. 23. Roof mounted.

Fig. 50: Measured normalized covariance function (correlation factor) for various antenna combinations within the antenna configuration of Fig. 23. Roof not mounted.

Fig. 51: Measured normalized covariance function (correlation factor) for various antenna combinations within the antenna configuration of Fig. 23. Roof mounted.

3. Introduction

During military operations in built-up areas (MOBA) there is a severe problem concerning wireless command transmission. Due to reflections and scattering effects caused by dielectric and conductive objects (houses, trees, light masts, etc.) a very complex electromagnetic field distribution with maximums and deep minimums will be formed from the transmitted electromagnetic wave. This is particularly true if the wavelength of the radiated signal is in the order of magnitude as or less than the measures of the obstacles. In urban and suburban vicinities this determines a frequency range of above 20 MHz to be disturbed by these effects.

Fig. 1 shows a typical distribution of the local antenna output voltage (in dB) in a built-up area at 80 MHz compared to the measures of a military truck. This distribution represents the electrical component of the electromagnetic field multiplied by the receiving behaviour of the antennas on the car. If the car passes through this field a single antenna, for instance antenna 1 of the shown car, would present an output voltage as shown on bottom of Fig. 1. Along the way of 15 meters, which is about 4 wavelengths, the antenna-output voltage magnitude shows 2 deep minimums. During a normal drive repeated break-downs of the radio link will occur. It could happen that the car has to stop in a position where its antenna 1 is located in a field-strength minimum. In this case the command transmission to antenna 1 can drop out for a longer time period in spite of the fact that at very close distances sufficient signal power would be available.

It is well-known that the problem of interference fading

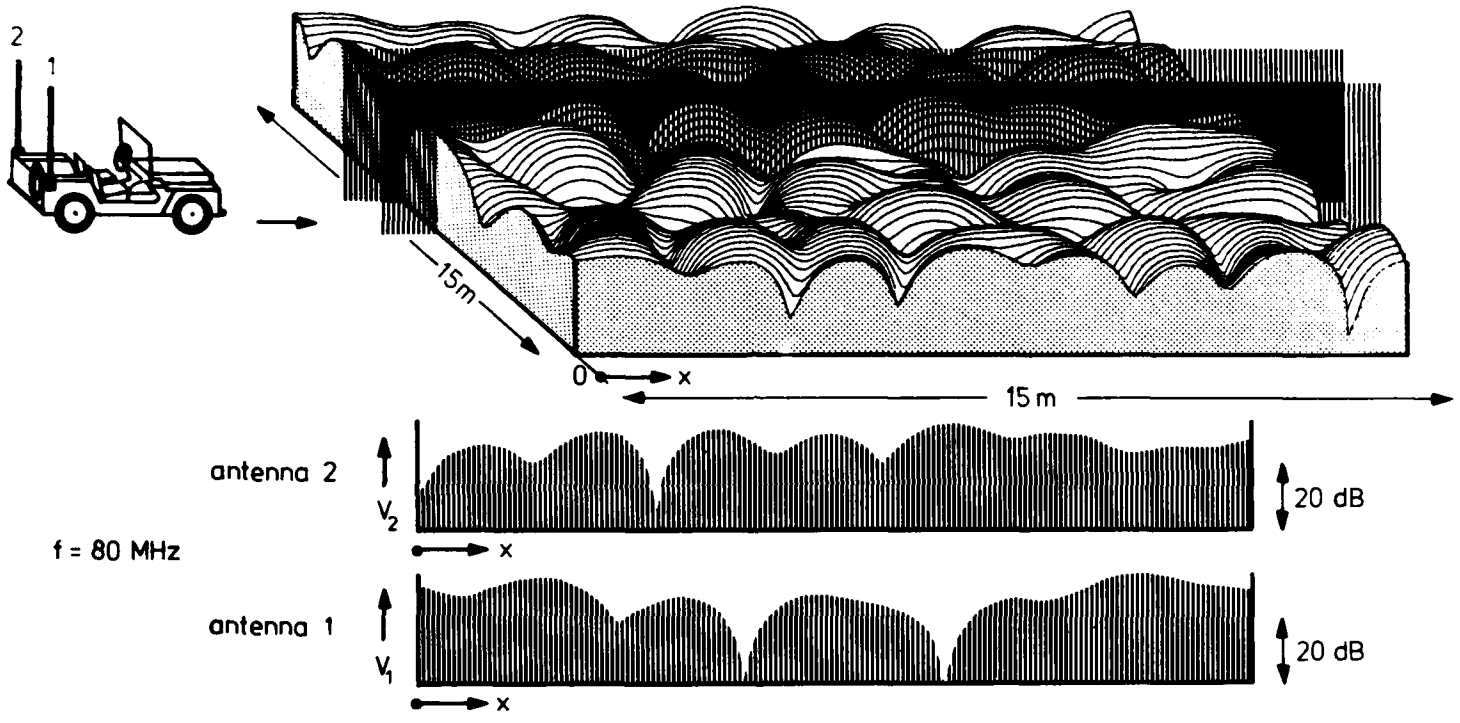

Fig. 1: Example of a spatial field distribution and locally received voltages of two car antennas.

can be reduced by using diversity systems. As in our case the field-strength magnitude changes with the location a space-diversity system can be used. In this system two antennas (or even more) are mounted spaced apart. If the dimensions of the car allow a sufficient distance between the antennas there is a certain probability that the second antenna will receive if the first antenna fails due to the passing of a field-strength minimum.

In the example of Fig. 1 the second antenna is mounted on the opposite side of the car with respect to antenna 1. As is shown in Fig. 1 the instantaneous magnitudes of the output voltages of both antennas differ. This is due to the local distribution of the electrical field-strength. It is obvious from Fig. 1 that the probability of a reception breakdown decreases if the radio receiver in the car has access to both antennas and can use both output voltages by means of a switching or combining process regarding the instantaneous output voltages.

From diversity techniques the following four major diversity systems are known [1]:

1. Selection diversity.
   The radio receiver is always connected to that antenna which has the higher output voltage at that instant.

2. Equal-gain diversity.
   The output voltages of both antennas are processed from the radio receiver with the same amplification factor and are combined at the RF-stage, or at the IF-stage, or at the base-band stage. Combinations at the RF- or at the IF-stage have to

be performed in consideration of the phase angle of the voltages, i.e. after a phase shifter, which continuously alters one of the phase angles to equal the other one.

3. Maximal-ratio diversity.
   This system is similar to the equal-gain diversity system. The difference in comparison with the latter system lies in the use of gain control stages in both branches which adjust the amplification factors proportional to the instantaneous magnitude of the antenna output voltage of the respective branch.

4. Scanning diversity.
   The radio receiver is connected to one antenna as long as this antenna voltage exceeds a prescribed threshold value. As soon as the output voltage of the selected antenna becomes smaller than the threshold value the receiver is switched over to the other antenna. The switching is performed with no regard to the output voltage of the other antenna.

Fig. 2 shows block diagrams of diversity combiners for these four diversity systems.

The performance of the four systems is slightly different. The more sophisticated systems (equal gain and maximal ratio) show a higher improvement than the simpler systems (selection and scanning). The increase in availability of all systems, however, depends on the correlation of the output voltages of the two antennas. If the changes of the output voltages are very similar the voltages are highly

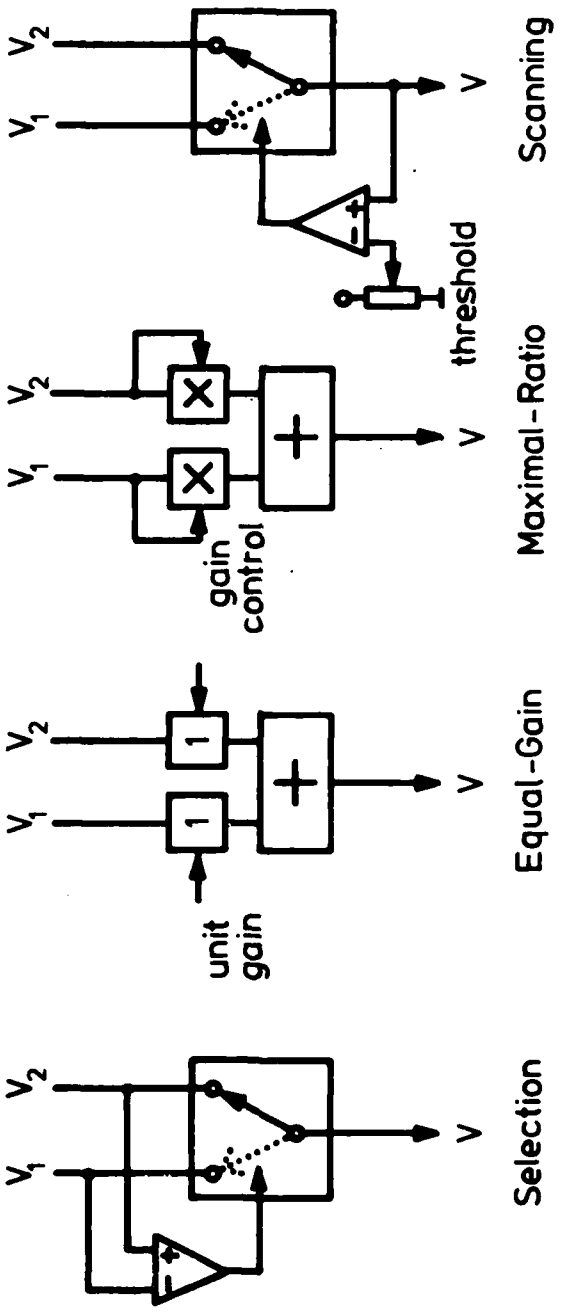

Fig. 2: Block diagrams of four basic diversity-combining systems.

correlated. In this case it is very probable that the second antenna shows also a minimum of its output voltage if the first antenna does. If, in contrast, the output voltages change more independently depending on the location of the car the voltages are of low correlation. In this case there is a higher probability that antenna 2 will show a sufficient output voltage while antenna 1 crosses a minimum or a zero.

The improvement of a diversity system over a single-antenna system can be expressed in terms of diversity gain or fade-reduction factor. The diversity gain expresses how much a reception-threshold level can be increased in a diversity system as compared to a single branch system to achieve the same exceeding probability for the signal power or S/N ratio, respectively. This is a function of the threshold value [6].

The fade-reduction factor is the ratio of the probabilities that the input signal is below a specified threshold value ("fading") in the diversity system and in a single-branch system, respectively. It is a function of the threshold value, too.

Both, diversity gain and fade-reduction factor, increase with decreasing correlation between the output voltages of the two antennas. Many papers dealt with the influence of the correlation factor on the improvement which can be obtained with the different diversity systems [2-5]. A very recent paper [6] considers the effect of the correlation factor in systems with different antenna behaviour (gain difference) and different noise (internal and external) within the two branches. Thus, if the correlation factor of the output voltages of two antennas is known the

improvement of each diversity system can be calculated with the help of well-known formulas.

The correlation between the output voltages of two antennas, however, can only be calculated for very simple antenna arrangements. The correlation factor has been calculated for the case of a vertically polarized field over an indefinitely extended conductive plane (autocovariance function of the electrical field component). If the magnitude of the electrical field component shows a Rayleigh distribution (many incident waves with about the same magnitude, random angle of incidence, and random phase) the correlation factor ρ has a value of

$$\rho = J_o^2 \left(2\pi \frac{d}{\lambda_o}\right) \qquad (1)$$

where J_o is the Bessel function of zero order, d is the distance between the two vertically mounted antennas, and λ_o is the free-space wavelength of the field.

The condition of the field to be of the Rayleigh type is less a restriction than one might assume. In [6] it is shown with the help of mathematical models and with measurements in real vicinities that the Rayleigh distribution is approached in nearly all cases of mobile reception, even within areas with a small number of scatterers around (suburban regions and open field).

A high influence on the correlation factor occurs if the ideal case of the conducting plane around the two antennas is not fulfilled. If, for instance, the two antennas are mounted upon the surface of a car there is a major interference from the currents along the car's surface. In this case the car is part of the antennas themselves and in-

fluences the receiving patterns of the antennas and can cause coupling effects between the antennas. Measurements of the correlation factor which have been performed during real test drives with a car bearing several antennas showed that Eqn. (1) cannot be used for mobile receiving systems [7]. The results of this paper point out that the correlation between two antennas on a car cannot be predicted just from the distance between the antennas. The influence of the car is too high. To find optimum mounting positions broadband measurements of the correlation have to be performed with the real arrangement, i.e. the real car and the real antennas, to avoid correlation peaks within the operating frequency band.

It was the purpose of this research work to perform correlation measurements for several antenna combinations mounted on the 1/4 ton truck M 151 A2 of the U.S. Army. The measurements cover the military frequency range 30 through 80 MHz. As antennas the U.S. Army type AS-2731/GRC with automatic matching box has been used. Further measurements have been done with small active rod antennas. These measurements have been extended to the frequency range 80 through 300 MHz. A detailed description of the active antenna in use is given in [7], pages 25 through 29.
Fig. 3 shows the mounting locations of the antennas on the truck. The numbering of the antennas will remain unchanged throughout the following report.

It is known from [7] that the measurement of the correlation is highly time-consuming if it is done with the help of real test drives. On the other hand this research work should carry out very detailed results with several antenna combinations and a very high frequency resolution. These results could not be achieved during test drives. On

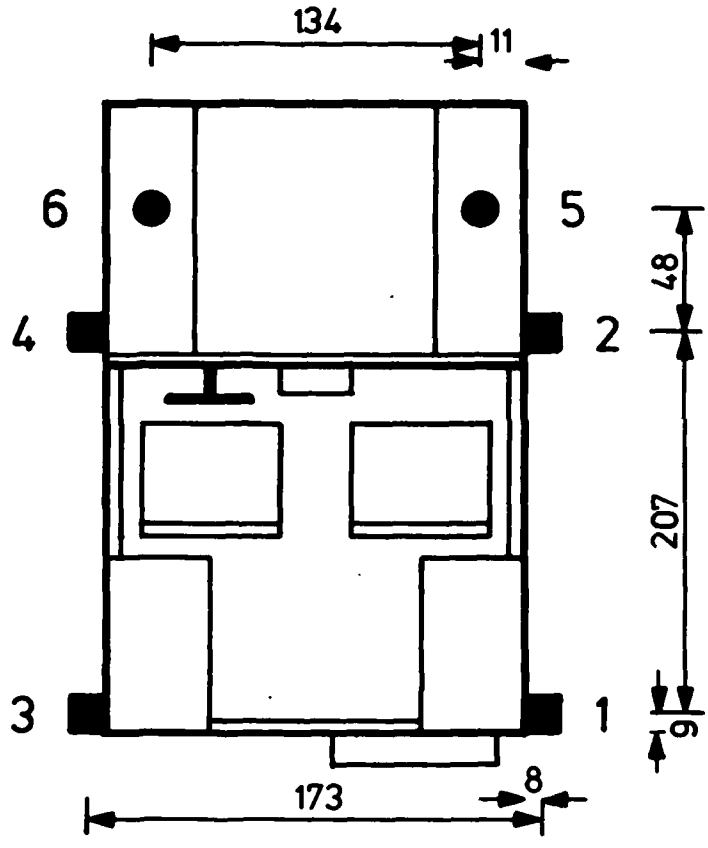

(all measures in cm)

Ant. 1 through 4: Passive rod antenna with automatic match box, Type AS-2731/GRC (height = 160 cm)

Ant. 5 and 6: Active rod antenna. See [7], pp. 19 through 20 (height = 40 cm)

Fig. 3: Mounting locations of the different antennas to be measured. Not all antennas shown here are always mounted simultaneously. (Ref. to Fig. 10, 23, 36, 59).

this account a new measuring method has been developed which is described in the following chapter.

4. Measuring method for the correlation factor

In the following it will be derived that the correlation between the output voltages of two antennas on a car can be calculated from the complex receiving patterns of both antennas. The expression "complex" shall point out that the receiving patterns have to be known with respect to magnitude and phase angle. With the help of the results of this chapter the time-consuming test drives can be substituted by pattern measurements in order to get the wanted correlation.

4.1 Basic theory

Fig. 4 shows a basic representation of the problem. The signal wave is splitted into multiple waves due to the reflections and scattering effects of the built-up vicinity. In urban and suburban areas the direct wave is missing in most cases since there is usually no direct sight from the transmitting antenna to the car. In all these cases the multiple incident waves are of about the same magnitude. Because of the different propagation paths the phase angles of the waves are randomly distributed as well as the angles of incidence.

If the car moves towards the x-direction the two antennas will be exposed to changing magnitudes of the electrical field strength depending on the local composition of the N waves. It has to be taken into account, however, that the antennas respond to the different angles of incidence depending on the receiving pattern of the antennas. If we assume the receiving patterns of the two antennas to be known the output voltage of each antenna along the traveling path x can be calculated. In the real arrangement the antennas will show output voltage magnitudes

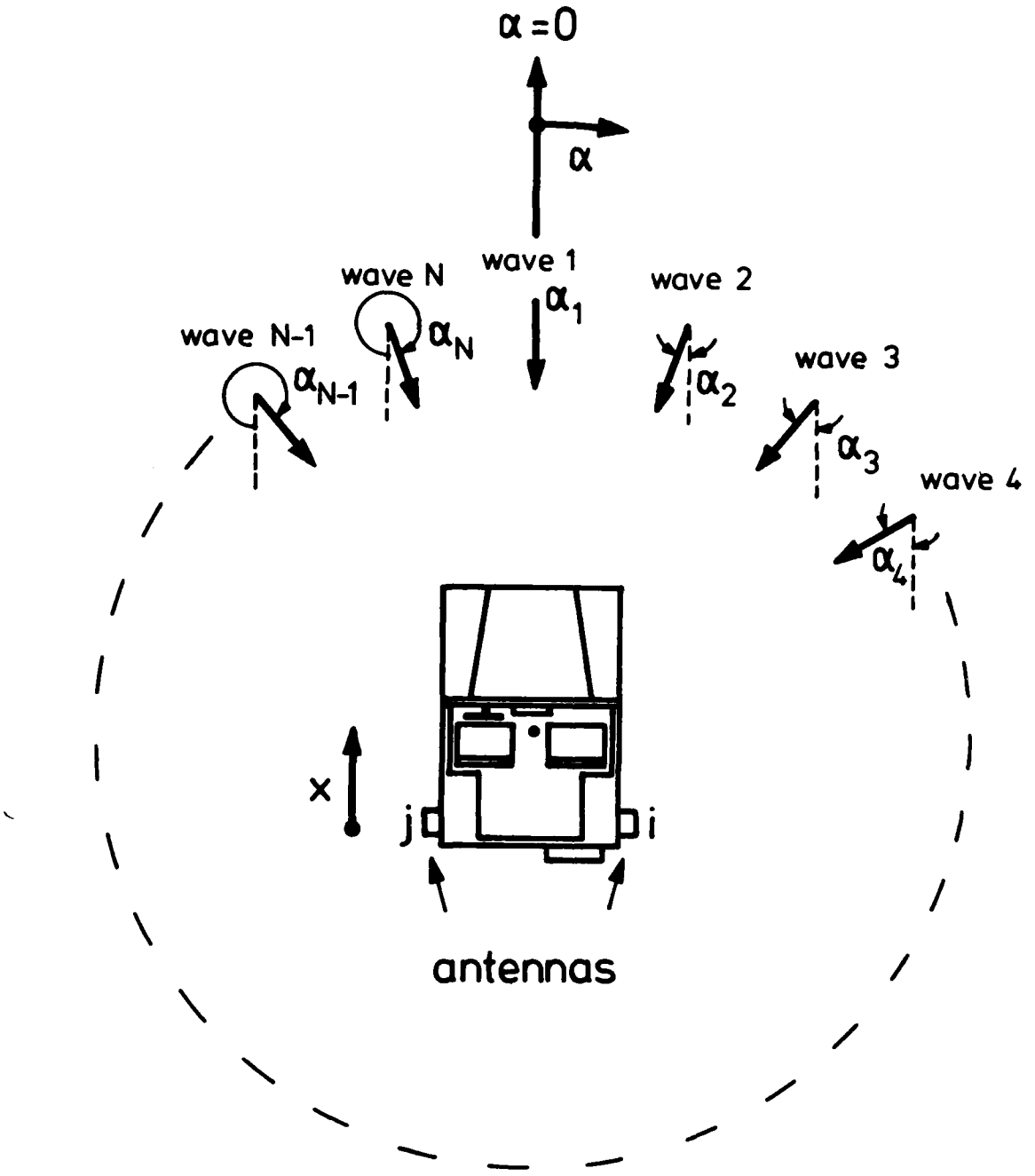

Fig. 4: Basic representation of N incident waves.

$$\underline{V}_i = \sum_{n=1}^{N} \underline{h}_{effi}(\alpha_n) \cdot \underline{E}_n \qquad (2)$$

where i is the number of the respective antenna, N is the total number of incident waves, and $\underline{E}_n$ is the complex magnitude of the n-th wave.

$$\underline{h}_{eff}(\alpha) = \left. \frac{\underline{V}}{\underline{E}} \right|_{\alpha} \qquad (3)$$

is the complex effective length for a single incident wave with an angle of incidence α. Eqn. (2) uses the law of superposition.

If we define the normalized receiving pattern functions

$$\underline{C}(\alpha) = \frac{\underline{h}_{eff}(\alpha)}{\underline{h}_{effmax}} \qquad (4)$$

Eqn. (2) can be written for the i-th antenna

$$\underline{V}_i = \underline{h}_{effimax} \cdot \sum_{n=1}^{N} \underline{C}(\alpha_n) \cdot \underline{E}_n \; . \qquad (5)$$

Within the Equations (2) through (5) the phase reference for the incident waves has been fixed to a reference point on the car. If the car is moving along the x axis the phase angles of the incident waves related to the car change and, therefore, the output voltage $\underline{V}_i$ in Eqn. (5) becomes a function of x:

$$\underline{V}_i(x) = \underline{h}_{effimax} \cdot \sum_{n=1}^{N} \underline{C}_i(\alpha_n) \cdot \underline{E}_n(x=0) \cdot e^{j\, x \cos\alpha_n} \qquad (6)$$

This equation can be used as a base for the calculation of the correlation between different antennas.

For the calculation of the diversity gain and the fade-reduction factor the correlation factor of the voltage magnitudes

$$\rho_{Rij} = \frac{\overline{(V_i - \overline{V_i}) \cdot (V_j - \overline{V_j})}}{\sqrt{\overline{(V_i - \overline{V_i})^2} \cdot \overline{(V_j - \overline{V_j})^2}}} \tag{7}$$

or the correlation factor of the signal powers

$$\rho_{Sij} = \frac{\overline{(S_i - \overline{S_i}) \cdot (S_j - \overline{S_j})}}{\sqrt{\overline{(S_i - \overline{S_i})^2} \cdot \overline{(S_j - \overline{S_j})^2}}} \tag{8}$$

(S_i = instantaneous available signal power of the i-th antenna; $\overline{S_i}$ = average of S_i) is needed. In [8] it is shown that

$$\rho_S \approx \rho_R \tag{9}$$

in the case of a Rayleigh distribution of the magnitudes of the antenna output voltages V_i. If in our case N is chosen sufficiently high, i.e. $N > 10$, with a rectangular distribution of the angle of incidence α throughout 0 to 2π, the Rayleigh distribution of the single-antenna voltage also can be assumed to be true. This is shown in Fig. 5. For $N = 5$ and $N = 20$ statistical results of the cumulative probability density function

$$\Pr (V \leq V_{min}) = P (V_{min}) \tag{10}$$

have been calculated and plotted in a Rayleigh net. The pure Rayleigh distribution is represented by the straight line. The statistics are derived from 100 random fields each with random incident waves, $\underline{C}_{(\alpha)}$ = const, and 1000 independent samples [6]. It is obvious from Fig. 5 that $N = 20$ is sufficient high to assume the Rayleigh distribution for the voltage magnitudes, if the antennas do not

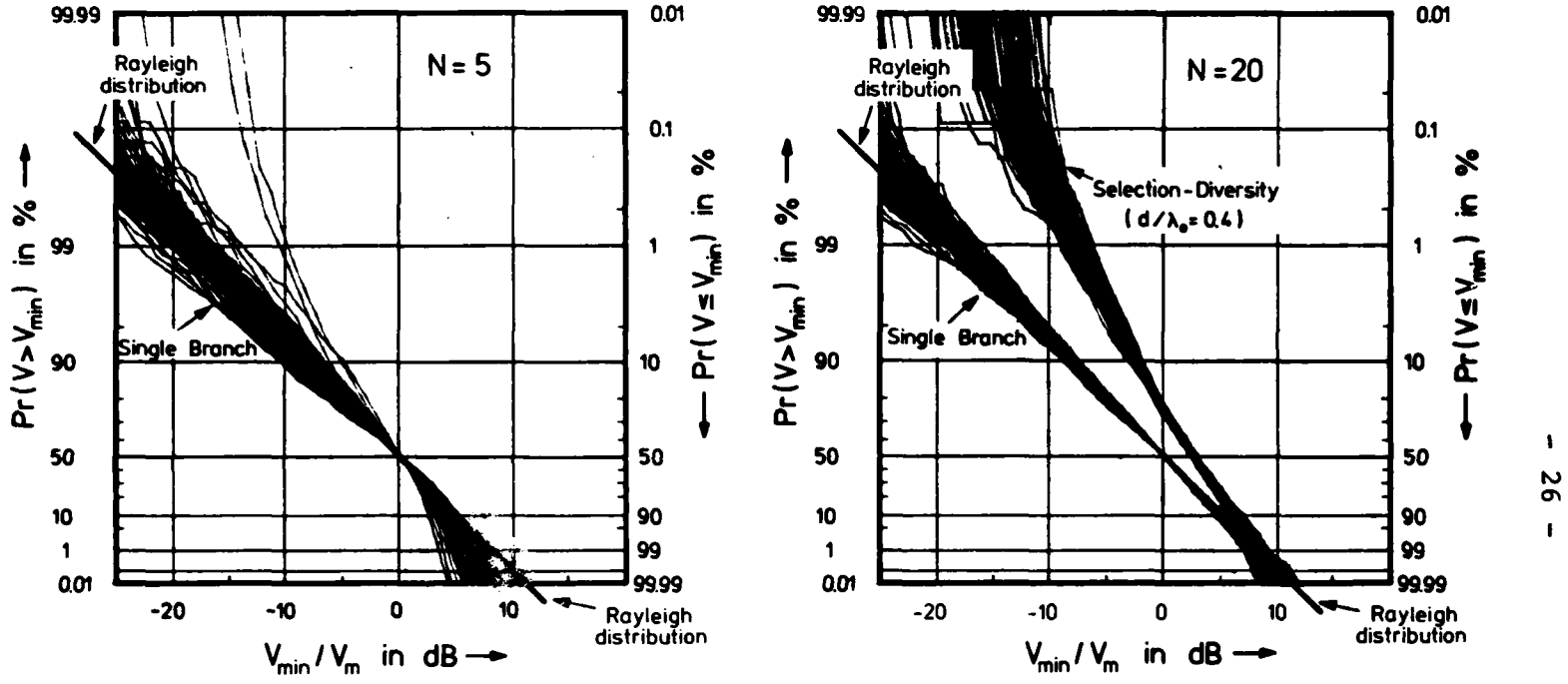

Fig. 5: Distribution of the magnitude of the electrical field strength in a field built up from N = 5 and N = 20 randomly distributed waves, respectively, compared to the Rayleigh distribution.
(100 calculated cases, each case represented by 1000 independent samples).
The representation for N = 20 is completed with the probability function of a selection-diversity system exposed to the different calculated fields.

show high gain, which is true in our case.

On that account we assume Eqn. (9) to be true in our case and restrict ourselves to the calculation of ρ_S which can be done easier than the calculation of ρ_R basing on Eqn. (6). For the differences between ρ_S and ρ_R see [8].
Eqn. (8) can be modified to

$$\rho_{Sij} = \frac{\overline{S_i S_j} - \overline{S_i} \cdot \overline{S_j}}{\sqrt{(\overline{S_i^2} - \overline{S_i}^2)(\overline{S_j^2} - \overline{S_j}^2)}} \tag{11}$$

All terms in Eqn. (11) can be calculated from Eqn. (6). Using (6) and

$$\underline{E}_n(0) = E_n(0) \cdot e^{j\varphi_{En}} \quad \text{and} \quad \underline{C}_i(\alpha_n) = C_i(\alpha_n) \cdot e^{j\varphi_{Ci}} \tag{12}$$

we get the normalized available output power of the i-th antenna

$$S_i(x) = \frac{1}{2} \left| \underline{V}_i(x) \right|^2 \tag{13}$$

$$= \frac{1}{2} h_{effimax}^2 \cdot \left| \sum_{n=1}^{N} C_i(\alpha_n) \cdot E_n(0) \cdot e^{j[x\cos\alpha_n + \varphi_{En} + \varphi_{Ci}(\alpha_n)]} \right|^2$$

or

$$S_i(x) = \frac{1}{2} h_{effimax}^2 \cdot \left[\sum_{m=1}^{N} C_i(\alpha_m) \cdot E_m(0) \cdot e^{j[\cos\alpha_m + \varphi_{Em} + \varphi_{Ci}(\alpha_m)]} \right] \times$$

$$\times \left[\sum_{n=1}^{N} C_i(\alpha_n) \cdot E_n(0) \cdot e^{-j[\cos\alpha_n + \varphi_{En} + \varphi_{Ci}(\alpha_n)]} \right] \tag{14}$$

The average of $S_i(x)$ is given by the averaging process

$$\overline{S_i} = \lim_{x_o \to \infty} \frac{1}{x_o} \int_o^{x_o} S_i(x)\,dx \tag{15}$$

Evaluating (15) with S_i from (14) it can be noticed that only terms of the sum product contribute to $\overline{S_i}$ which show a constant exponent that is not a function of x, i.e. m=n. Thus,

$$\overline{S_i} = \frac{1}{2} h^2_{effimax} \cdot \sum_{n=1}^{N} C_i^2(\alpha_n) \cdot E_n^2(o) \tag{16}$$

and

$$\overline{S_i}^2 = \frac{1}{4} h^4_{effimax} \left[\sum_{n=1}^{N} C_i^2(\alpha_n) \cdot E_n^2(o) \right]^2$$

In a similar way $\overline{S_i^2}$ can be calculated.

$$\overline{S_i^2} = \lim_{x_o \to \infty} \frac{1}{x_o} \int_o^{x_o} S_i^2(x)\, dx$$

$$= \lim_{x_o \to \infty} \frac{1}{x_o} \frac{1}{4} h^2_{effimax} \int_o^{x_o} \left| \sum_{n=1}^{N} C_i(\alpha_n) E_n(O) \cdot e^{j[x\cos\alpha_n + \varphi_{En} + \varphi_{Ci}(\alpha_n)]} \right|^4 dx \tag{17}$$

or

$$\overline{S_i^2} = \lim_{x_o \to \infty} \frac{1}{x_o} \frac{1}{4} h^4_{effimax} \cdot \int_o^{x_o} \left[\sum_{m=1}^{N} C_i(\alpha_m) \cdot E_m \cdot e^{j[x\cos\alpha_m + \varphi_{Em} + \varphi_{Ci}(\alpha_m)]} \right] \times$$

$$\times \left[\sum_{n=1}^{N} C_i(\alpha_n)\, E_n \cdot e^{-j[x\cos\alpha_n + \varphi_{En} + \varphi_{Ci}(\alpha_n)]} \right] \times$$

$$\times \left[\sum_{o=1}^{N} C_i(\alpha_o)\, E_o \cdot e^{j[x\cos\alpha_o + \varphi_{Eo} + \varphi_{Ci}(\alpha_o)]} \right] \times$$

$$\times \left[\sum_{p=1}^{N} C_i(\alpha_p)\, E_p \cdot e^{-j[x\cos\alpha_p + \varphi_{Ep} + \varphi_{Ci}(\alpha_p)]} \right] dx \tag{18}$$

Within the quadruple product only those terms contribute to $\overline{S_i^2}$ which give a constant exponent, i.e. the combinations

$$\text{and} \quad \begin{matrix} (m = n \quad \text{and} \quad o = p) & (19) \\ (m = p \quad \text{and} \quad n = o). & (20) \end{matrix}$$

It has to be regarded that the combinations m=n=o=p are included twice in Eqns. (19) and (20) when Eqn. (18) is reduced to the contributing terms.

Thus,

$$\overline{S_i^2} = \frac{1}{4} h_{effimax}^4 \left\{ 2 \left[\sum_{n=1}^{N} C_i^2(\alpha_n) E_n^2 \right]^2 - \left| \sum_{n=1}^{N} C_i^4(\alpha_n) E_n^4 \right| \right\} \qquad (21)$$

Furthermore, the covariance between two antennas i and j is

$$\overline{S_i S_j} = \lim_{x_o \to \infty} \frac{1}{x_o} \cdot \frac{1}{2} h_{effimax}^2 \cdot \frac{1}{2} h_{effjmax}^2 \times$$

$$\times \int_o^{x_o} \left| \sum_{n=1}^{N} C_i(\alpha_n) \cdot E_n \cdot e^{j[x\cos\alpha_n + \varphi_{En} + \varphi_{Ci}(\alpha_n)]} \right|^2 \times$$

$$\times \left| \sum_{n=1}^{N} C_j(\alpha_n) \cdot E_n \cdot e^{j[x\cos\alpha_n + \varphi_{En} + \varphi_{Cj}(\alpha_n)]} \right|^2 dx$$

$$= \lim_{x_o \to \infty} \frac{1}{x_o} \cdot \frac{1}{2} h_{effimax}^2 \cdot h_{effjmax}^2 \times$$

$$\times \int_o^{x_o} \left[\sum_{m=1}^{N} C_i(\alpha_m) E_m \cdot e^{j[x\cos\alpha_m + \varphi_{Em} + \varphi_{Ci}(\alpha_m)]} \right] \times$$

$$\times \left[\sum_{n=1}^{N} C_i(\alpha_n) E_n \cdot e^{-j[x\cos\alpha_n + \varphi_{En} + \varphi_{Ci}(\alpha_n)]} \right] \times$$

$$\times \left[\sum_{o=1}^{N} C_j(\alpha_o) E_o \cdot e^{j[x\cos\alpha_o + \varphi_{Eo} + \varphi_{Ci}(\alpha_o)]} \right] \times$$

$$\times \left[\sum_{p=1}^{N} C_j(\alpha_p) E_p \cdot e^{-j[x\cos\alpha_p + \varphi_{Ep} + \varphi_{Ci}(\alpha_p)]} \right] dx \qquad (22)$$

Again, only those terms in the quadruple product contribute to the integral which fulfil the conditions

$$(m = n \quad \text{and} \quad o = p) \tag{23}$$

and

$$(m = p \quad \text{and} \quad n = o) \tag{24}$$

wherein the combinations m=n=o=p are contained twice. On this account,

$$\overline{S_i S_j} = \frac{1}{4} h^2_{effimax} \cdot h^2_{effjmax} \times$$

$$\times \left\{ \left[\sum_{n=1}^{N} C_i^2(\alpha_n) E_n^2 \cdot \sum_{n=1}^{N} C_j^2(\alpha_n) E_n^2 \right] \right.$$

$$+ \left[\sum_{n=1}^{N} C_i(\alpha_n) C_j(\alpha_n) E_n^2 \cos[\varphi_{Ci}(\alpha_n) - \varphi_{Cj}(\alpha_n)] \right]^2$$

$$+ \left[\sum_{n=1}^{N} C_i(\alpha_n) C_j(\alpha_n) E_n^2 \sin[\varphi_{Ci}(\alpha_n) - \varphi_{Cj}(\alpha_n)] \right]^2$$

$$\left. - \sum_{n=1}^{N} C_i^2(\alpha_n) C_j^2(\alpha_n) E_n^4 \right\} \tag{25}$$

Summarizing Eqns. (16) through (25) in Eqn. (11) and denoting

$$C_i(\alpha_n) = C_i$$

$$C_j(\alpha_n) = C_j$$

$$\varphi_{Ci}(\alpha_n) = \varphi_{Ci}$$

$$\varphi_{Cj}(\alpha_n) = \varphi_{Cj} \tag{26}$$

one obtains Equation (27);

$$\rho_{Sij} = \frac{\left[\sum_{n=1}^{N} C_i C_j E_n^2 \cos(\varphi_{Ci}-\varphi_{Cj})\right]^2 + \left[\sum_{n=1}^{N} C_i C_j E_n^2 \sin(\varphi_{Ci}-\varphi_{Cj})\right]^2 - \sum_{n=1}^{N} C_i^2 C_j^2 E_n^4}{\left[\sum_{n=1}^{N} C_i^2 E_n^2\right] \cdot \left[\sum_{n=1}^{N} C_j^2 E_n^2\right] \cdot \sqrt{\left[1 - \frac{\sum_{n=1}^{N} C_i^4 E_n^4}{\left[\sum_{n=1}^{N} C_i^2 E_n^2\right]^2}\right] \cdot \left[1 - \frac{\sum_{n=1}^{N} C_j^4 E_n^4}{\left[\sum_{n=1}^{N} C_j^2 E_n^2\right]^2}\right]}} \qquad (27)$$

Equation (27) can be written as

$$\rho_{Sij} = \underbrace{\frac{\left[\sum_{n=1}^{N} C_i C_j E_n^2 \cos(\varphi_{Ci}-\varphi_{Cj})\right]^2 + \left[\sum_{n=1}^{N} C_i C_j E_n^2 \sin(\varphi_{Ci}-\varphi_{Cj})\right]^2}{\left[\sum_{n=1}^{N} C_i^2 E_n^2\right] \cdot \left[\sum_{n=1}^{N} C_j^2 E_n^2\right]}}_{\rho_{Sij\infty}} \cdot (1+\delta) \quad (28)$$

$$\rho_{Sij} = \rho_{Sij\infty} \cdot (1+\delta) \quad (29)$$

It can be shown that the value of δ in (29) decreases with increasing N and vanishes for $N \to \infty$. On this account, the first term in Equation (28) is called $\rho_{Sij\infty}$ as it is the exact correlation factor for the ideal Rayleigh field with an infinite number of incident waves.

As ρ_{Sij} can easily be calculated from the receiving patterns of the i-th and the j-th antenna it will be used as an approximation for ρ_{Sij}. For that purpose, δ acts as a relative error function. It can be estimated for the case of antennas with low gain, i.e.

$$C_1(\alpha) \approx \text{const}; \quad C_2(\alpha) \approx \text{const} \quad (30)$$

and uniform magnitude of the incident waves, i.e.

$$E_n = E_{n+1}, \quad 1 \leq n \leq N-1. \quad (31)$$

Under these assumptions we get the relative error

$$\delta \approx \frac{1}{N} \left(\frac{1}{\rho_{Sij\infty}} - 1\right) \quad (32)$$

and the absolute error

$$\Delta = \delta \cdot \rho_{Sij\infty} \approx \frac{1}{N} (1 - \rho_{Sij\infty}) \quad (33)$$

The following measurement will use a number of N = 18 incident waves which will cause a maximum absolute error of

$\Delta \approx 0.06$. With regard to other error sources during the measurements it is obvious that the approximation

$$\rho_{Sij} \approx \rho_{Sij\infty} = \frac{\left[\sum_{n=1}^{N} C_i C_j E_n^2 \cos(\varphi_{Ci} - \varphi_{Cj})\right]^2 + \left[\sum_{n=1}^{\infty} C_i C_j E_n^2 \sin(\varphi_{Ci} - \varphi_{Cj})\right]^2}{\sum_{n=1}^{N} C_i^2 E_n^2 \cdot \sum_{n=1}^{N} C_j^2 E_n^2} \quad (34)$$

is allowable.

The Eqns. (27) and (34) do not show a dependence on the phase angles of the incident waves. The main determining terms within the two equations are the receiving patterns C_i and C_j of the two antennas including the mutual phase difference $\varphi_{ci} - \varphi_{cj}$.

With (27) and (34) the determination of the correlation factor has been reduced to the measurement of the receiving patterns. As soon as these receiving patterns are known all possible cases with different numbers of incident waves and random distribution of the wave magnitudes can be simulated and calculated with the help of a computer.

It is known from the literature [9] that the distribution of the magnitudes of the incident waves does not effect the autocovariance function of the field if $N \to \infty$. If, as in our case, the antennas mounted on the car are of low directivity we can assume that the distribution of the magnitude of E_n is of low influence, too. On this account, Eqn. (34) can be further simplified by assuming equal values of E_n:

$$\rho_{ij} \approx \frac{\left[\sum_{n=1}^{N} C_i C_j \cos(\varphi_{Ci}-\varphi_{Cj})\right]^2 + \left[\sum_{n=1}^{N} C_i C_j \sin(\varphi_{Ci}-\varphi_{Cj})\right]^2}{\sum_{n=1}^{N} C_i^2 \cdot \sum_{n=1}^{N} C_j^2} \qquad (35)$$

In appendix 1 it is shown that (35) asymptotically approaches the autocovariance function of the electrical field component of a Rayleigh field, if $N \to \infty$ and $C_i = \text{const}$, $C_j = \text{const}$ in Eqn. (35).

If a finite number of N is chosen the result of (35) will differ a certain amount from the usual theoretical limit value. The maximum deviation is about 1/N. To achieve an accuracy of about .05 a wave number of $N \approx 20$ is sufficient. In the following a measurement equipment is described which we built up for the simultaneous measurement of the complex receiving patterns of several antennas mounted on a car.

4.2 Measuring equipment

For the measurements the truck has been placed on a turntable as shown in Fig. 6a. The turntable is a simple self-built construction with three wheels and a fixed bearing at one corner. When rotating the turntable the truck moves around its right front corner. The turntable is located on a paved site which is sized about 100 x 200 meters. The nearest reflecting and scattering objects have a distance of at least 200 meters. In a distance of about 70 meters from the turntable an illuminating transmission antenna is mounted. This is shown in Fig. 6b.

During the field measurements the whole measuring equipment is assembled on the truck, as can be seen in Fig. 7. A block diagram of the equipment is shown in Fig. 8. The

a)

b)

Fig. 6 a): Truck on the turntable
b): Measuring area.

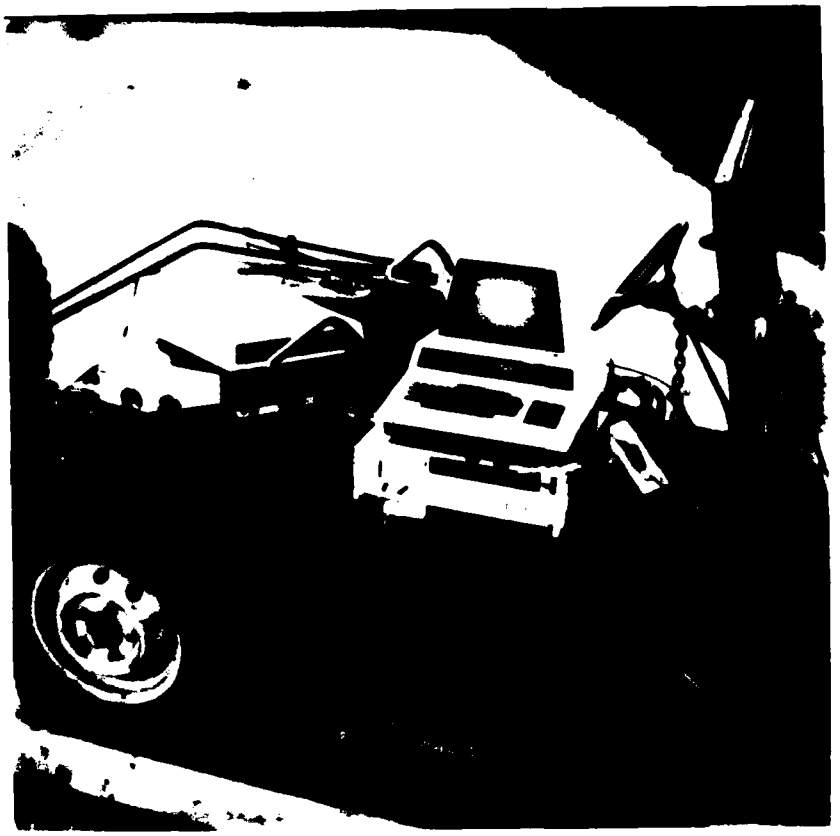

Fig. 7: Measuring equipment on the truck during function tests.

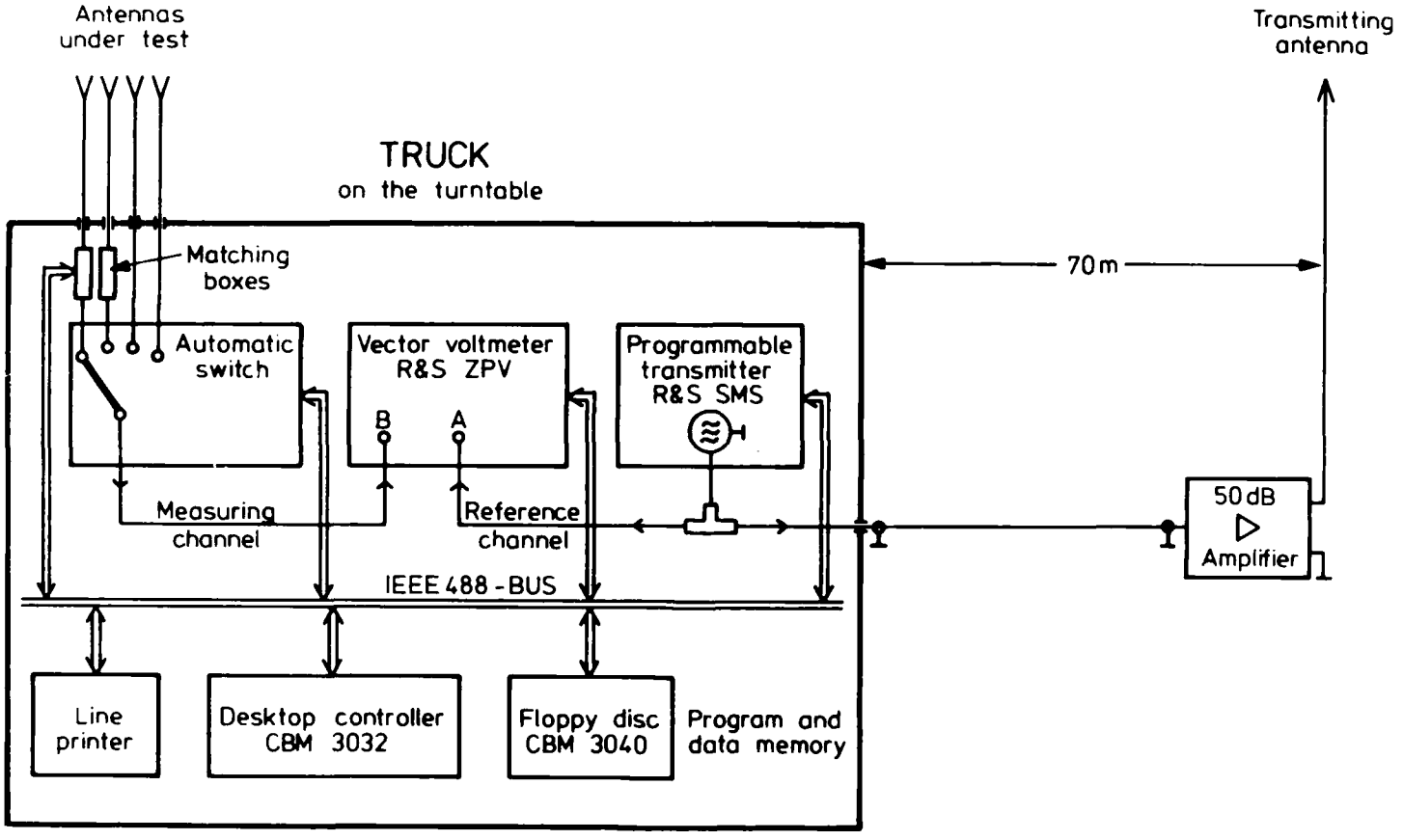

Fig. 8: Block diagram of the measuring equipment.

measurements are managed by a desktop controller (Commodore CBM 3032) via an IEEE 488 bus.

The controller asks for a specified direction of the turntable. If this direction is adjusted and acknowledged by the measuring personal, the controller starts to scan the frequency by adjusting the synthesizer transmitter and the vector voltmeter. During the real measurements the frequency steps in general have been chosen 1 MHz, in some cases 2 MHz or 5 MHz, respectively. At each frequency the response of all connected antennas is measured concerning magnitude and phase, the latter with respect to the reference channel. All data are stored in the memory (Floppy disk, Commodore CBM 3040). After covering the whole frequency range the controller requests the next angle position of the turntable.

All measurements have been done with an angle increment of the turntable of 20 degrees, i.e. 18 measurements have been performed at each frequency to achieve the receiving patterns. In Eqn. (35) the number of waves, on this account, is $N = 18$.

The straight-forward method to measure receiving patterns would have been to rotate the truck at a constant frequency. With this method, however, the truck has to be fully rotated for each measuring frequency and each antenna combination. With our measurement the truck only has to be rotated once for each antenna combination. Our measurement, however, requests a high accuracy of the frequency adjustment to avoid phase-shift errors throughout the angle variations of the turntable. This fact has been considered sufficiently by using a quartz-controlled synthesizer transmitter with extremely high long-time-frequency stabil-

ity.

The stored data can be evaluated afterwards by plotting the receiving patterns and by calculating the wanted covariance functions. These results are given in the following chapter.

5. Results of the measurements

In the following the measurement results are listed in detail. The measured receiving patterns are only intermediate results in order to get the covariance functions. On the other hand, the measured receiving patterns could be of interest for some other purposes, too. On this account the measured receiving patterns are also plotted in the following section. Since the phase angle of the receiving pattern is of no interest in general cases only the magnitude has been plotted in the common polar representation.

Within the frequency range of 30 through 80 MHz the measurements have been performed with frequency steps of 1 MHz. As the receiving patterns change only slowly with frequency we restricted the representation of the patterns to frequency increments of 5 MHz in this report. For interested persons the receiving patterns with the 1 MHz-frequency resolution are available on request.

As can be seen from the measuring results the tall passive antennas show mutual influences on the receiving patterns. This is due to the fact that these antennas guide higher antenna currents and disturb the electromagnetic field on account of power consumption and backscattering. Since this effect is influenced by the load impedances of the antennas we always maintained a 50 ohms termination of each antenna simultaneously on the truck.

The short active antennas (rod length = 40 cm) are loaded with a high ohmic input-impedance amplifier. Due to the high ohmic load and the short rod length the currents along the rods and the backscattering effects can be neglected. On this account, the two active antennas were mounted

throughout all measurements.

The receiving pattern of each antenna depends on the configuration of the passive antennas mounted on the car. The pattern of antenna 1, for instance, is different if antenna 2 or antenna 3 is mounted, respectively. Due to this fact each antenna pattern has to be measured for each configuration of the passive antennas. The following representation, therefore, is splitted into groups of equal antenna configuration (as given in the photographs of the Figures 10, 23, and 36).

As only one example Fig. 9 gives a complete set of the measured complex receiving patterns for one antenna combination (antenna 2 and antenna 6) out of the antenna configuration of Fig. 10 at a frequency of 50 MHz. The measured points with an increment of 20 degrees for the angle of incidence are marked. The representation on top shows the various values of C_2 and C_6 to be processed in Eqn. (35). in order to evaluate ρ_{26}. On the bottom of Fig. 9 the values of $\varphi_2 - \varphi_6$ can be seen depending on α_n. This phase dependence on α_n mainly determines the value of ρ_{26} via Eqn. (35). If $\varphi_i - \varphi_j$ remains nearly constant the correlation is high. With increasing phase swing of $\varphi_i - \varphi_j$ the correlation decreases.

5.1 Receiving patterns

The following receiving patterns are splitted into three groups:

a) Antenna configuration of Fig. 10:
   2 long passive rod antennas (right rear and right front)
   2 short active antennas (right front and left front)
   The relating results are given in Figures 11 through 22.

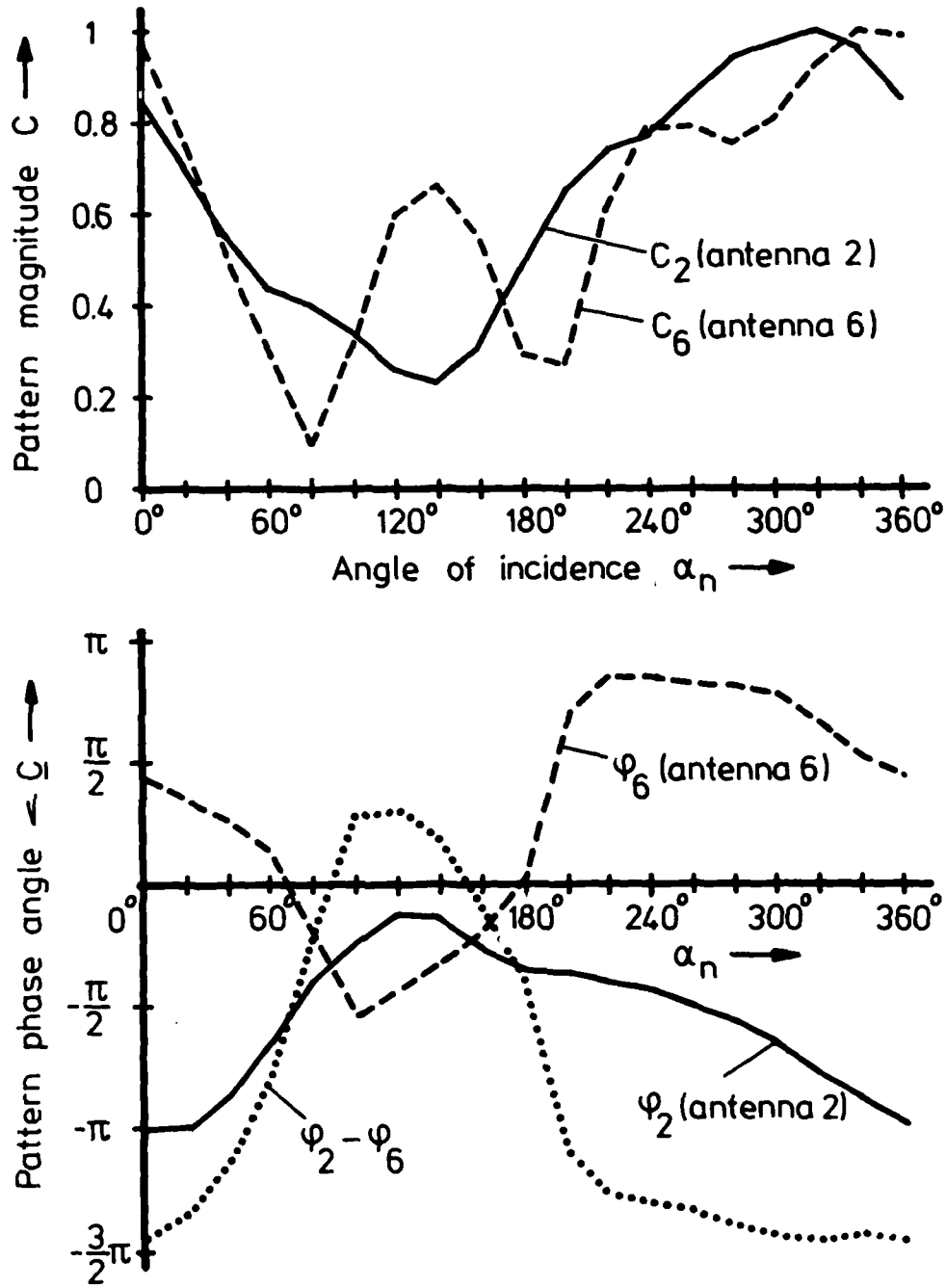

Fig. 9: Magnitude and phase angle of the receiving patterns $\underline{C}_2$ and $\underline{C}_6$ of antenna 2 and antenna 6, respectively. f = 50 MHz.

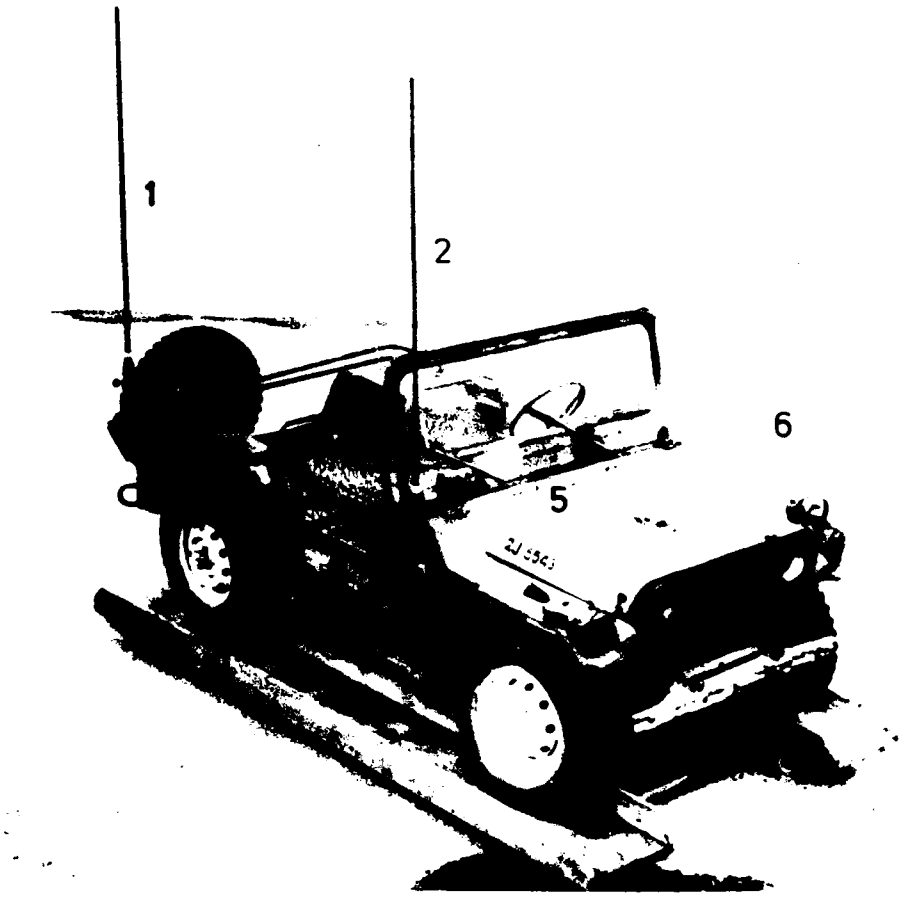

Fig. 10: Antenna configuration for Fig. 11 through 22.

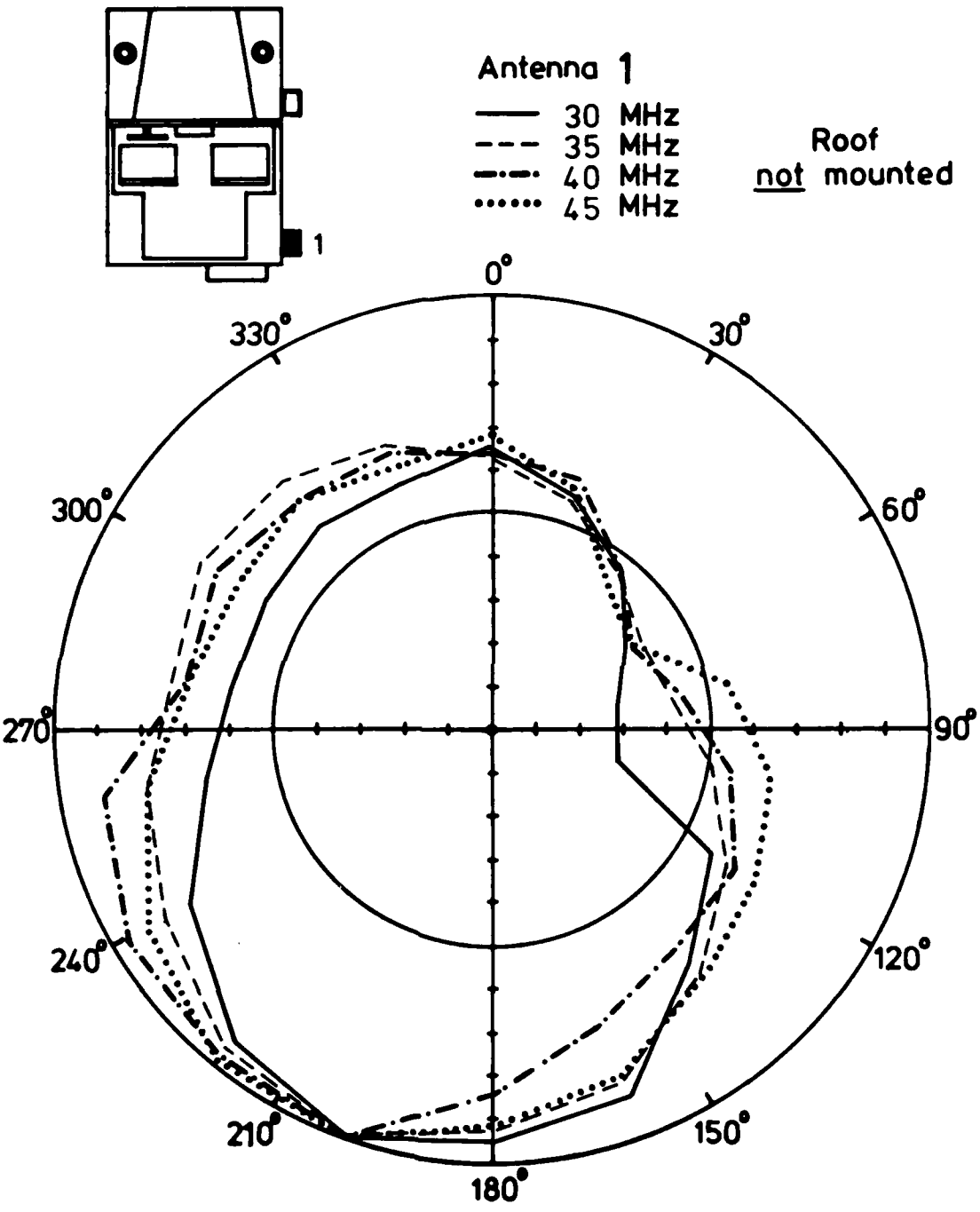

Fig. 11: Receiving pattern of antenna 1 for f = 30/35/40/45 MHz. Roof not mounted. (Antenna configuration as in Fig. 10)

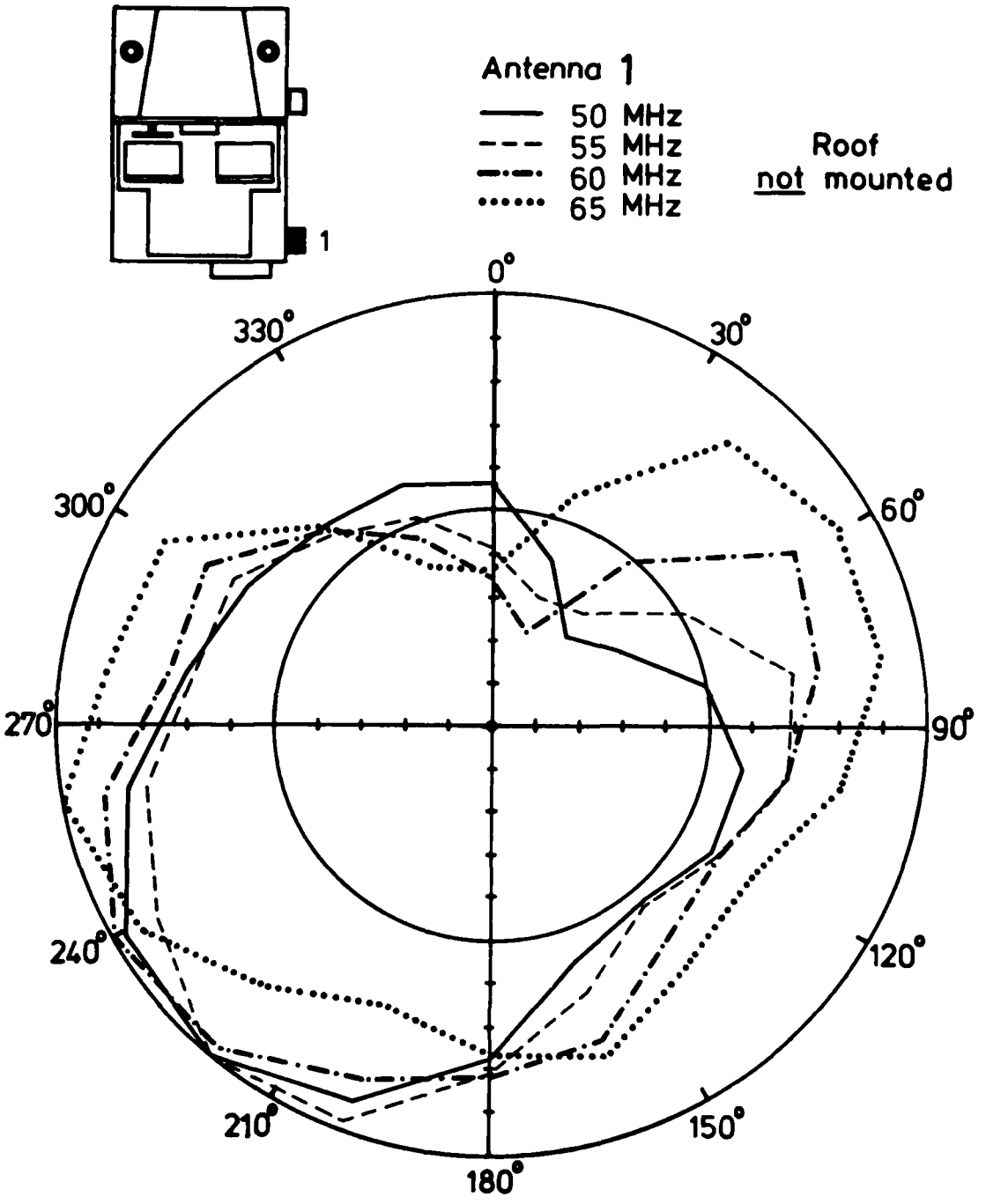

Fig. 12: Receiving pattern of antenna 1 for f = 50/55/60/65 MHz. Roof not mounted. (Antenna configuration as in Fig. 10)

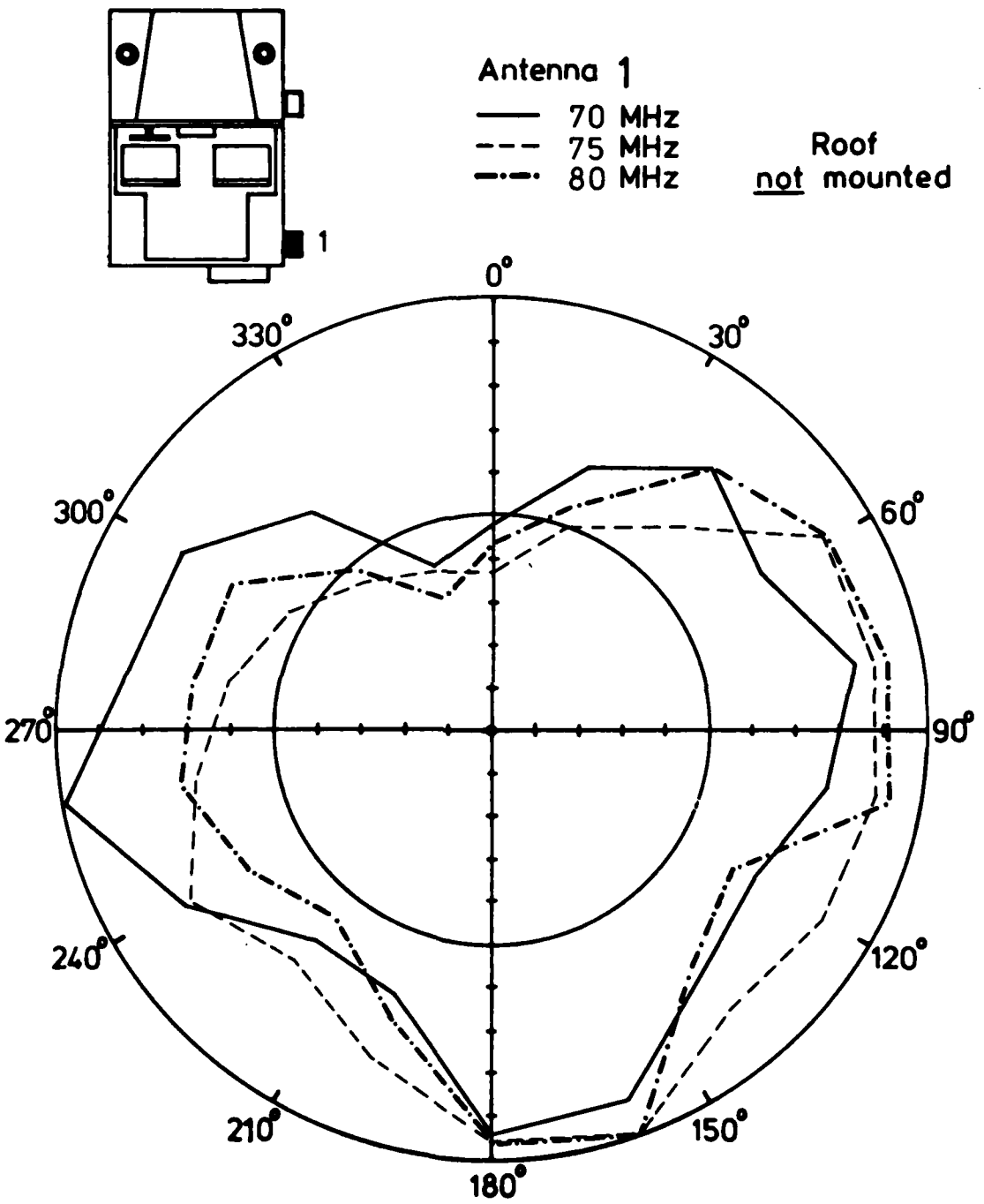

Fig. 13: Receiving pattern of antenna 1 for f = 70/75/80 MHz. Roof not mounted. (Antenna configuration as in Fig. 10)

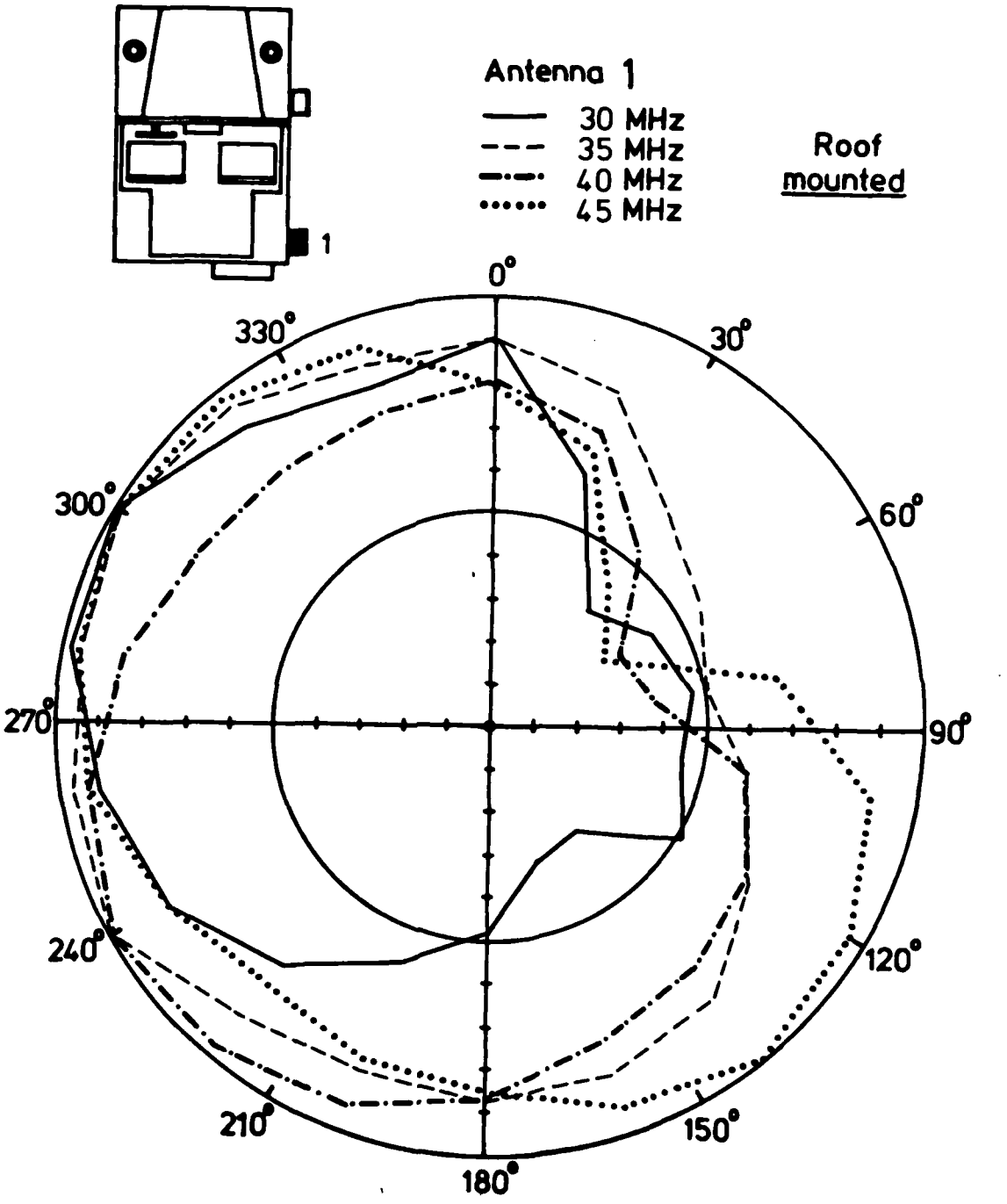

Fig. 14: Receiving pattern of antenna 1 for f = 30/35/40/45 MHz. Roof mounted. (Antenna configuration as in Fig. 10)

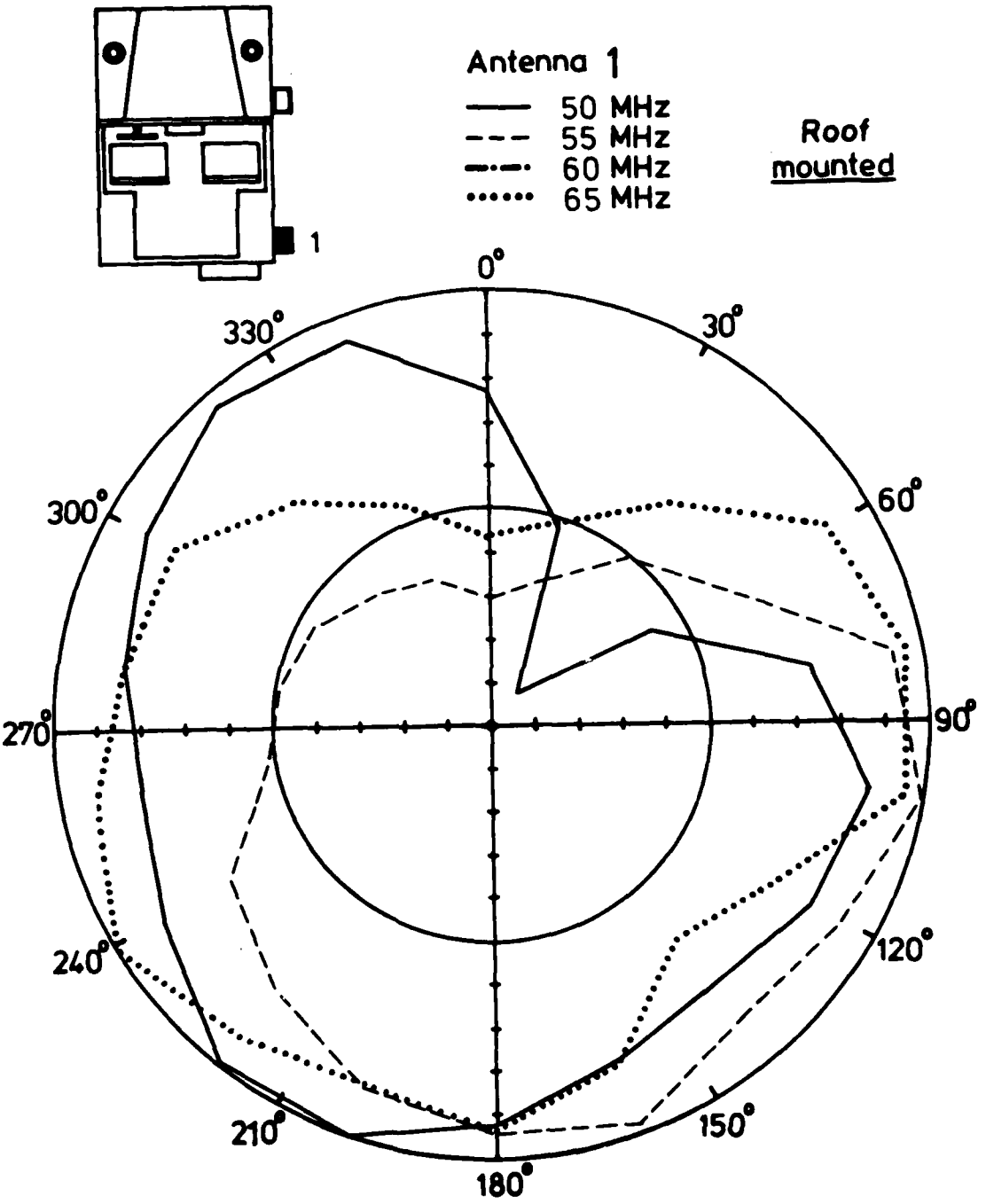

Fig. 15: Receiving pattern of antenna 1 for f = 50/55/60/65 MHz. Roof mounted. (Antenna configuration as in Fig. 10)

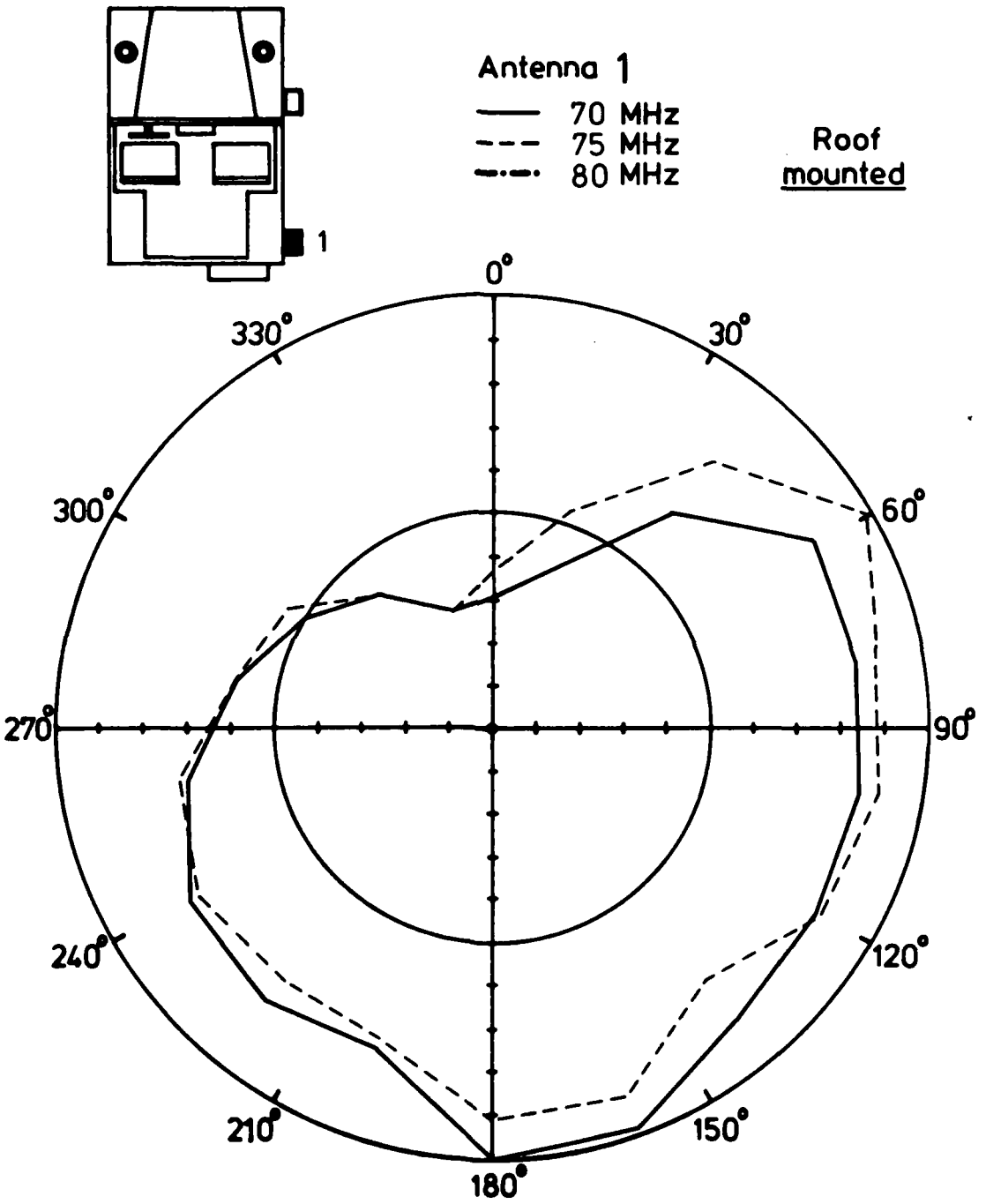

Fig. 16: Receiving pattern of antenna 1 for f = 70/75/80 MHz. Roof mounted. (Antenna configuration as in Fig. 10)

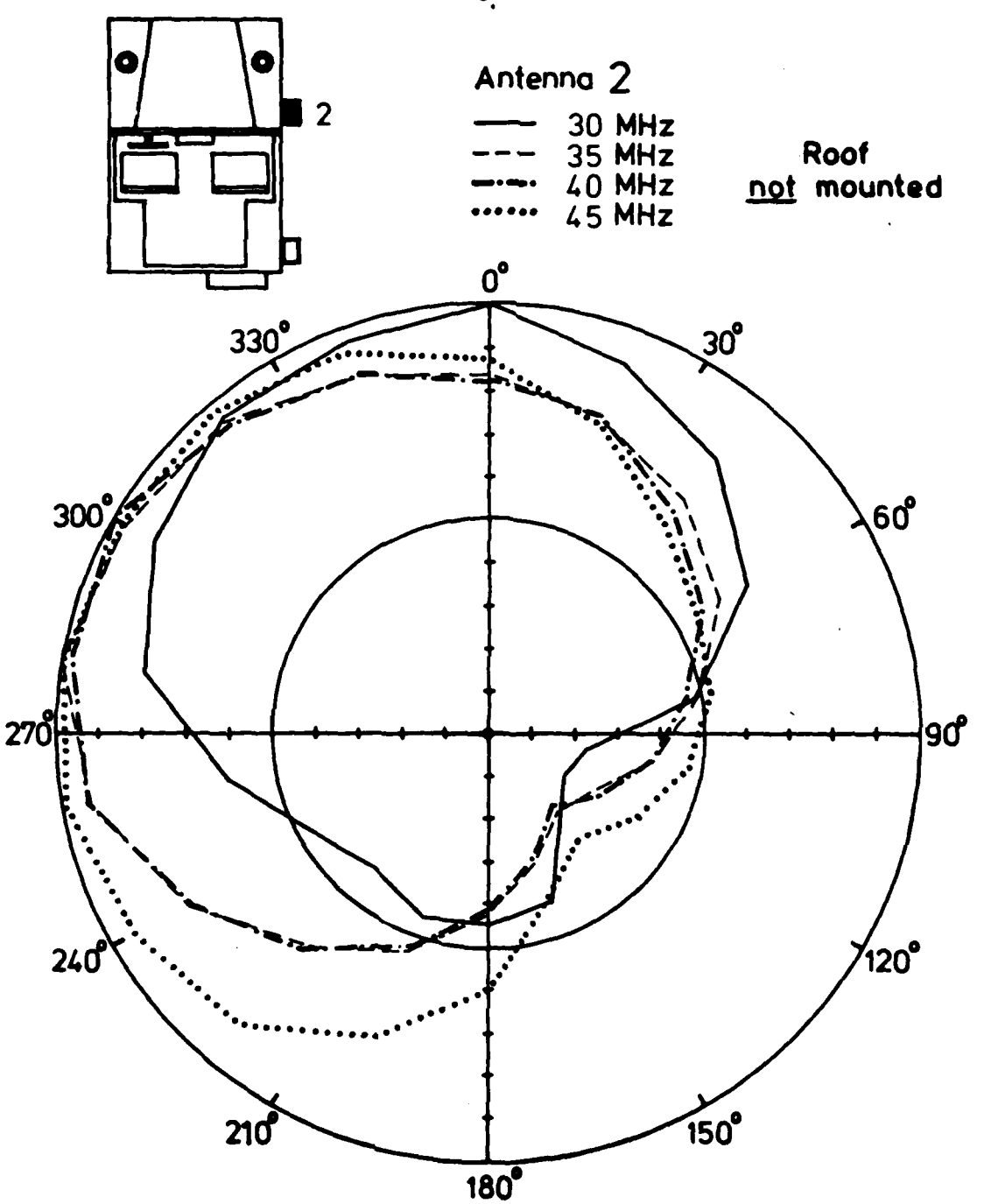

Fig. 17: Receiving pattern of antenna 2 for f = 30/35/40/45 MHz. Roof not mounted. (Antenna configuration as in Fig. 10)

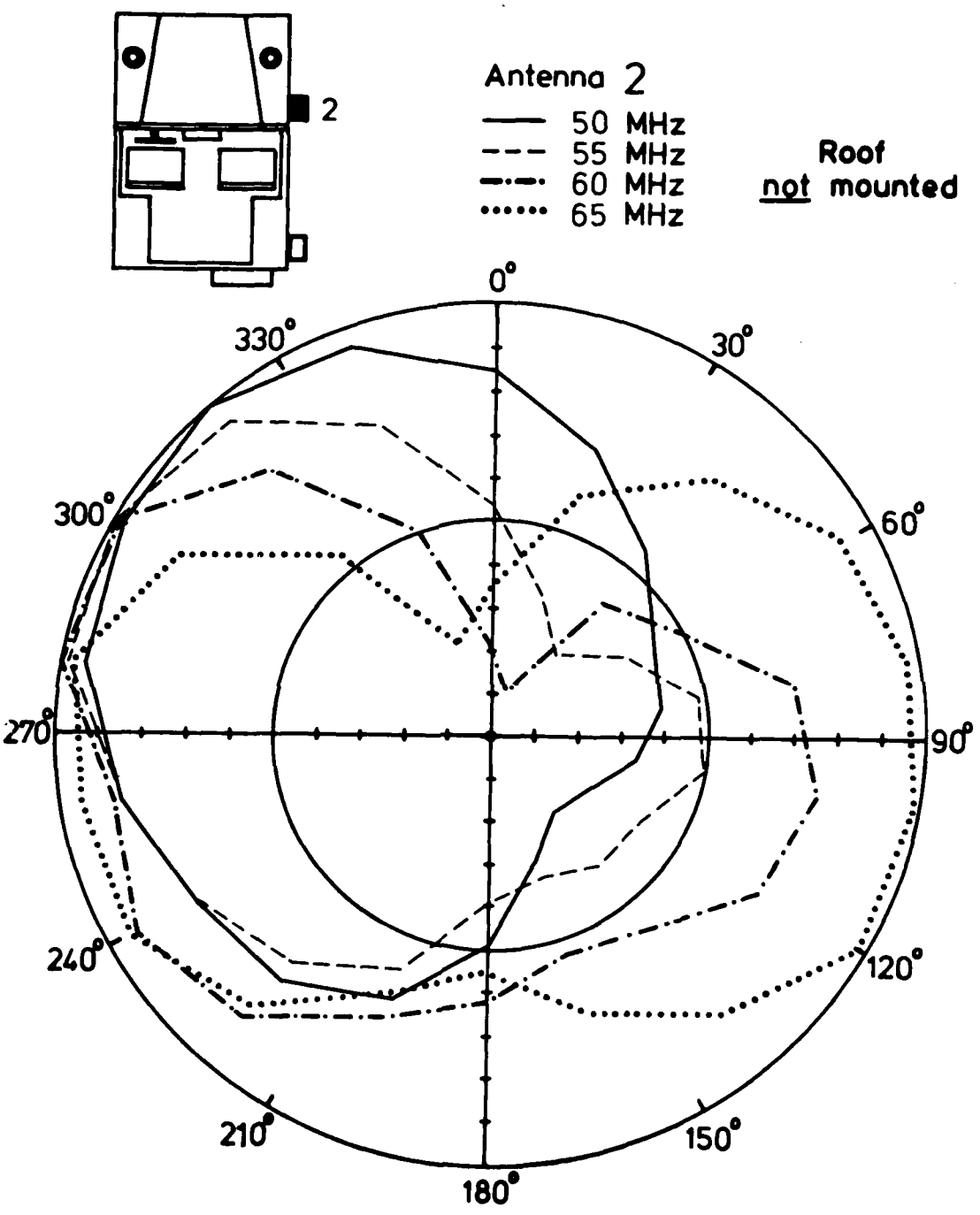

Fig. 18: Receiving pattern of antenna 2 for f = 50/55/60/65 MHz. Roof not mounted. (Antenna configuration as in Fig. 10)

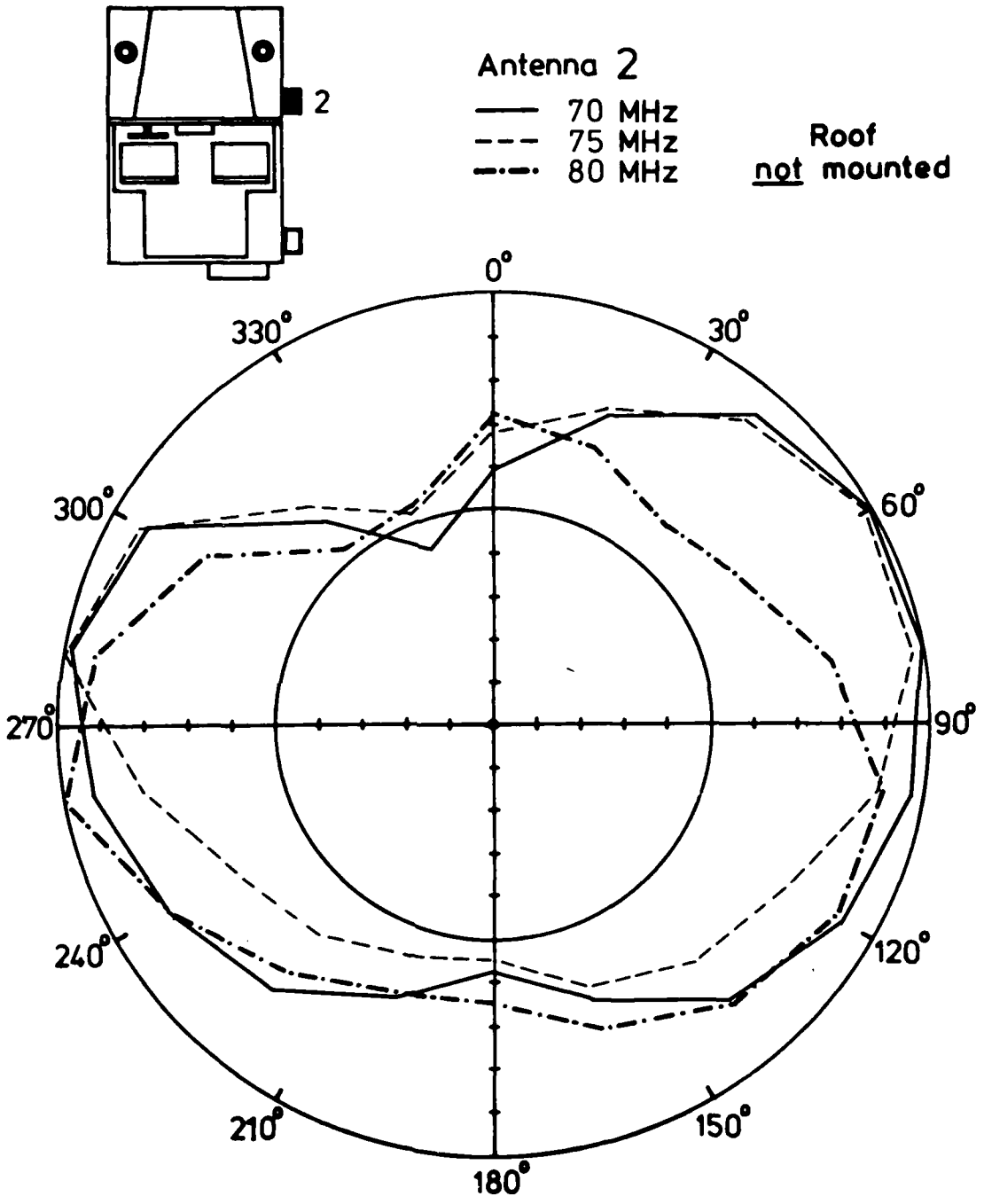

Fig. 19: Receiving pattern of antenna 2 for f = 70/75/80 MHz. Roof not mounted. (Antenna configuration as in Fig. 10)

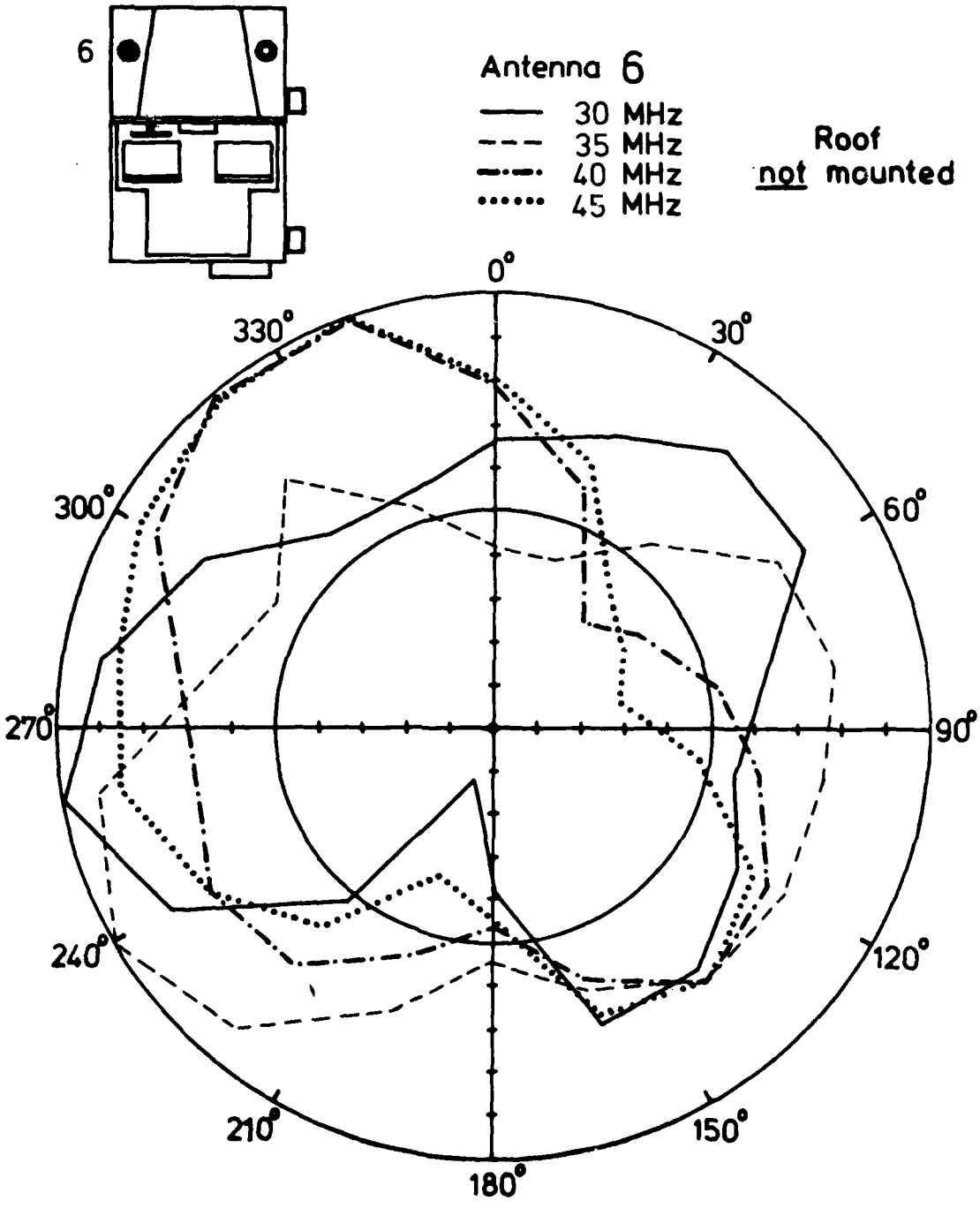

Fig. 20: Receiving pattern of antenna 6 for f = 30/35/40/45 MHz. Roof not mounted. (Antenna configuration as in Fig. 10)

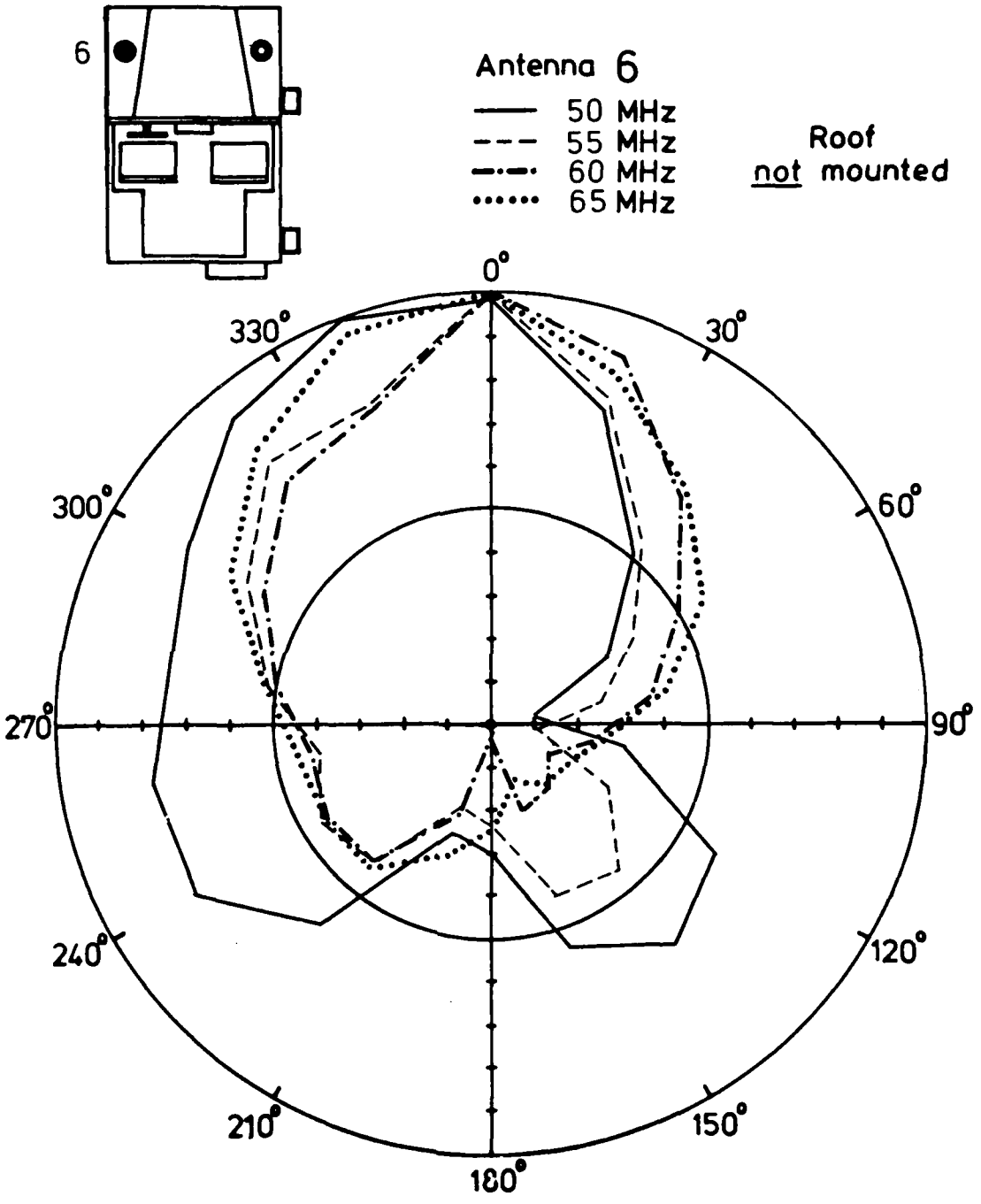

Fig. 21: Receiving pattern of antenna 6 for f = 50/55/60/65 MHz. Roof not mounted. (Antenna configuration as in Fig. 10)

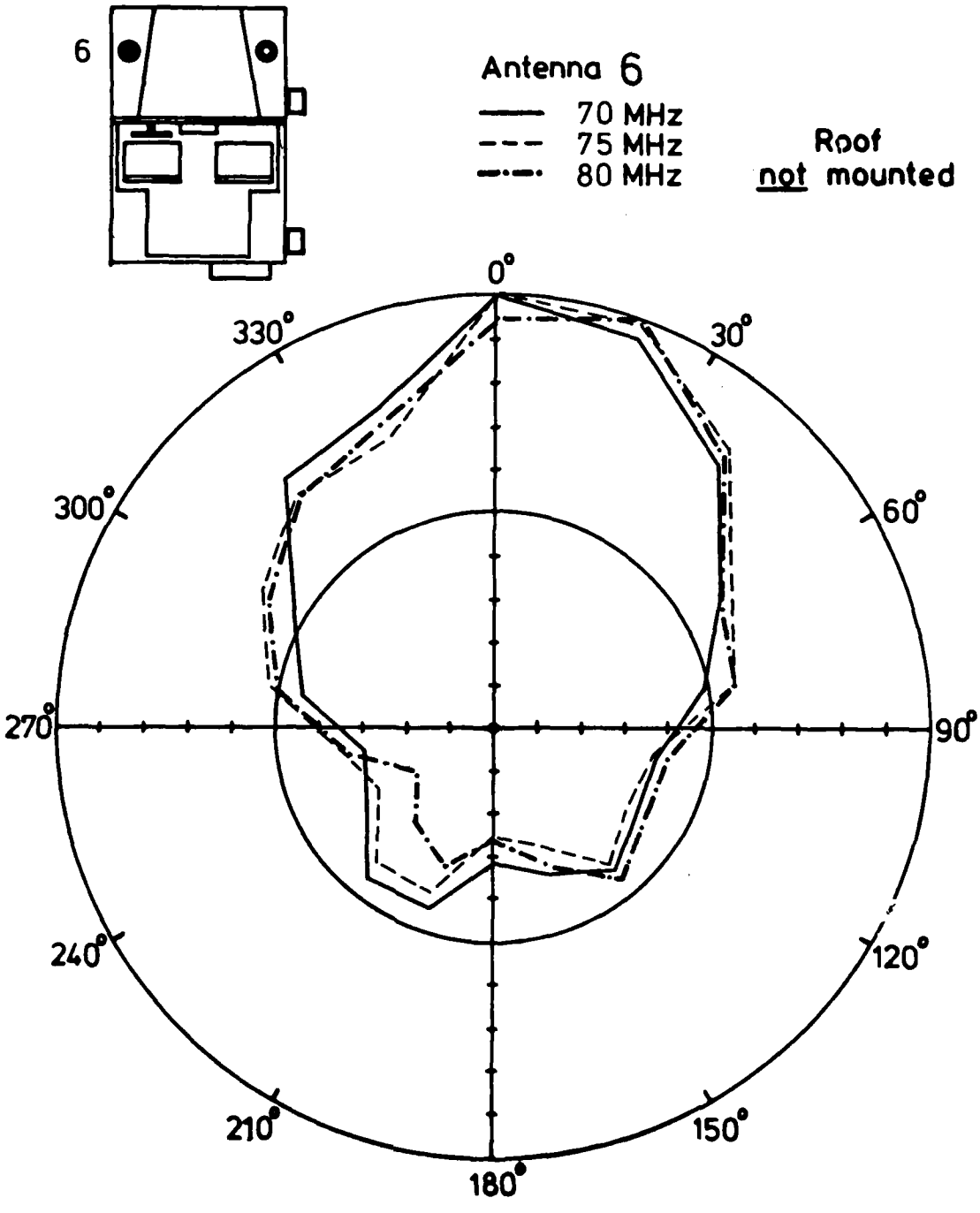

Fig. 22: Receiving pattern of antenna 6 for f = 70/75/80 MHz. Roof not mounted. (Antenna configuration as in Fig. 10)

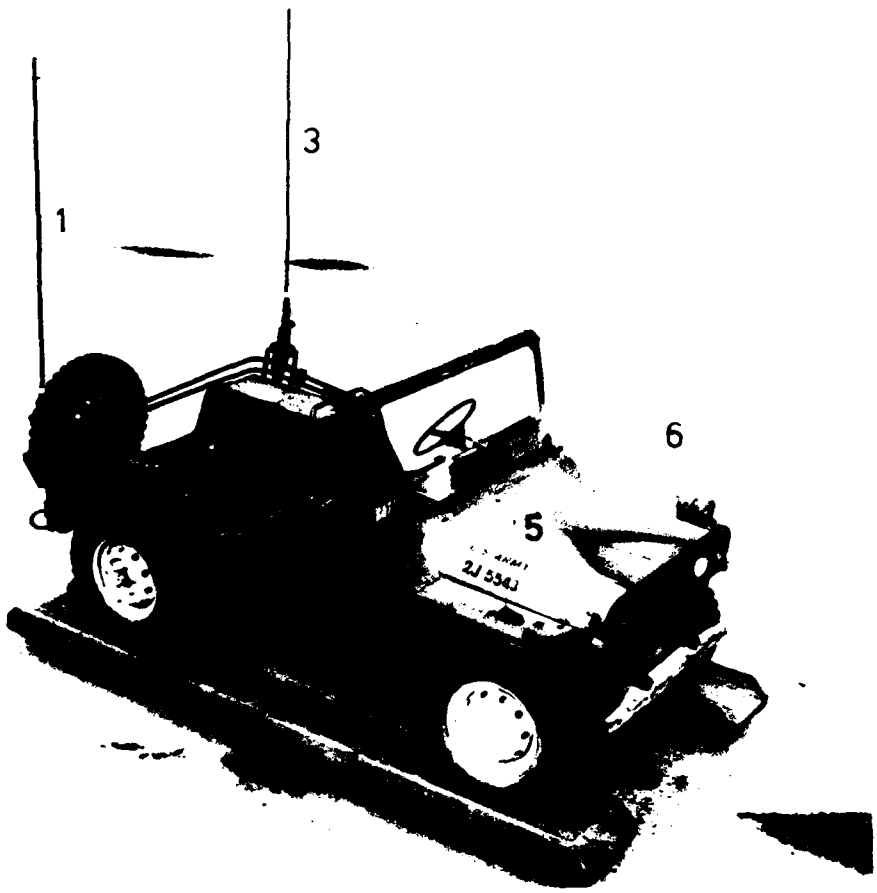

Fig. 23: Antenna configuration for Fig. 24 through 35.

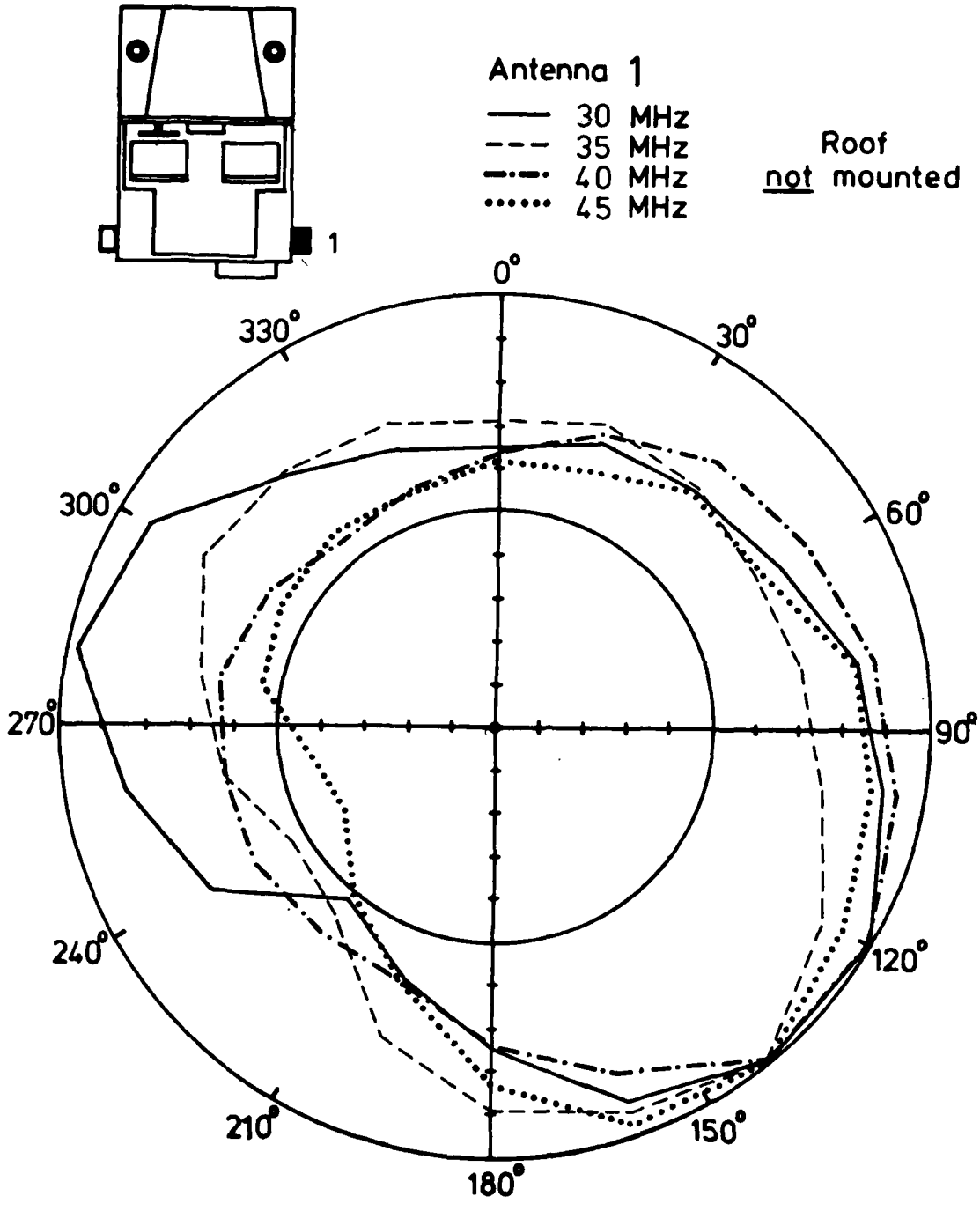

Fig. 24: Receiving pattern of antenna 1 for f = 30/35/40/45 MHz. Roof not mounted. (Antenna configuration as in Fig. 23)

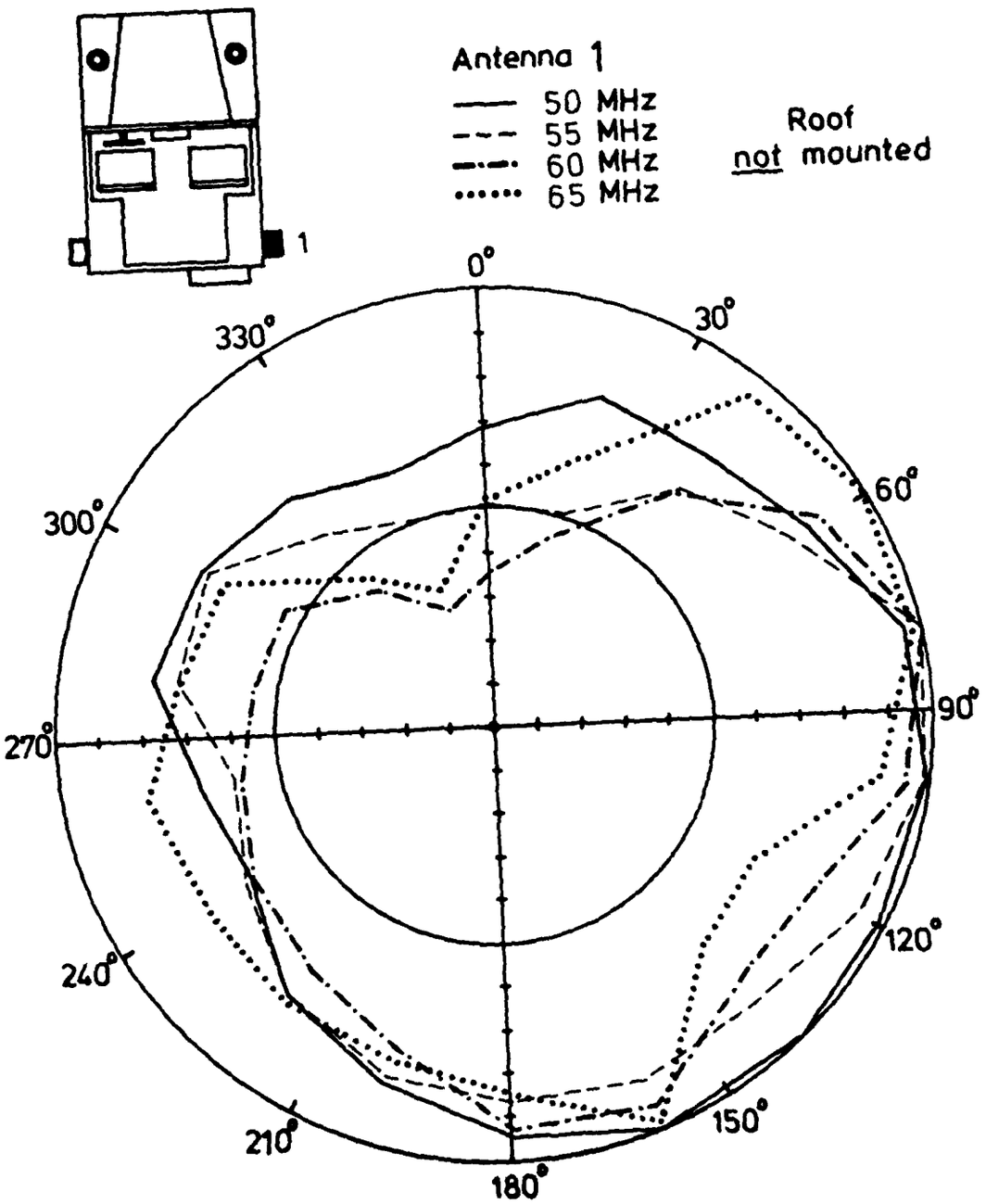

Fig. 25: Receiving pattern of antenna 1 for f = 50/55/60/65 MHz. Roof not mounted. (Antenna configuration as in Fig. 23)

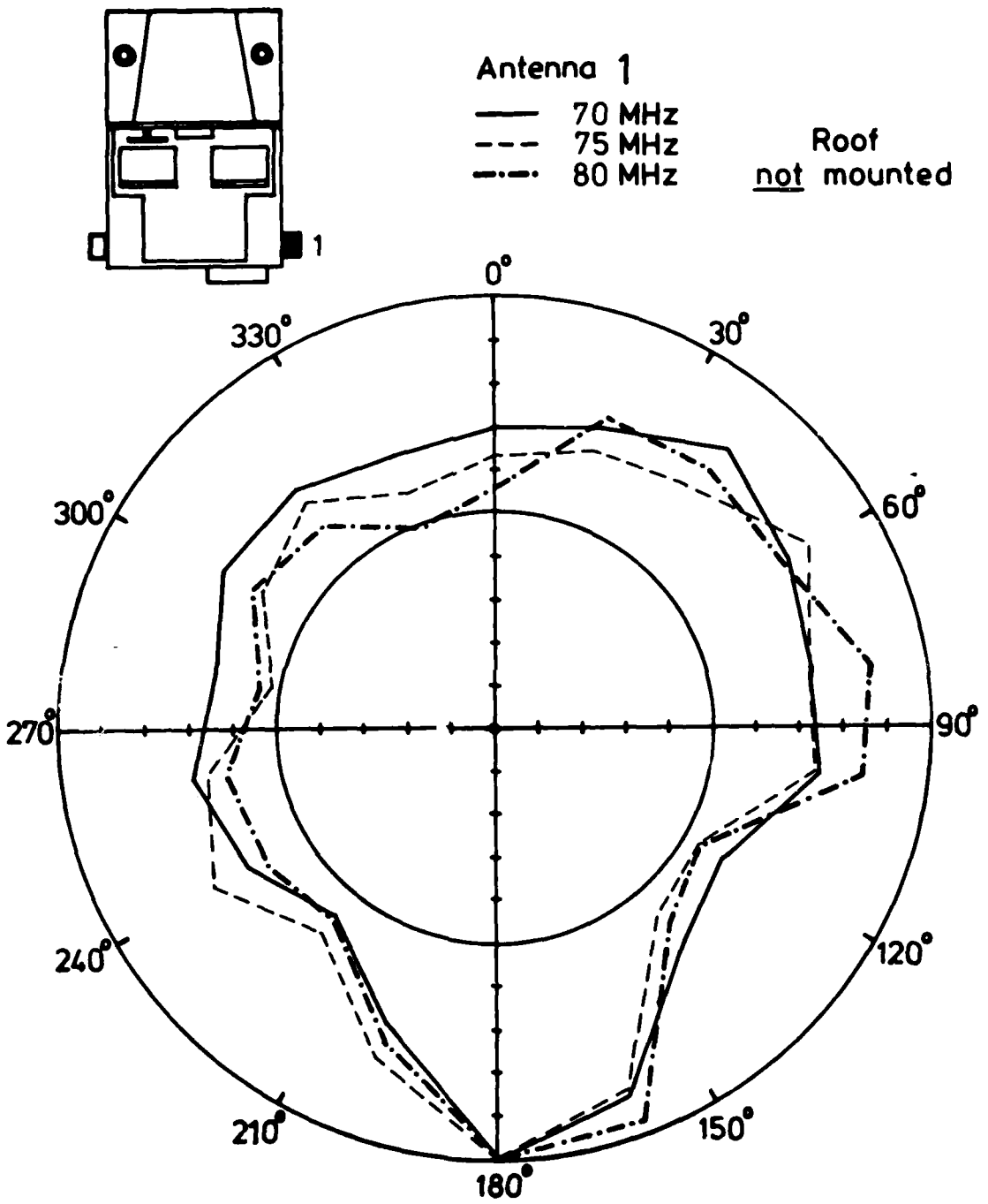

Fig. 26: Receiving pattern of antenna 1 for f = 70/75/80 MHz. Roof not mounted. (Antenna configuration as in Fig. 23)

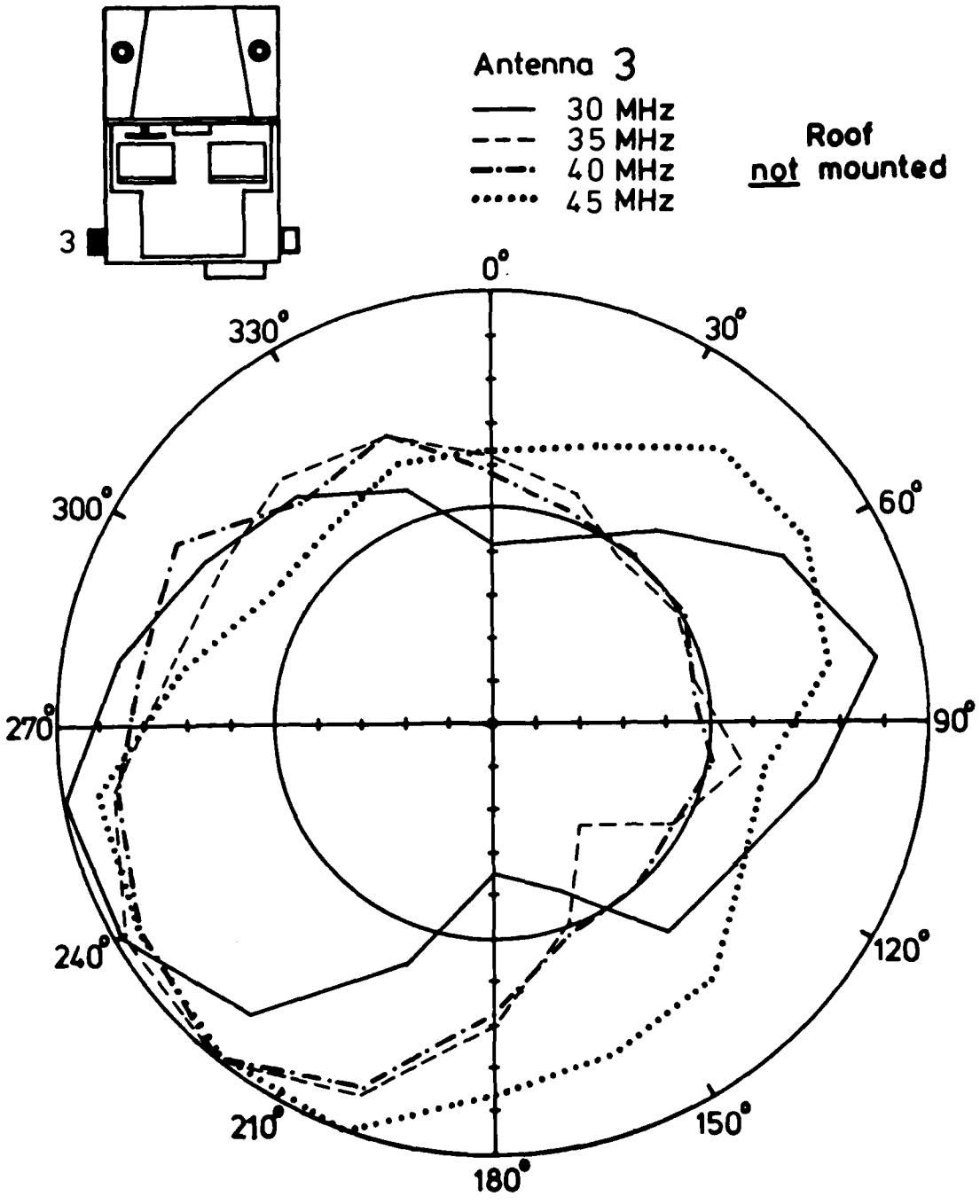

Fig. 27: Receiving pattern of antenna 3 for f = 30/35/40/45 MHz. Roof not mounted. (Antenna configuration as in Fig. 23)

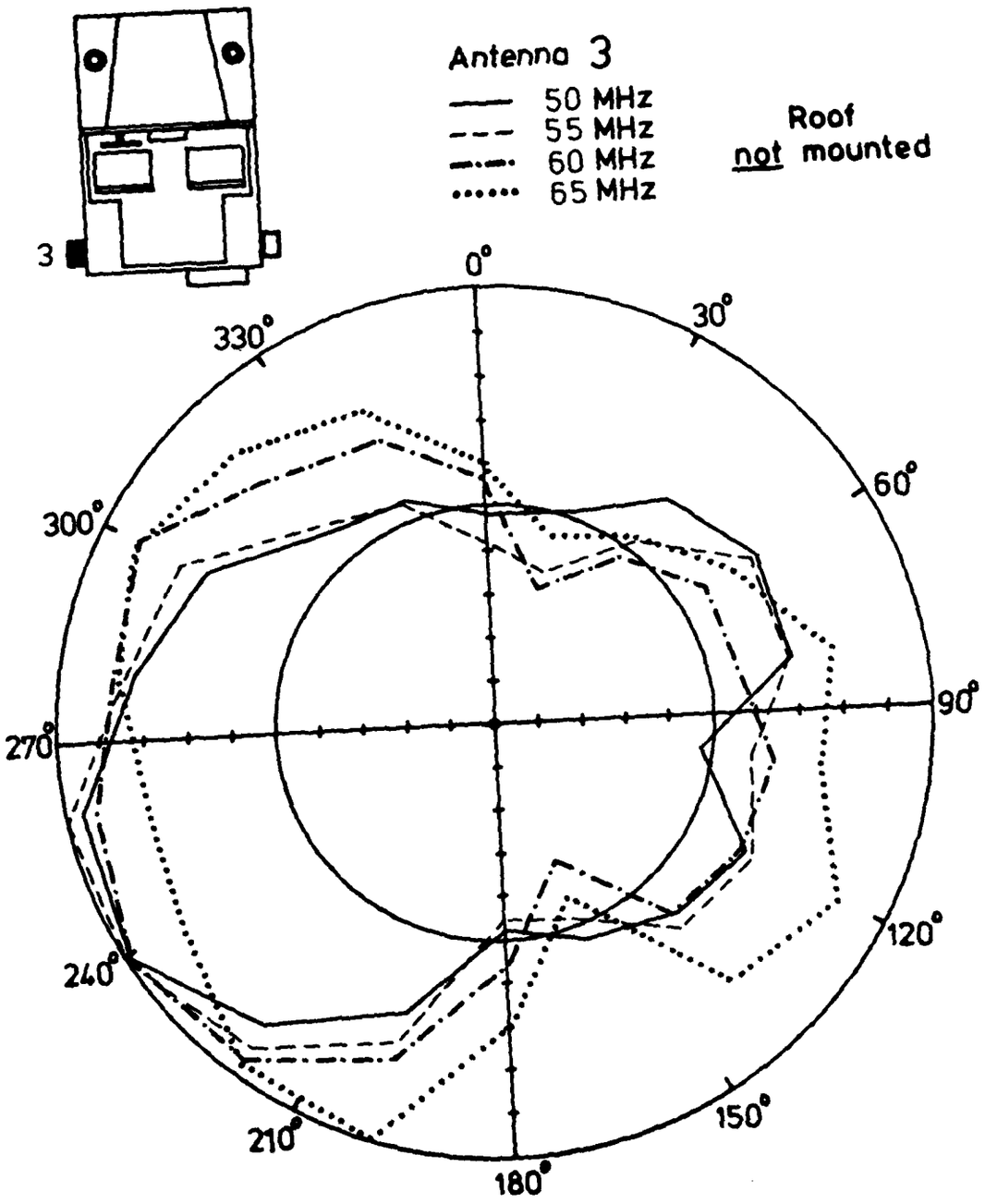

Fig. 28: Receiving pattern of antenna 3 for f = 50/55/60/65 MHz. Roof not mounted. (Antenna configuration as in Fig. 23)

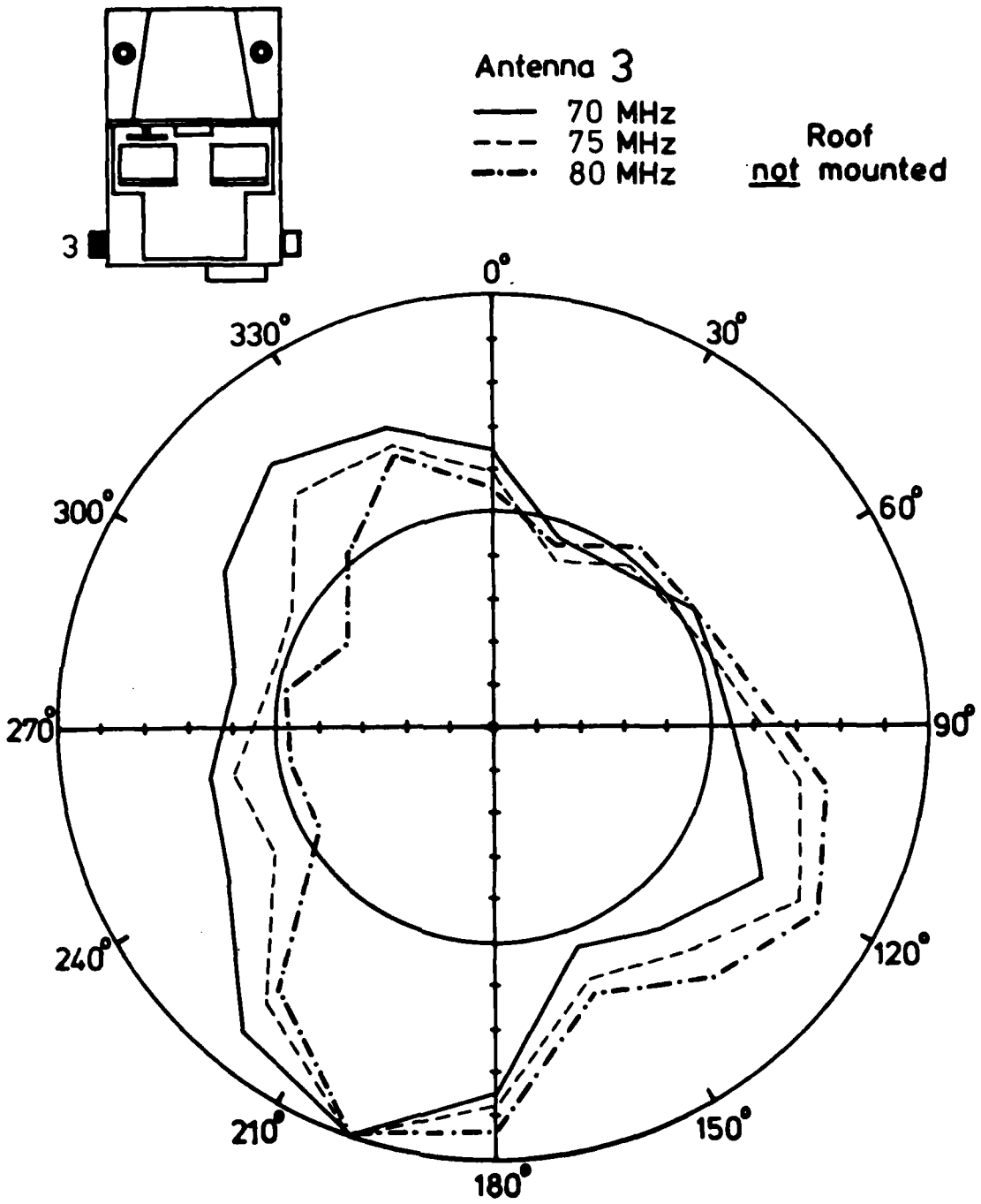

Fig. 29: Receiving pattern of antenna 3 for f = 70/75/80 MHz. Roof not mounted. (Antenna configuration as in Fig. 23)

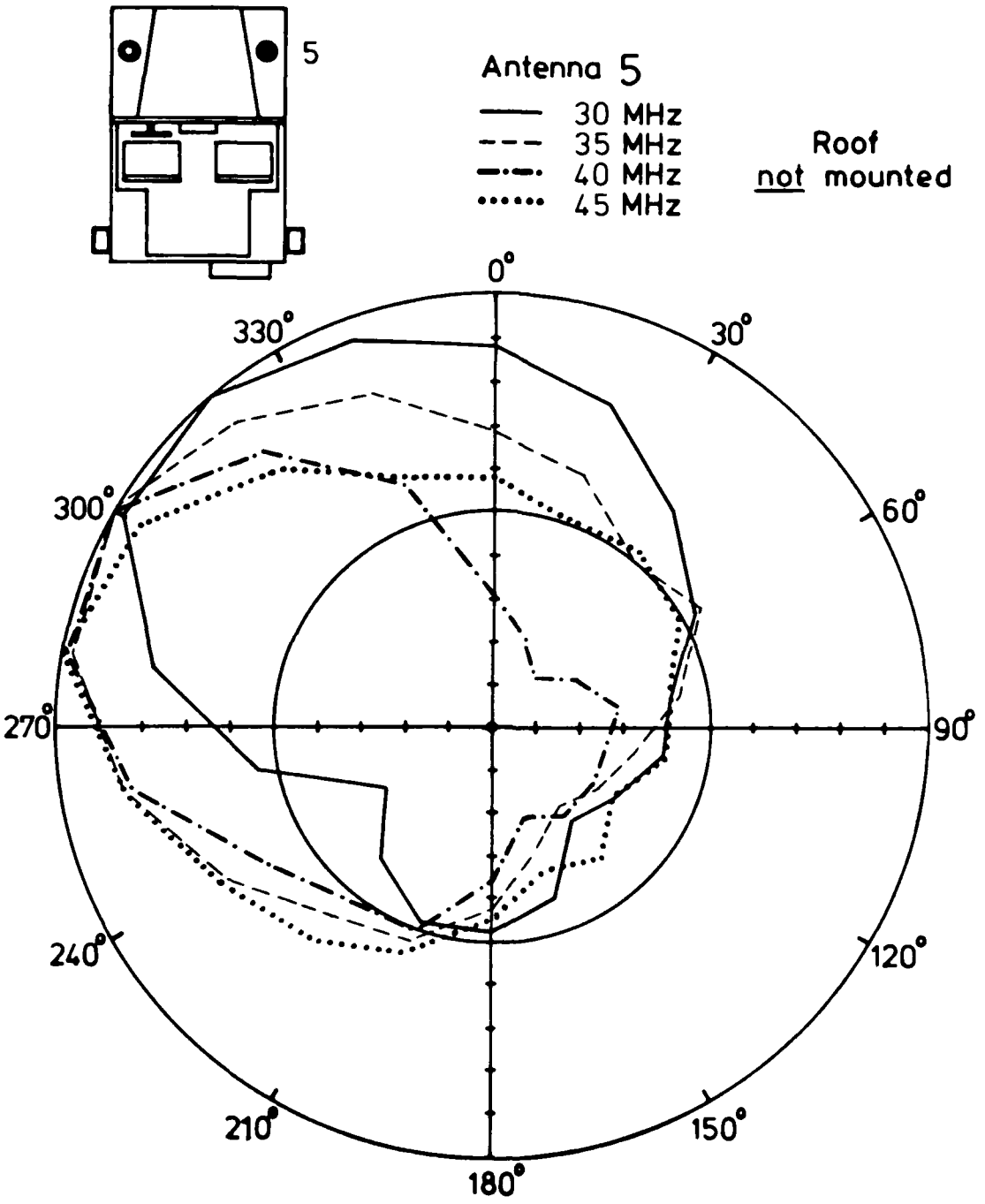

Fig. 30: Receiving pattern of antenna 5 for f = 30/35/40/45 MHz. Roof not mounted. (Antenna configuration as in Fig. 23)

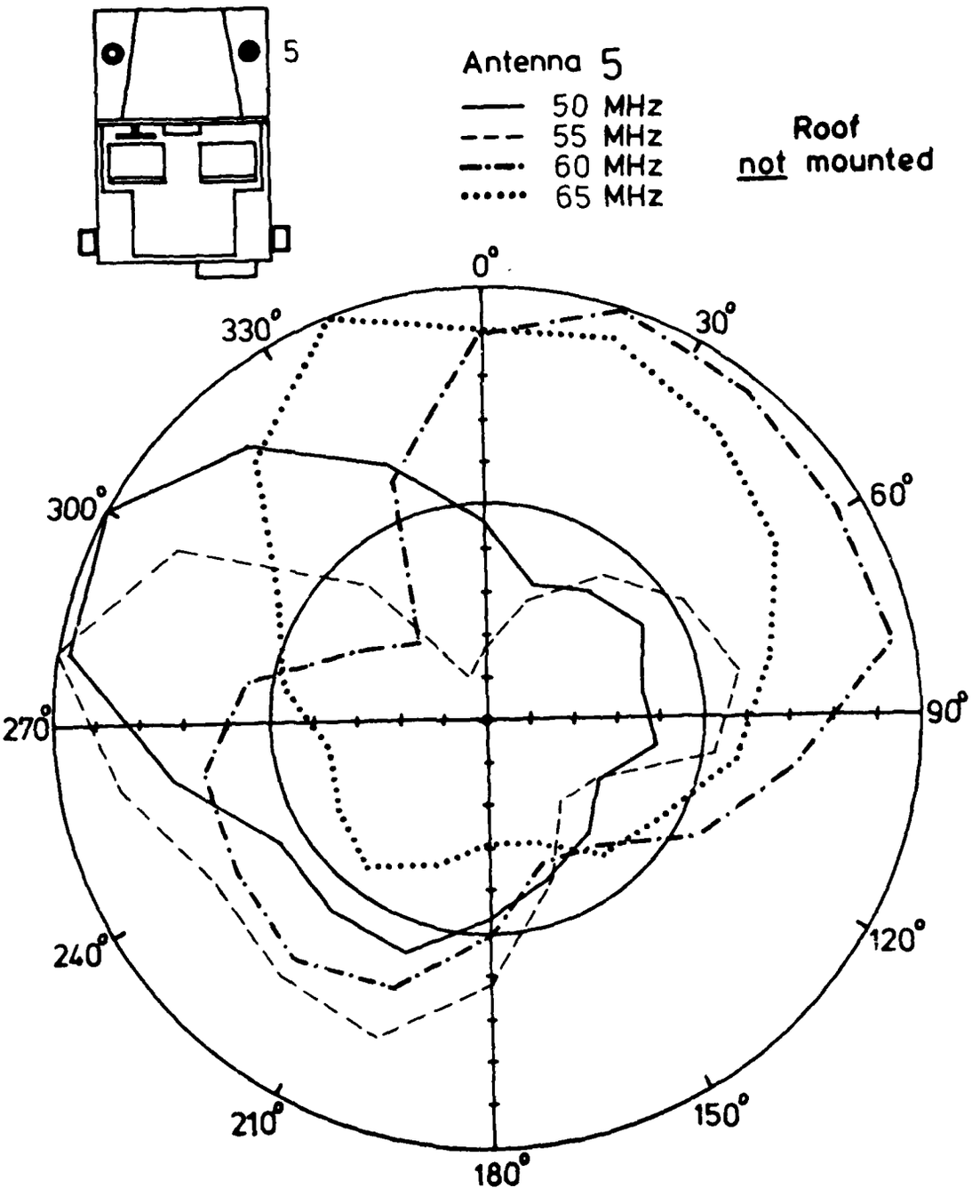

Fig. 31: Receiving pattern of antenna 5 for f = 50/55/60/65 MHz. Roof not mounted. (Antenna configuration as in Fig. 23)

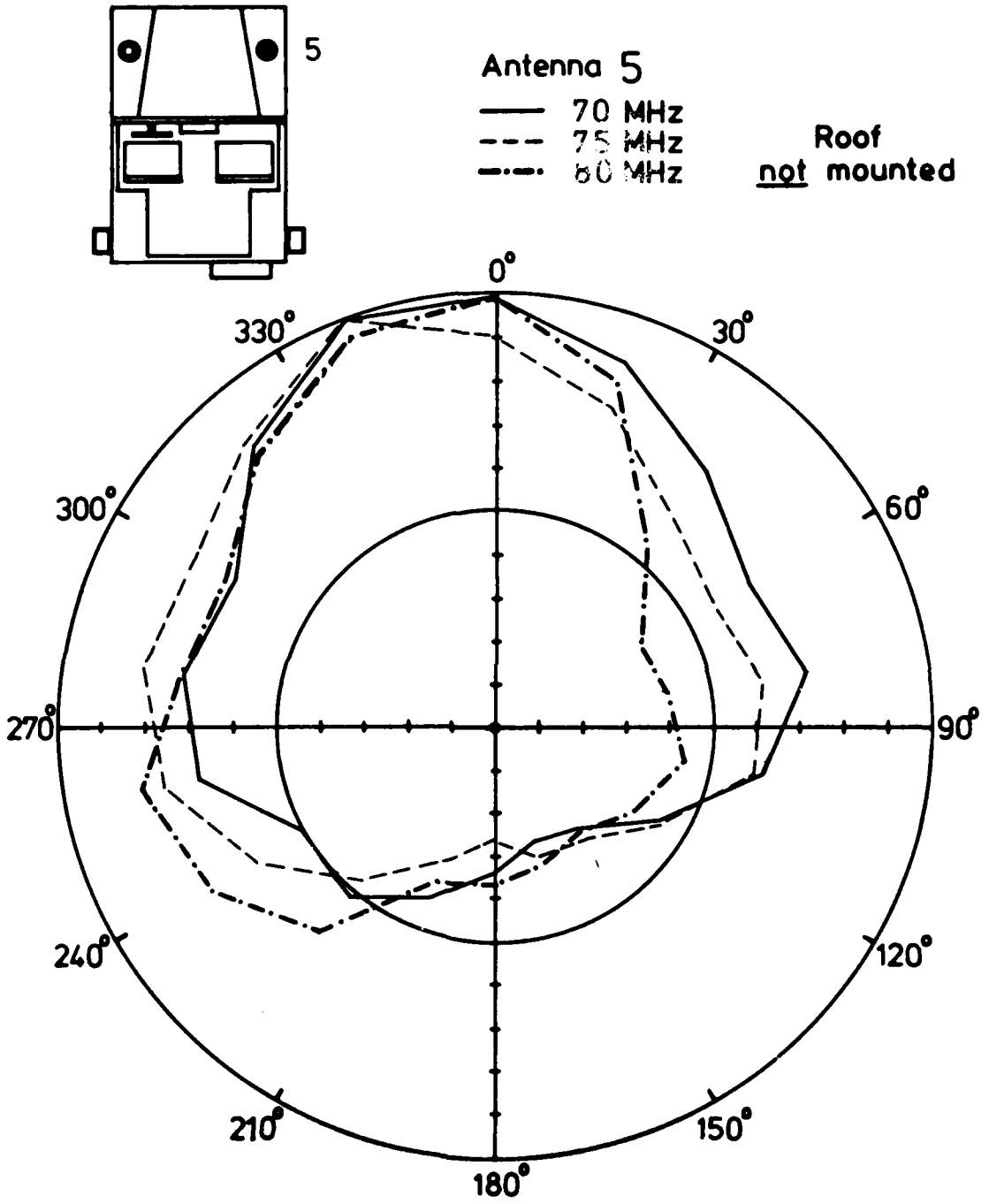

Fig. 32: Receiving pattern of antenna 5 for f = 70/75/80 MHz. Roof not mounted. (Antenna configuration as in Fig. 23)

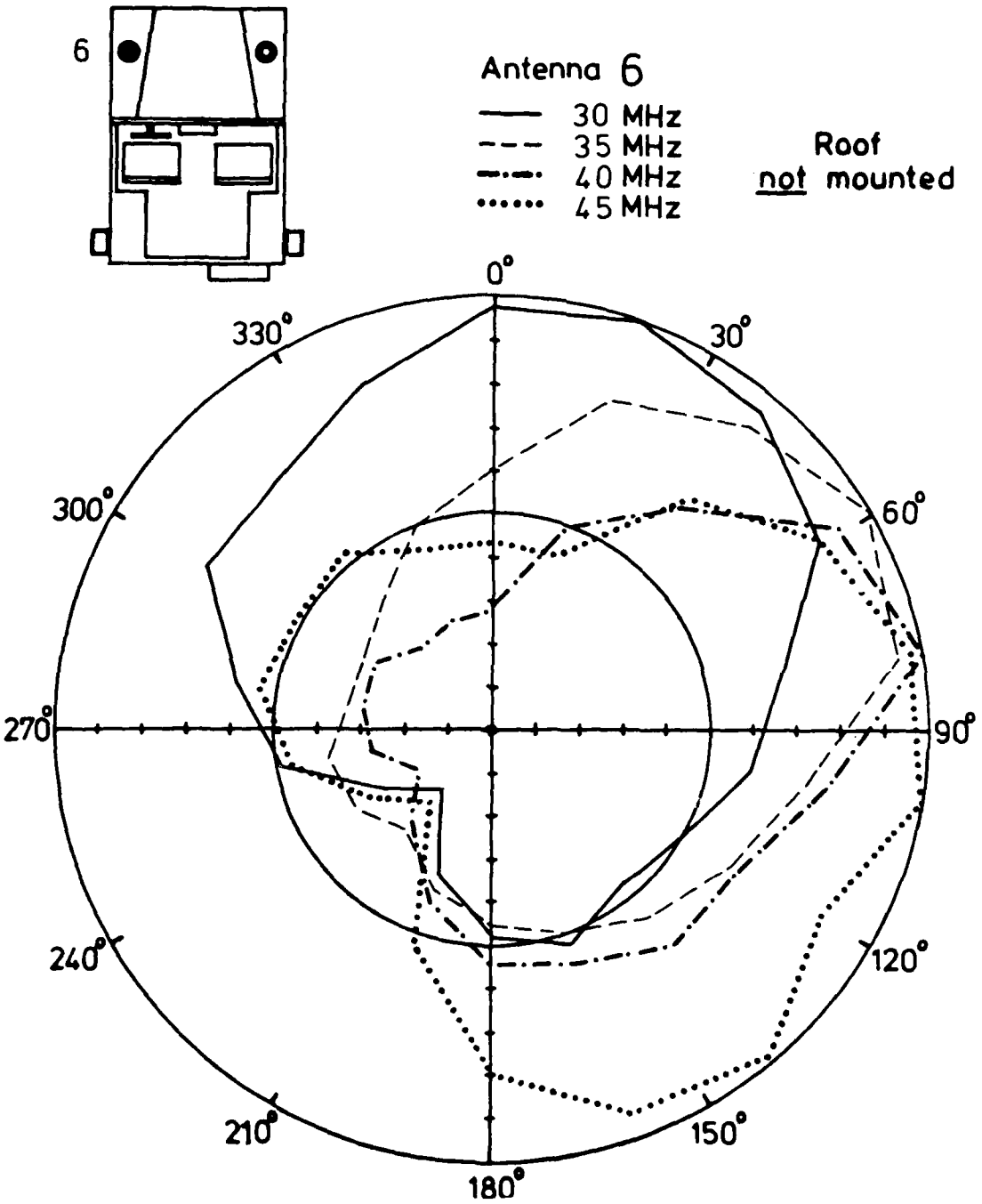

Fig. 33: Receiving pattern of antenna 6 for f = 30/35/40/45 MHz. Roof not mounted. (Antenna configuration as in Fig. 23)

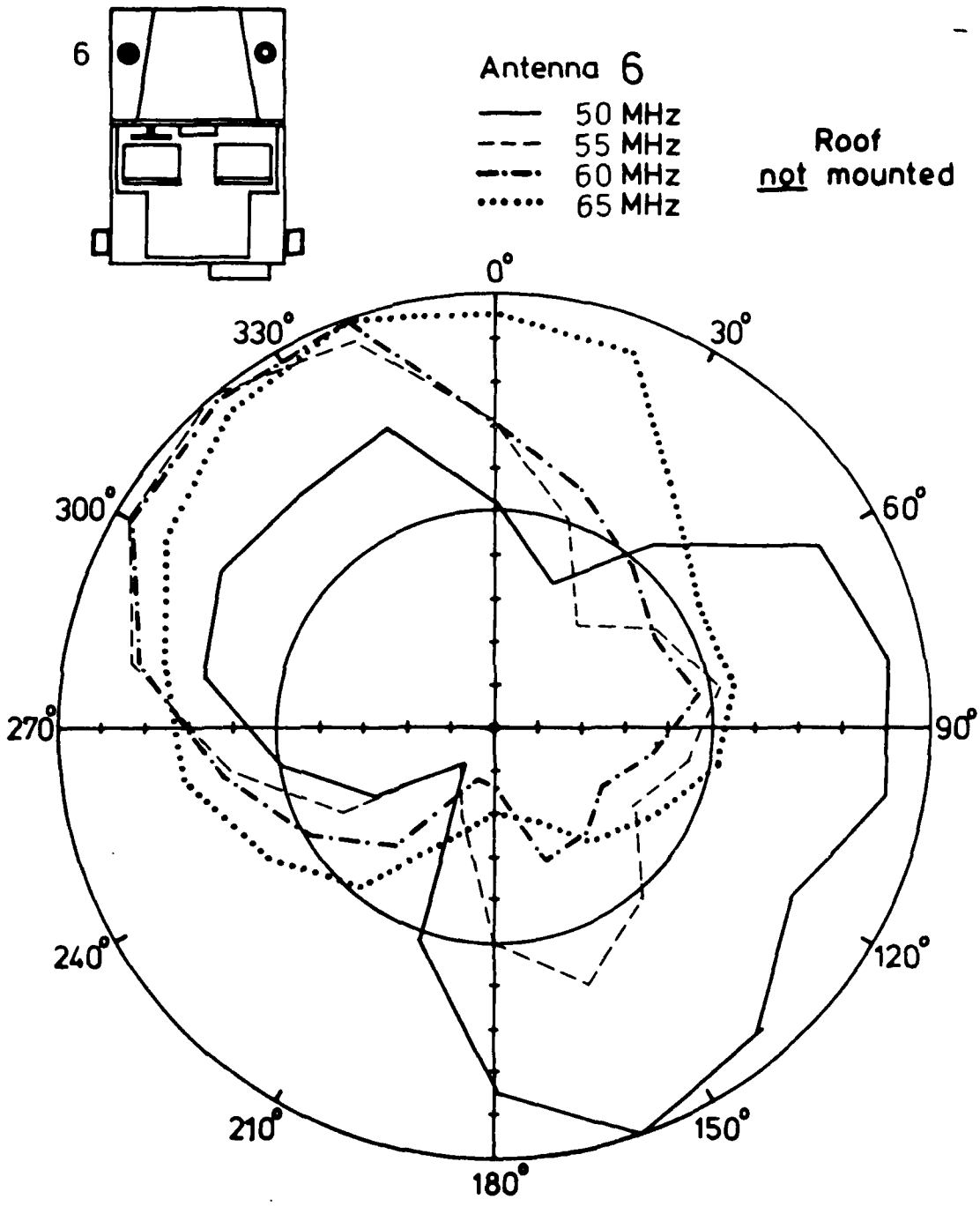

Fig. 34: Receiving pattern of antenna 6 for f = 50/55/60/65 MHz. Roof not mounted. (Antenna configuration as in Fig. 23)

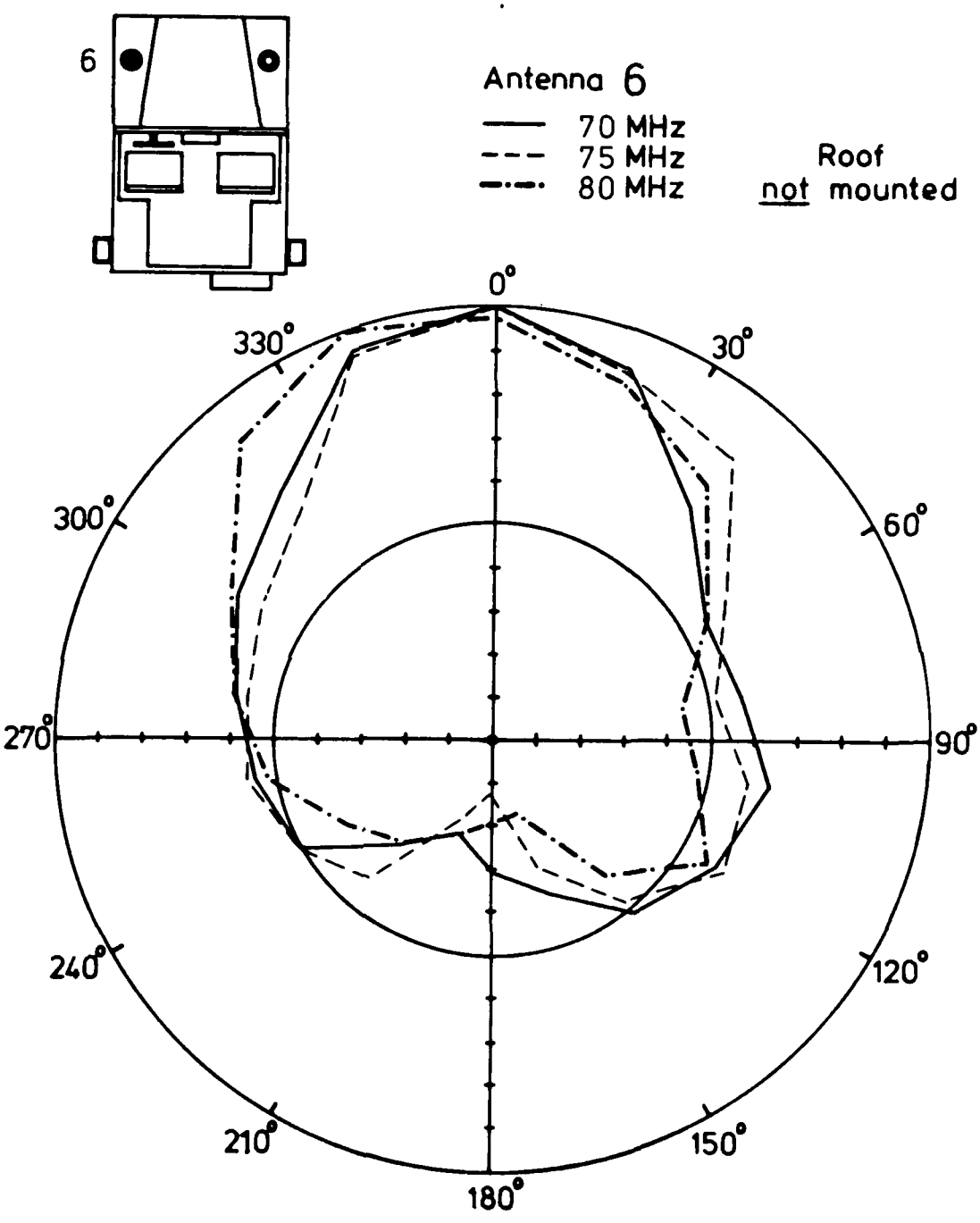

Fig. 35: Receiving pattern of antenna 6 for f = 70/75/80 MHz. Roof not mounted. (Antenna configuration as in Fig. 23)

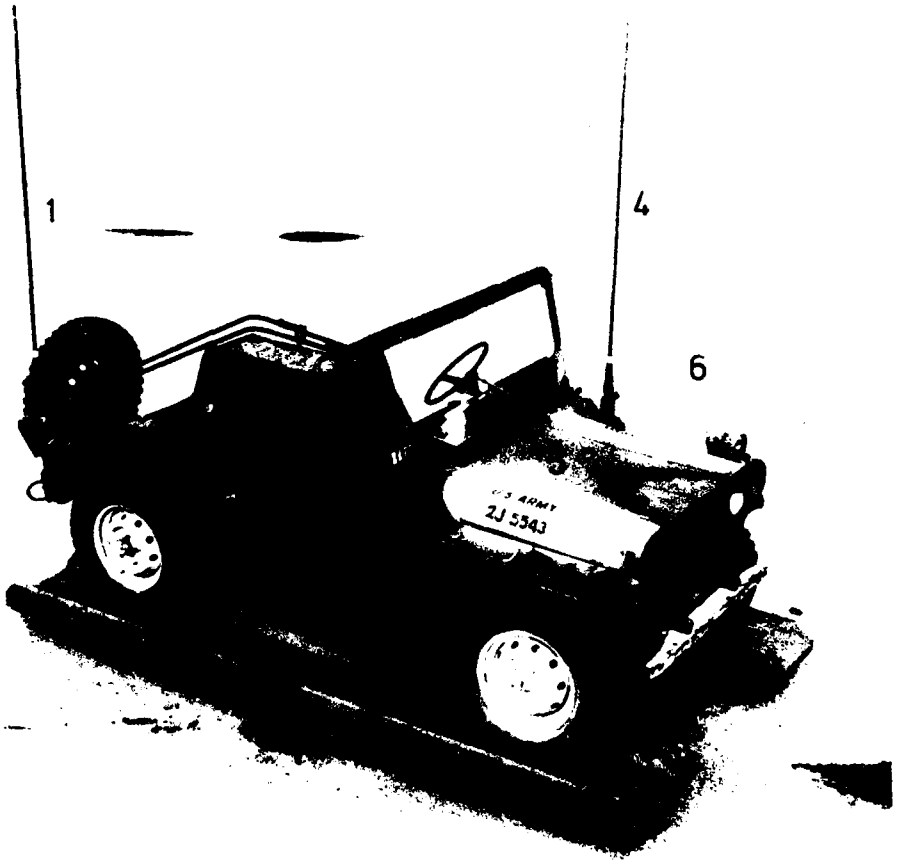

Fig. 36: Antenna configuration for Figs. 37 through 45.

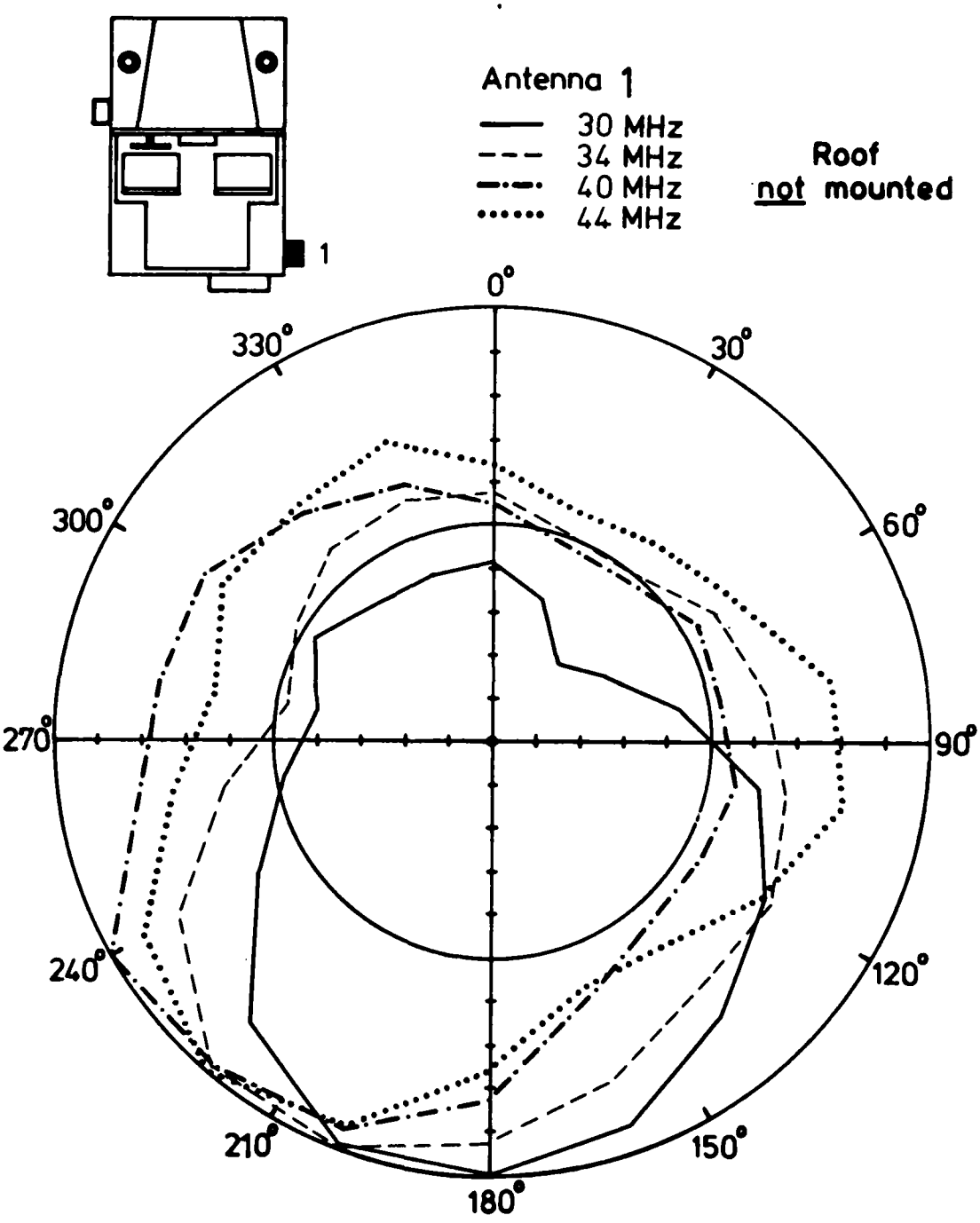

Fig. 37: Receiving pattern of antenna 1 for f = 30/34/40/44 MHz. Roof not mounted. (Antenna configuration as in Fig. 36)

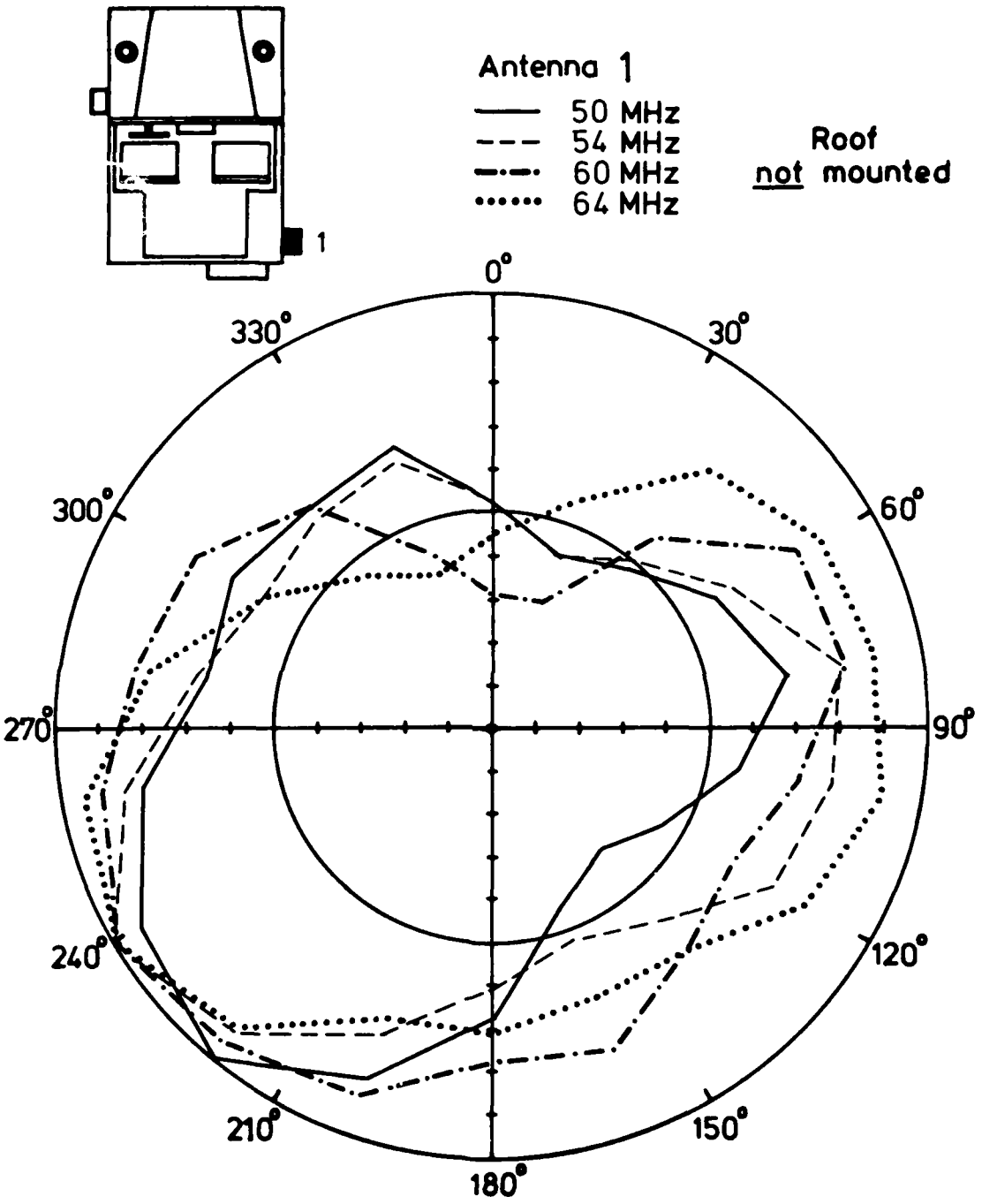

Fig. 38: Receiving pattern of antenna 1 for f = 50/54/60/64 MHz. Roof not mounted. (Antenna configuration as in Fig. 36)

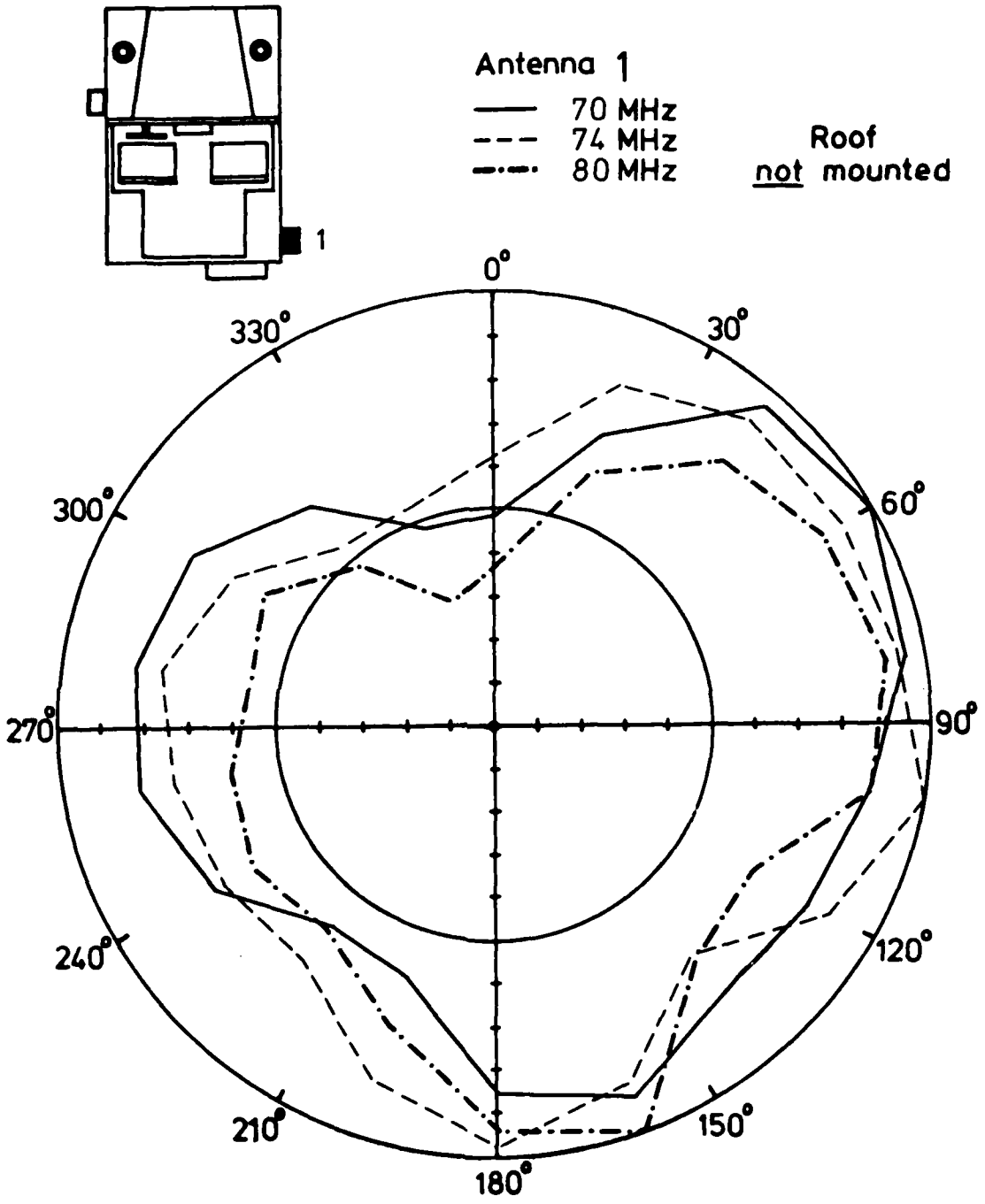

Fig. 39: Receiving pattern of antenna 1 for f = 70/74/80 MHz. Roof not mounted. (Antenna configuration as in Fig. 36)

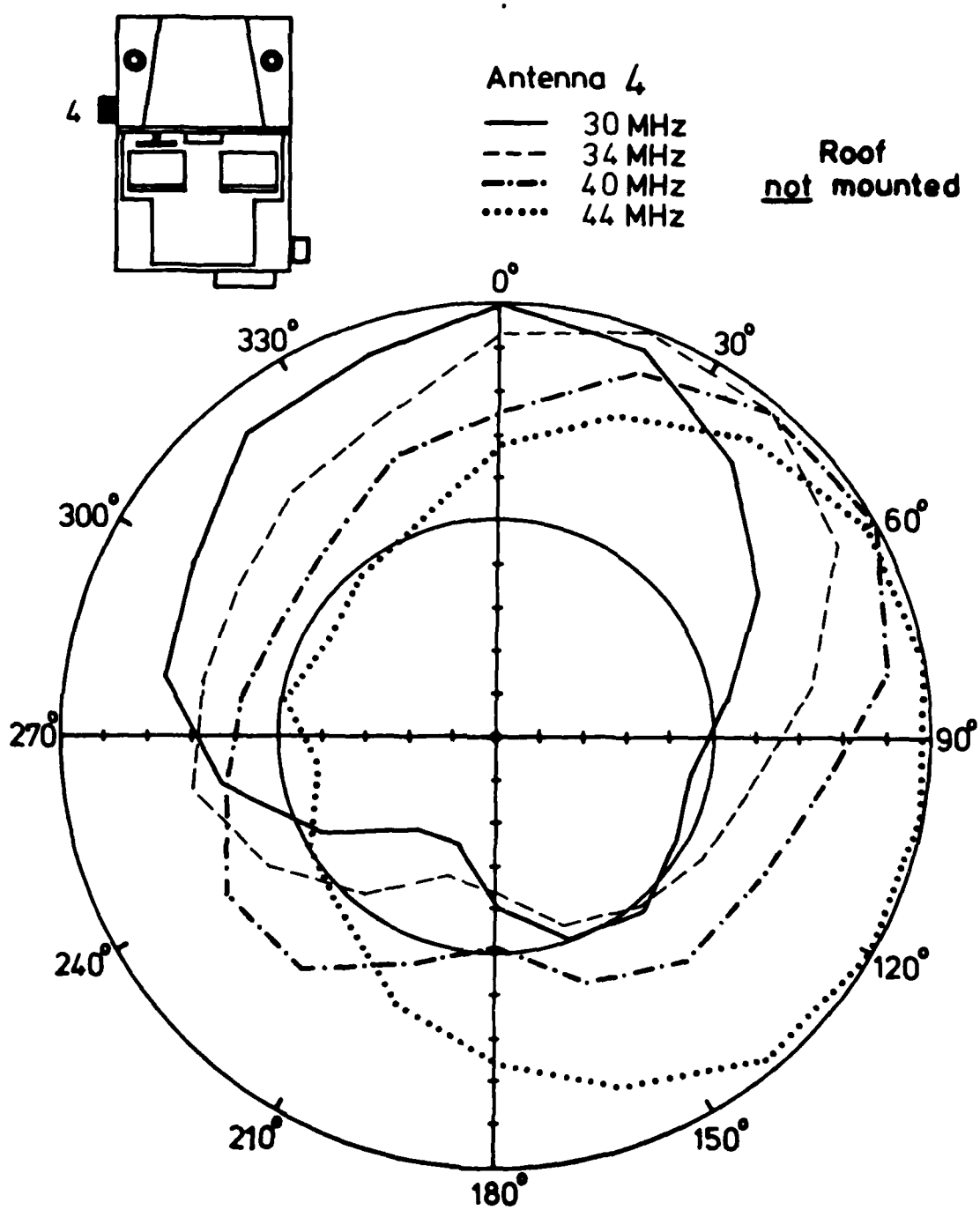

Fig. 40: Receiving pattern of antenna 4 for f = 30/34/40/44 MHz. Roof not mounted. (Antenna configuration as in Fig. 36)

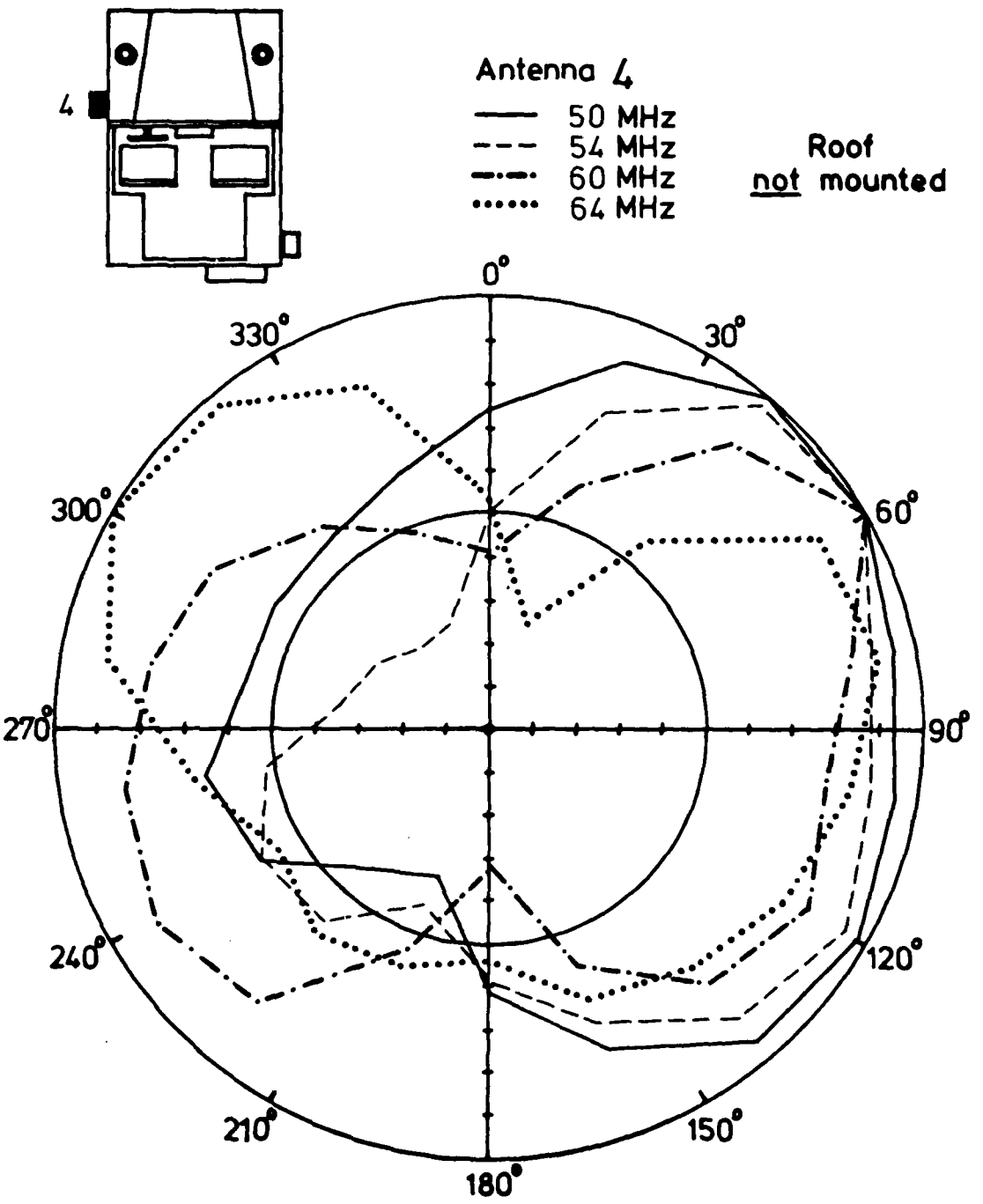

Fig. 41: Receiving pattern of antenna 4 for f = 50/54/60/64 MHz. Roof not mounted. (Antenna configuration as in Fig. 36)

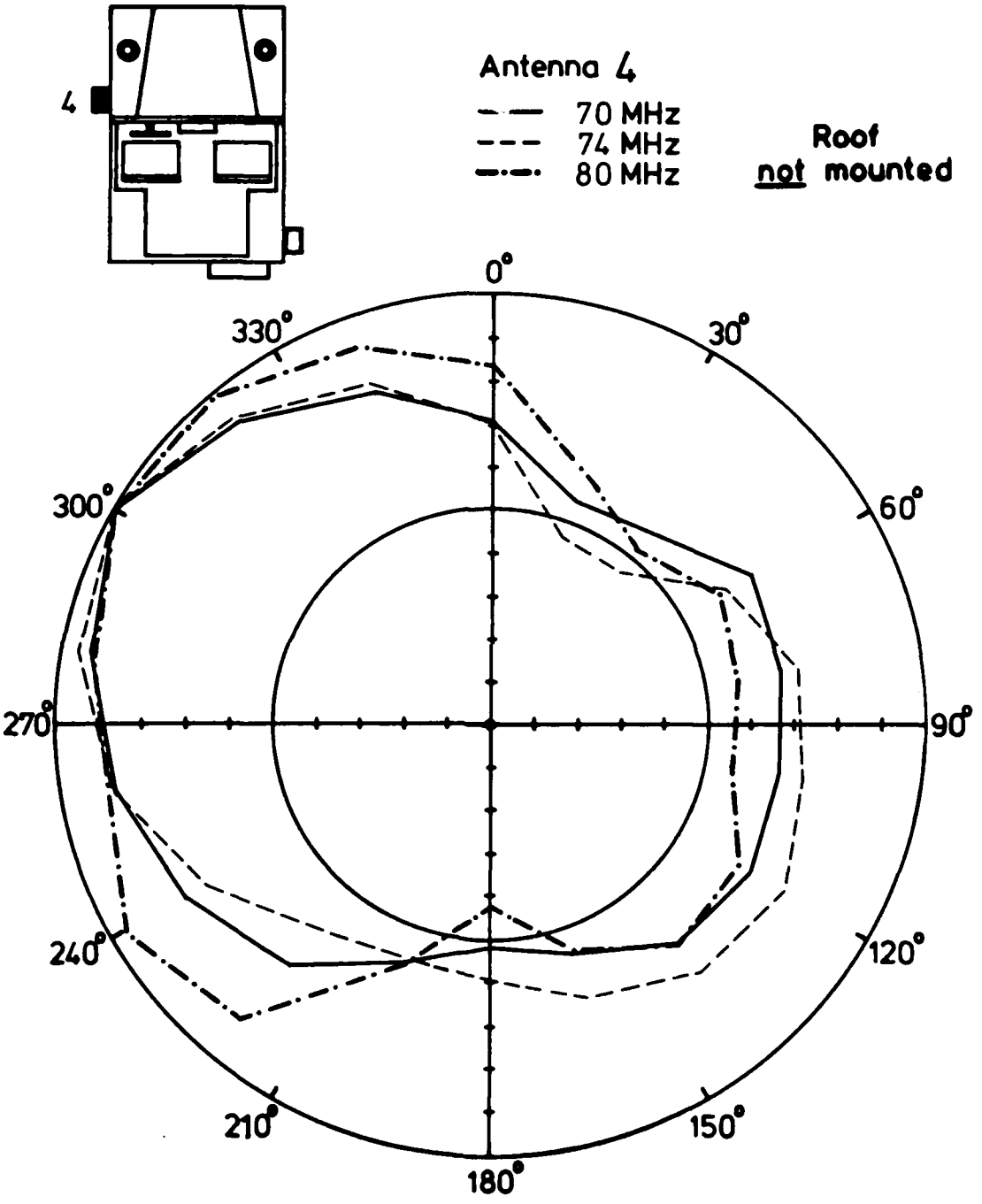

Fig. 42: Receiving pattern of antenna 4 for f = 70/74/80 MHz. Roof not mounted. (Antenna configuration as in Fig. 36)

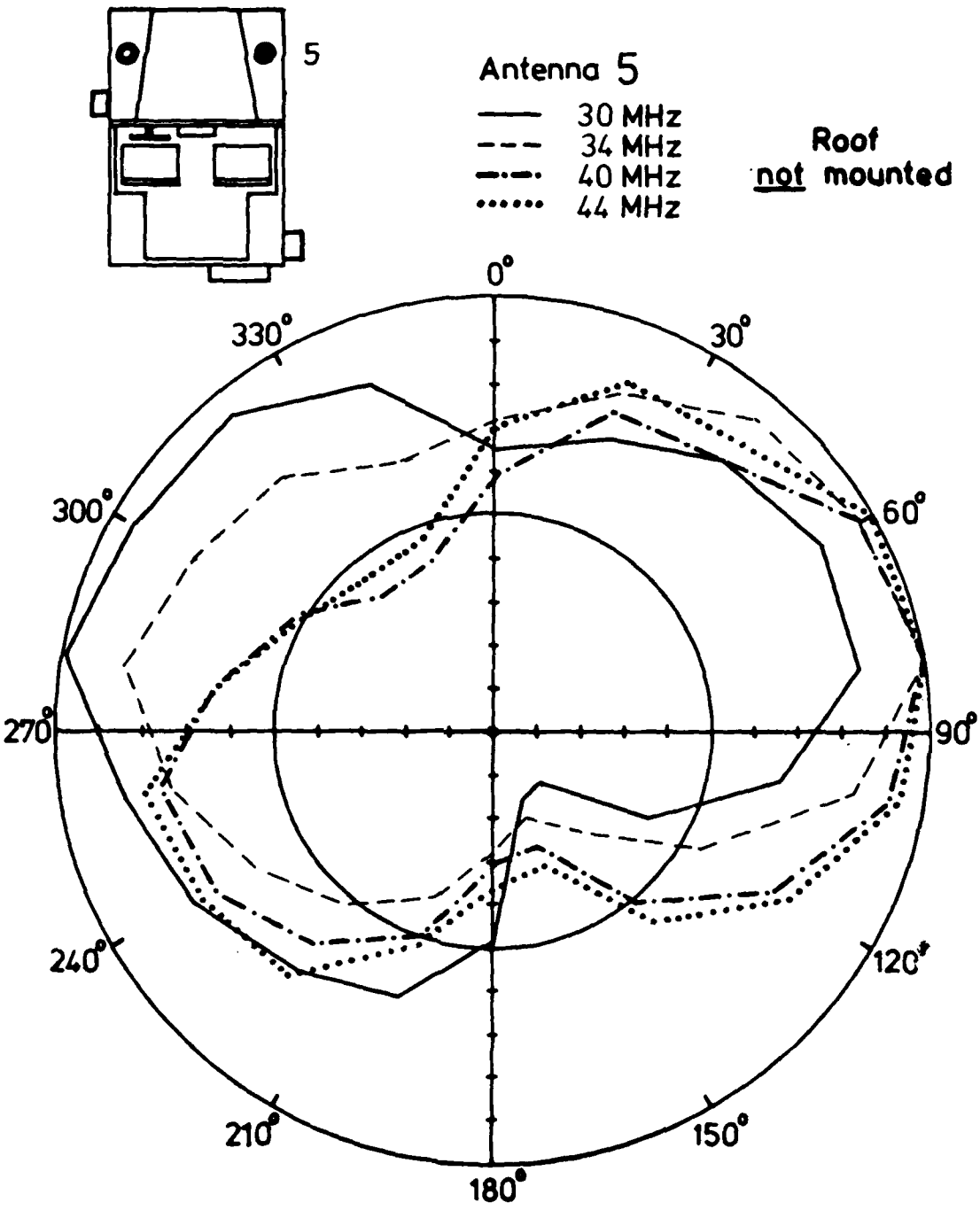

Fig. 43: Receiving pattern of antenna 5 for f = 30/34/40/45 MHz. Roof not mounted. (Antenna configuration as in Fig. 36)

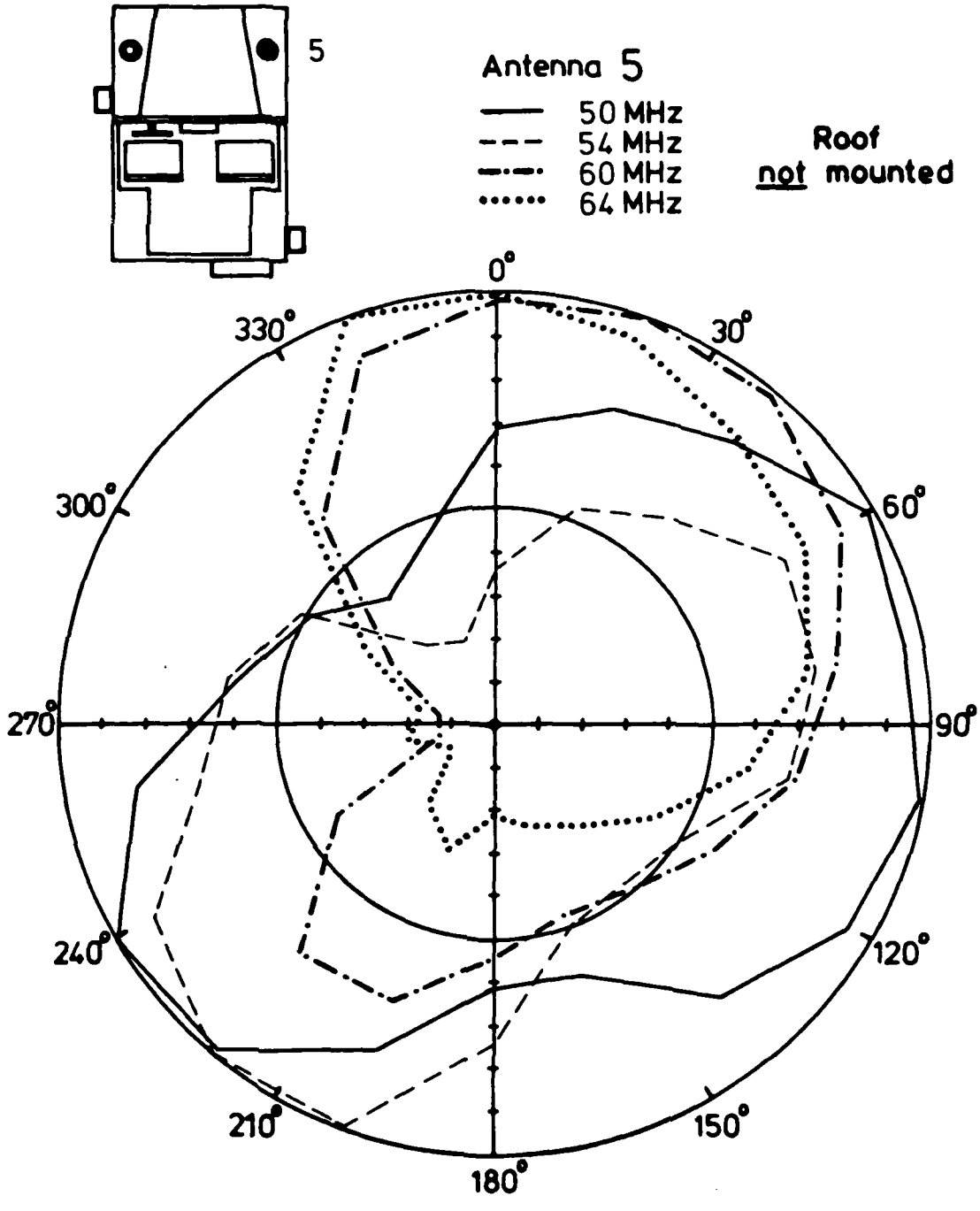

Fig. 44: Receiving pattern of antenna 5 for f = 50/54/60/64 MHz. Roof not mounted. (Antenna configuration as in Fig. 36)

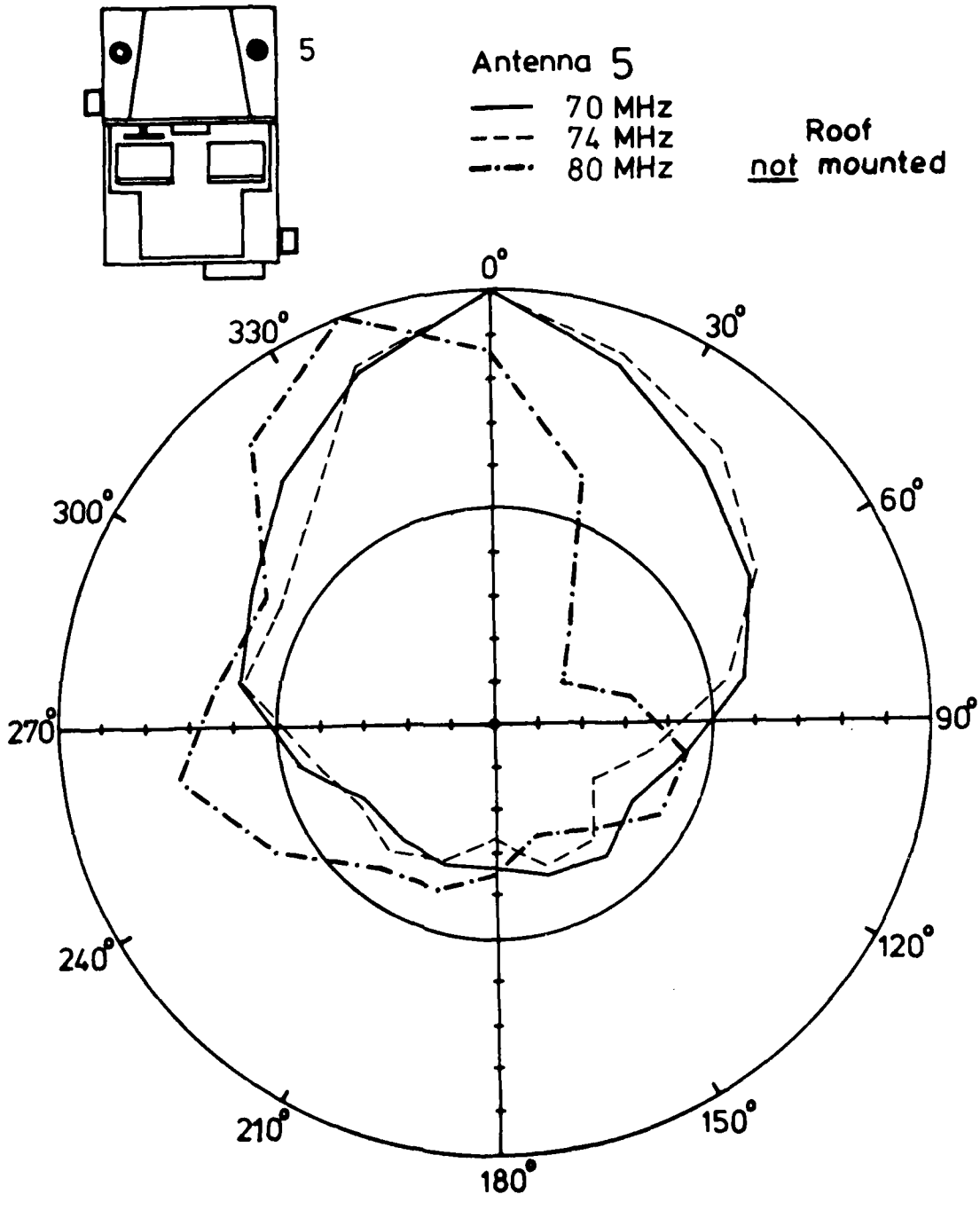

Fig. 45: Receiving pattern of antenna 5 for f = 70/74/80 MHz. Roof not mounted. (Antenna configuration as in Fig. 36)

b) Antenna configuration of Fig. 23:
   2 long passive rod antennas (right rear and left rear)
   2 short active antennas (right front and left front)
   The relating results are given in Figures 24 through 35.

c) Antenna configuration of Fig. 36:
   2 long passive rod antennas (right rear and left front)
   2 short active antennas (right front and left front)
   The relating results are given in Figures 37 through 45.

It should be observed that some results are gained with the standard roof mounted to point out the influence of the mounting rods on the antennas nearby.

Separate measurements have been performed with a single passive rod antenna with a length of 2.7 m, mounted on the right rear and bent down to the right front of the truck. These measurements are not related to diversity systems and should only show the pattern influence of the practice to bend down long rod antennas. The results are given in Appendix 2.

5.2 Discussion of the receiving patterns

As all antennas are of the vertical rod type exposed to a vertically polarized electromagnetic field one might assume to get omnidirectional reception in each case. The measurements show, however, that the uniform pattern of the rod is influenced by the car and the adjacent antennas.

At low frequencies there is already a variation of the pattern magnitudes of about 3 to 1 which can be seen from Figures 11 and 17 for the antennas 1 and 2, for instance.

The tall passive rod antennas obviously cause a "shadowing"

for the other antennas. This fact can be observed with the help of the following examples (refer to Fig. 3):

- Antenna 1 shows a minimum towards 0° through 60° (Fig. 11 to 13) if antenna 2 is mounted.
- Antenna 1 shows a minimum towards 210° through 270° (Fig. 24 to 26) if antenna 3 is mounted.
- Antenna 1 shows a minimum towards 270° through 0° (Fig. 37 to 39) if antenna 4 is mounted.

The same behaviour is shown from the patterns of the other antennas. There is always a minimum to be found which is directed about to the location of another mounted tall passive rod antenna. The pattern minimums are not directed exactly to the adjacent passive rod antenna. The reason is that the car itself has a major influence on the antenna patterns, too.

A comparison of Figures 11 through 13 to Figures 14 through 16 shows that there is only a small effect of a mounted roof to the receiving patterns. On this account, no further measurements are presented in this report concerning a mounted roof despite of the fact that all measurements have been performed with and without a mounted roof.

5.3 Normalized covariance function (correlation factor)

With the measured complex receiving patterns the correlation factors have been calculated for the various antenna combinations throughout the different antenna configurations. In contrast to the receiving patterns the covariance function is represented here on the base of the full measured frequency resolution, i.e. in general with frequency increments of 1 MHz.

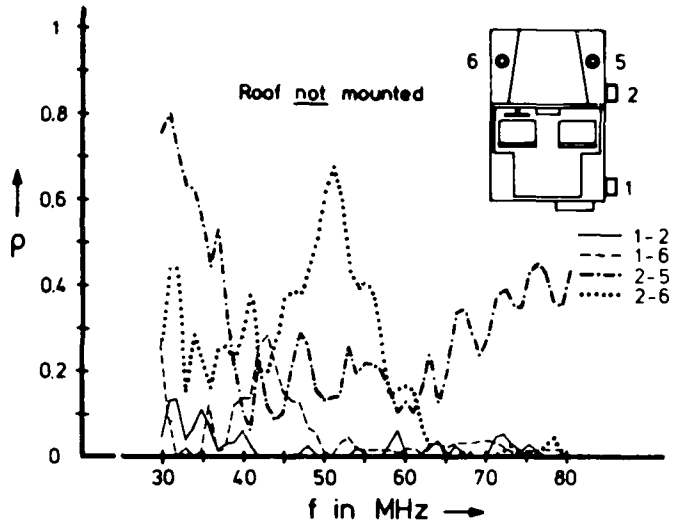

Fig. 46: Measured normalized covariance function (correlation factor) for various antenna combinations within the antenna configuration of Fig. 10. Roof not mounted.

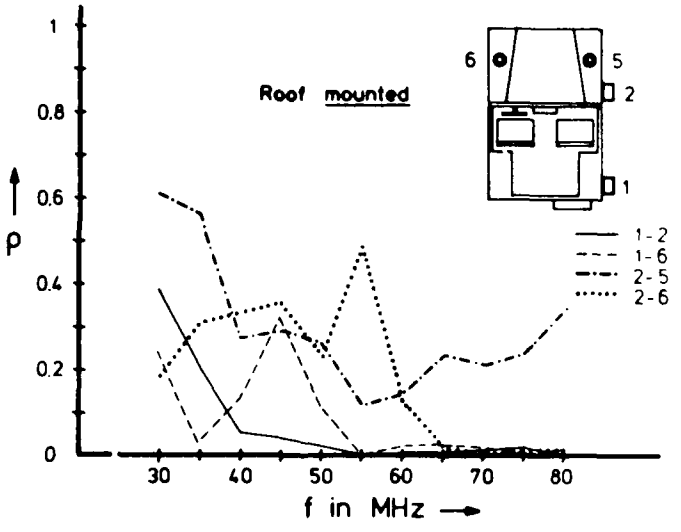

Fig. 47: Measured normalized covariance function (correlation factor) for various antenna combinations within the antenna configuration of Fig. 10. Roof mounted.

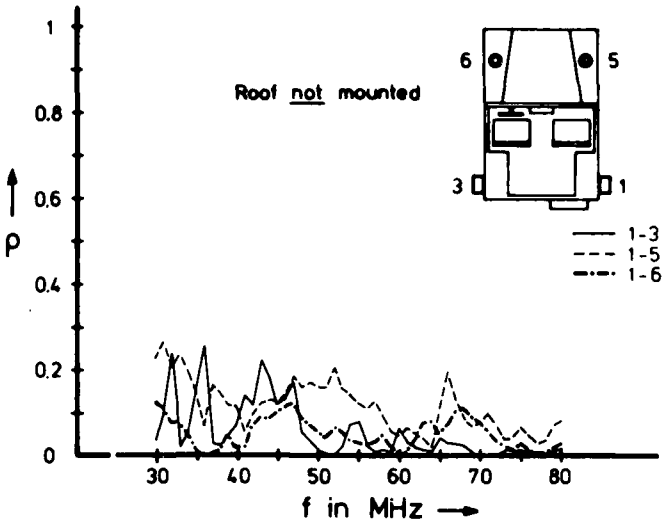

Fig. 48: Measured normalized covariance function (correlation factor) for various antenna combinations within the antenna configuration of Fig. 23. Roof not mounted.

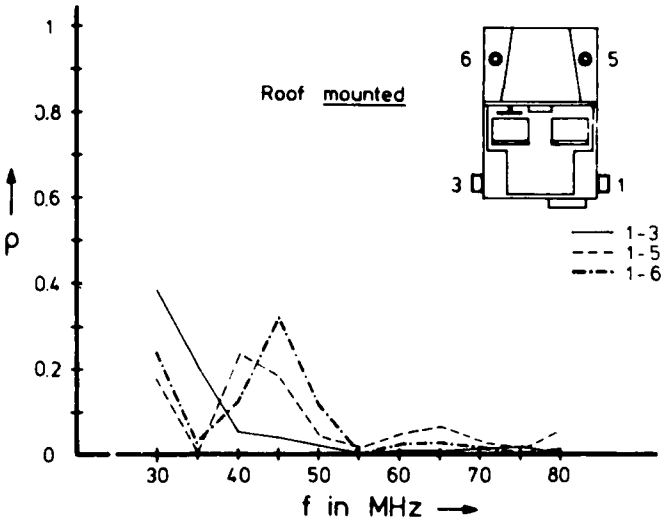

Fig. 49: Measured normalized covariance function (correlation factor) for various antenna combinations within the antenna configuration of Fig. 23. Roof mounted.

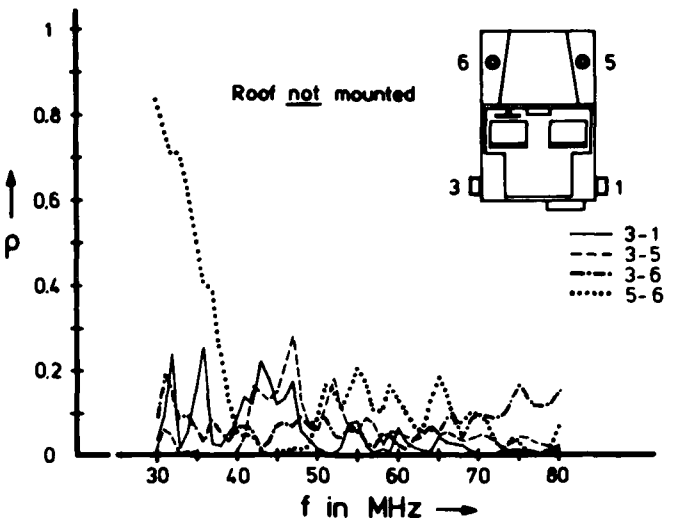

Fig. 50: Measured normalized covariance function (correlation factor) for various antenna combinations within the antenna configuration of Fig. 23. Roof not mounted.

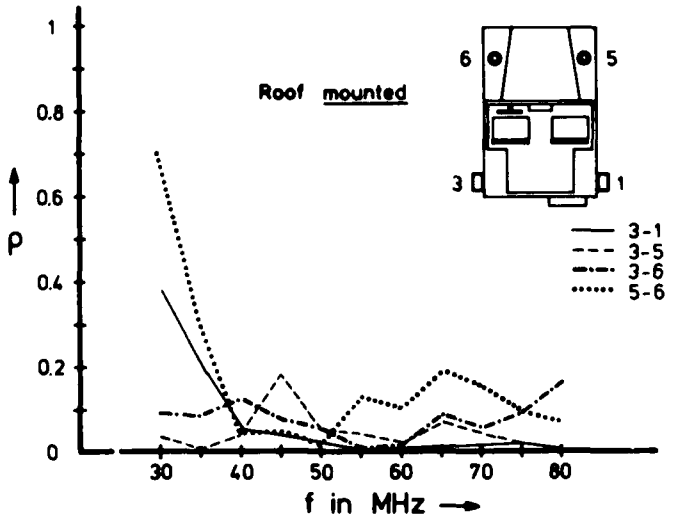

Fig. 51: Measured normalized covariance function (correlation factor) for various antenna combinations within the antenna configuration of Fig. 23. Roof mounted.

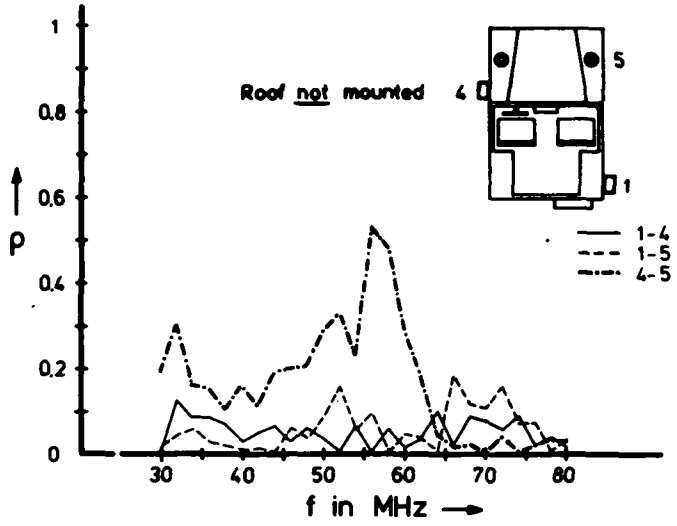

Fig. 52: Measured normalized covariance function (correlation factor) for various antenna combinations within the antenna configuration of Fig. 36. Roof not mounted.

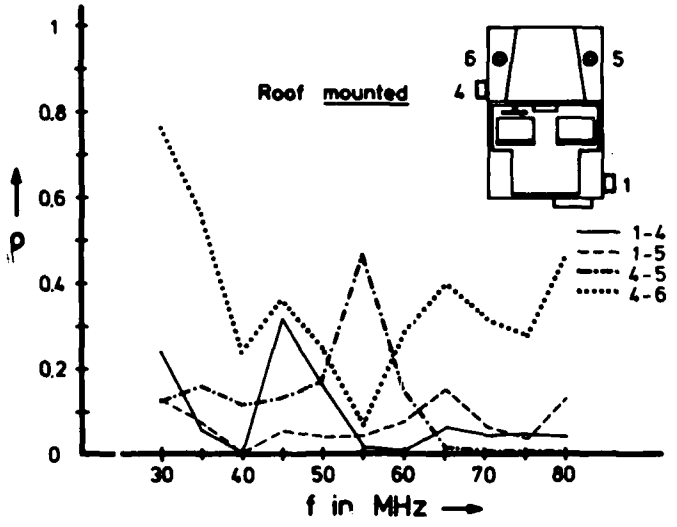

Fig. 53: Measured normalized covariance function (correlation factor) for various antenna combinations within the antenna configuration of Fig. 36. Roof mounted.

The results are given in

- Fig. 46 and 47 for the antenna configuration of Fig. 10 (roof mounted and not mounted, respectively)
- Fig. 48 through 51 for the antenna configuration of Fig. 23 (roof mounted and not mounted, respectively)
- Fig. 52 and 53 for the antenna configuration of Fig. 36 (roof mounted and not mounted, respectively).

6. Discussion and conclusions

In the following the measured correlation factors will be discussed on the basis of the Figs. 46 through 53.

a) Antenna configuration of Fig. 10;
without roof: Fig. 46,
with mounted roof: Fig. 47.

The differences between the cases of a mounted or a not mounted roof are not essential. There are are only slight differences between both cases at certain frequencies.

The correlation between the tall passive antennas (1-2) is below .15 all over the frequency band in the case of a not mounted roof and is below .15 for frequencies over 36 MHz in the case of a mounted roof.

The correlation between the right rear passive antenna (1) and the left front active antenna (6) is slightly higher, particularly in the frequency range of about 45 MHz. This should be due to resonance effects between the high-ohmic probing active antenna and the back-scattered field of antenna 1.

The antenna combinations 2-5 and 2-6 would not be expected for use in a diversity system. The results are more of theoretical interest. On the other hand, it can be seen that even the antenna combination 2-5 shows sufficient low correlation between 40 and 60 MHz. The antenna combination 2-6 shows a correlation peak at about 50 MHz in both cases, with and without mounted roof, respectively.

b) Antenna configuration of Fig. 23;
without roof: Figs. 48 and 50,
with mounted roof: Figs. 49 and 51.

The passive antennas (1 and 3)again show a low mutual correlation factor. The mounted roof increases this correlatien only around the lower end of the frequency range.

Also the combinations of one passive and one active antenna (1-5, 1-6, 3-5, and 3-6) show a low covariance. Each combination promises a sufficient diversity gain.

Only the combination of the two front mounted active antennas shows an increased correlation, which, of course, is restricted to low frequencies (< 40 MHz).

A comparison of symmetrical cases (1-5 against 3-6 and 1-6 against 3-5) shows sufficient accordance. The small differences can be caused by the the asymmetrical components of the structure of the truck.

c) Antenna configuration of Fig. 36;
without roof: Fig. 52,
with mounted roof: Fig. 53.

In this case of the diagonal mounting of the passive antennas (1-4) the influence of the mounted roof is a little bit higher than in the cases mentioned above. The higher influence, however, is restricted to the frequency range of 40 through 55 MHz. It is not essential as the correlation factor with a mounted roof remains below .3 in all cases.

The antenna combinations 4-5 and 5-6 are symmetrical cases to the antenna combinations 2-6 and 5-6 of Figs. 46 and 47. A comparison of the results shows a very good accordance of the basic frequency dependence and the absolute values of the correlation factor. A certain frequency shift (particularly of the correlation peak of the antenna combination 2-6 in Fig. 46 against the antenna combination 4-5 in Fig. 53) can be caused from the asymmetry of the car.

In general, the results mentioned above show that the dimensions of the 1/4 ton truck M 151 A2 are sufficient large to establish an effective space-diversity system. If two passive antennas are used each combination out of the possibilities: right-rear and left-rear, front and rear single-sided, front and rear across, respectively, can be used with only minor differences.

In the case of a combination of one passive and one active antenna the passive antenna should be located on the rear of the car and the active antenna on the front. The differences between a single sided mounting or an arrangement across are of no importance in this case.

The correlation factors measured with our method approach the correlation of the fast Rayleigh fading. With real test drives the results will always be a little bit higher. This is due to the fact that at real test drives the influence of a variable v.m.s. of the whole field never can be eliminated completely. For the calculation of the fade-reduction factor and the diversity gain, however, the correlation factor determined with our method is the more suited one to describe the behaviour in a pure Rayleigh field.

For a final decision for a diversity system it should be kept in mind that a second tall passive antenna increases the optical detectibility of the car. The use of an active antenna for the second diversity branch would avoid this disadvantage.

In this report only the correlation between the antennas has been considered. From [6] it is known that gain differences or differences in the S/N ratio within the diversity branches also influence the diversity gain or the fade-reduction factor. Our measurements have been performed using the standard matching box of the antenna type AS-2731/GRC. As we found out there were often differences of about 3 through 8 dB between the two passive antenna outputs after the matching boxes. This gain difference reduces the improvement of the expected diversity system more than the measured correlation of the output voltages.

It is recommended to extend the measurements described within this report on the absolute values of the effective height or effective areas of the antennas, respectively, to obtain the influence of the mounting location on this antenna parameters, too. To eliminate the influences of matching-box inaccuracies these measurements should be performed without the matching boxes.

The recommended measurements can also be performed with the measurement method described here. The pattern measurements would have to be related to a calibrated field-strength. This could be done with some improvements of our measuring equipment.

7. References cited

[1] Brennan, D.G.: Linear Diversity Combining Techniques; Proceedings of the IRE, Vol. 47, pp. 1075-1102, 1959

[2] Vigants, A.: Space-Diversity Performance as a Function of Antenna Separation; IEEE Trans. on Communications, Vol. Com-16, No. 6, pp. 831-836, 1968

[3] Henze, E.: Theoretische Untersuchungen über einige Diversity-Verfahren; Archiv Elektr. Übertragung, Vol. 11, pp. 183-184, 1957

[4] Schmelovsky, K.H.: Einfluß der Korrelation zwischen Empfangsfeldstärken bei Diversity-Empfang; Hochfrequenztechnik und Elektroakustik, Vol. 65, pp. 74-76, 1956

[5] Staras, H.: Diversity Reception with Correlated Signals; Journal of Applied Physics, Vol. 27, pp. 93-94, 1956

[6] Tschimpke, L.: Raumdiversity beim mobilen Empfang von Meterwellen in bebauten Gebieten; Doctor's Thesis, University of the Bundeswehr Munich, 1981

[7] Flachenecker, G.: MOBA-Receiving System with High Availability; Final Technical Report, European Research Office - United States Army, Grant Number DA-ERO-77-G-049, 1978

[8] Pierce, J.N. and Stein, S.: Multiple Diversity with Nonindependent Fading; Proc. IRE, 1960, pp. 89-104

[9] Clarke, R.H.: A Statistical Theory of Mobile Radio Reception, B.S.T.J., 1968, pp. 957-1000

[10] Gradschteyn, I.S. and Ryzhik, I.M.: Table of Integrals, Series, and Products; Academic Press, New York, 1965

Appendix 1

If in Eqn. (35) the antennas are assumed to be omnidirectional (C_i = const, C_j = const) the calculated correlation factor ρ_{Sij} equals the autocorrelation function of the received field component, in our case the electrical field (see Eqns. (3) and (4)). Furthermore, if $N \to \infty$ is assumed the resulting field shows a Rayleigh distribution of the magnitude of the electrical field component. In this case the autocorrelation function is known to be

$$\rho_E = J_o^2 (2\pi d/\lambda_o) \tag{36}$$

where J_o is the Bessel function of zero order and d is the distance of the probing points.

With the above assumptions Eqn. (35) can be written

$$\rho_{Sij} = \lim_{N \to \infty} \frac{\left[\sum_{n=1}^{N} \cos(\varphi_i - \varphi_j)\right]^2 + \left[\sum_{n=1}^{N} \sin(\varphi_i - \varphi_j)\right]^2}{\left[\sum_{n=1}^{N} 1\right] \cdot \left[\sum_{n=1}^{N} 1\right]}$$

with the fact in mind that φ_i and φ_j are phase angles of the antenna-output voltages in response to a wave with an angle of incidence α_n. With the help of Fig. 54 it can be shown that the phase difference $\varphi_i - \varphi_j$ is

$$\varphi_i - \varphi_j = (2\pi d/\lambda_o) \cdot \cos(\alpha_n - \gamma) \tag{37}$$

where γ is the angle of the line between antenna i and antenna j related to the x-direction. Hence,

$$\cos(\varphi_i - \varphi_j) = \cos[(2\pi d/\lambda_o)\cos(\alpha_n - \gamma)] \tag{38}$$

$$\sin(\varphi_i - \varphi_j) = \sin[(2\pi d/\lambda_o)\cos(\alpha_n - \gamma)] \tag{39}$$

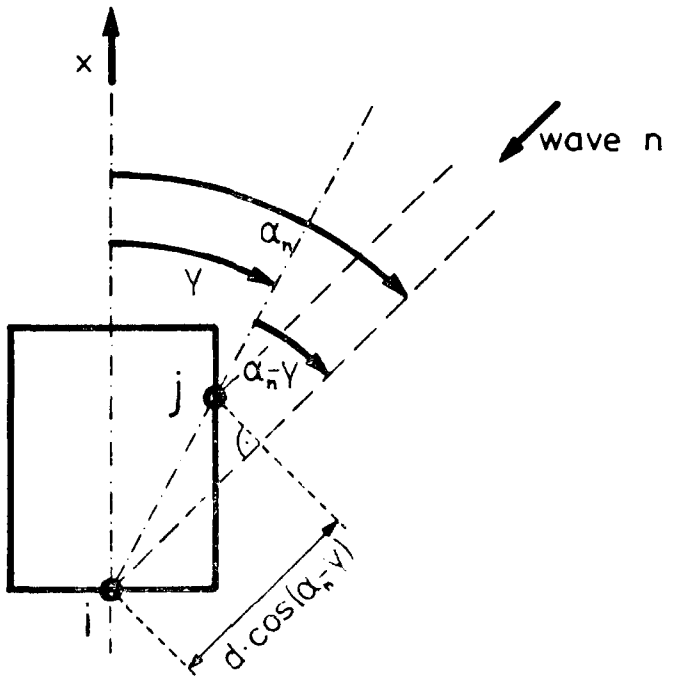

Fig. 54: Schematic diagram of two antennas i and j exposed to a wave with an angle of incidence α_n.

and the correlation factor can be written by replacing the limes of the sums by integrals

$$\rho_{Sij} = \frac{\left\{\frac{1}{2\pi}\int_0^{2\pi} \cos[2\pi \frac{d}{\lambda_o}\cos(\alpha_n-\gamma)]d\alpha\right\}^2+\left\{\frac{1}{2\pi}\int_0^{2\pi} \sin[2\pi \frac{d}{\lambda_o}\cos(\alpha_n-\gamma)]\right\}^2}{\frac{1}{2\pi}\int_0^{2\pi} d\alpha \cdot \frac{1}{2\pi}\int_0^{2\pi} d\alpha}$$

$$= \left\{\frac{1}{2\pi}\int_0^{2\pi} \cos[2\pi \frac{d}{\lambda_o}\cos(\alpha_n-\gamma)d\alpha\right\}^2+ \left\{\frac{1}{2\pi}\int_0^{2\pi} \sin[2\pi \frac{d}{\lambda_o}\cos(\alpha_n-\gamma)]\right\}^2 \quad (40)$$

It is known [10] that

$$\int_0^{2\pi} \cos[z \cdot \cos(x-\gamma)]dx = 2\pi J_o(z) \quad (41)$$

and

$$\int_0^{2\pi} \sin[z \cdot \cos(x-\gamma)]dx = 0 \quad (42)$$

Hence,

$$\rho_{Sij} = J_o^2(2\pi d/\lambda_o)$$

q.e.d.

Appendix 2

Receiving patterns of a bent-down rod antenna.

In some cases the older 2.7 m passive rod antenna is still in use. It is common practice to bend this antenna down if the extreme height of the antenna impedes the handling of the car. The bending-down of the antenna, on the other hand, strongly influences the pattern of the antenna.

The capabilities of the turntable have been used to measure the patterns of a bent-down antenna. Fig. 55 is a sketch of the mounting and Figures 56 through 58 show the measuring results.

AD-A107 114 BUNDESWEHR MUNICH UNIV (GERMANY F R) INST FOR HIGH-F--ETC F/G 9/5
CROSS CORRELATION IN A SPACE-DIVERSITY SYSTEM ON A MILITARY VEH--ETC(U)
AUG 81 G FLACHENECKER, L TSCHIMPKE DAJA37-80-C-0347

UNCLASSIFIED NL

2 ↓ 2

END
DATE FILMED
12-81
DTIC

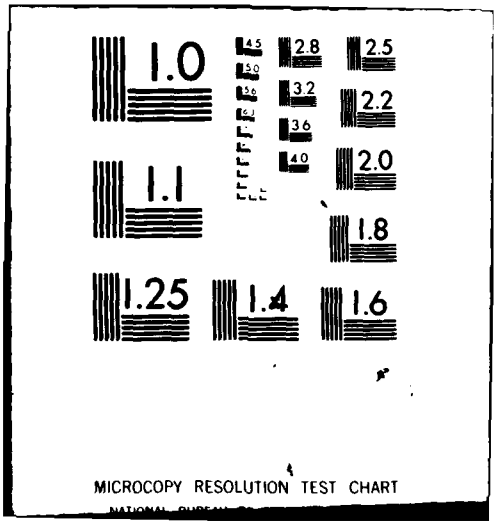
1.0
1.1
1.25
1.4
1.6
1.8
2.0
2.2
2.5
2.8
3.2
3.6
4.0
4.5
5.0
5.6
6.3
MICROCOPY RESOLUTION TEST CHART

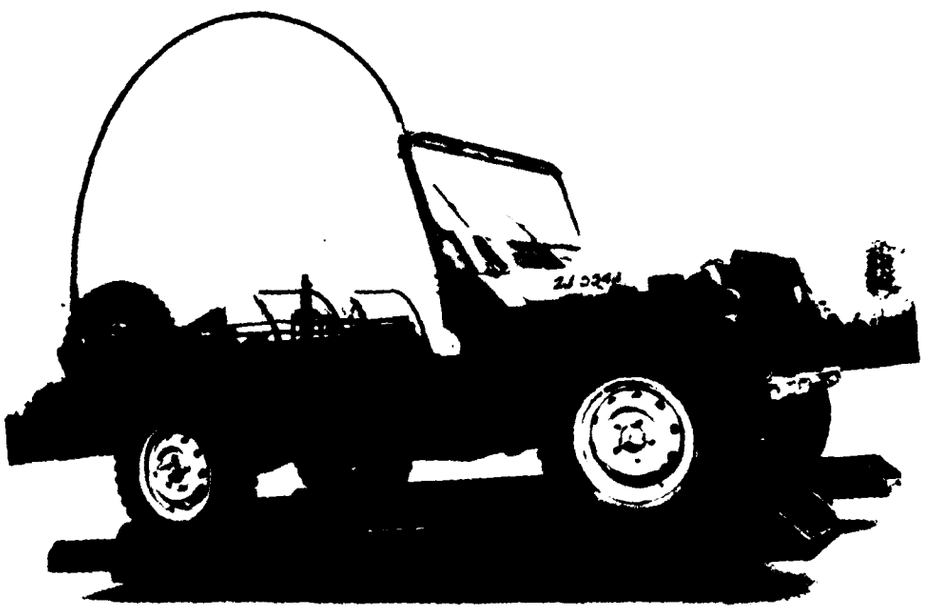

Fig. 55: Sketch of a bent-down rod antenna of 2.7 m length.

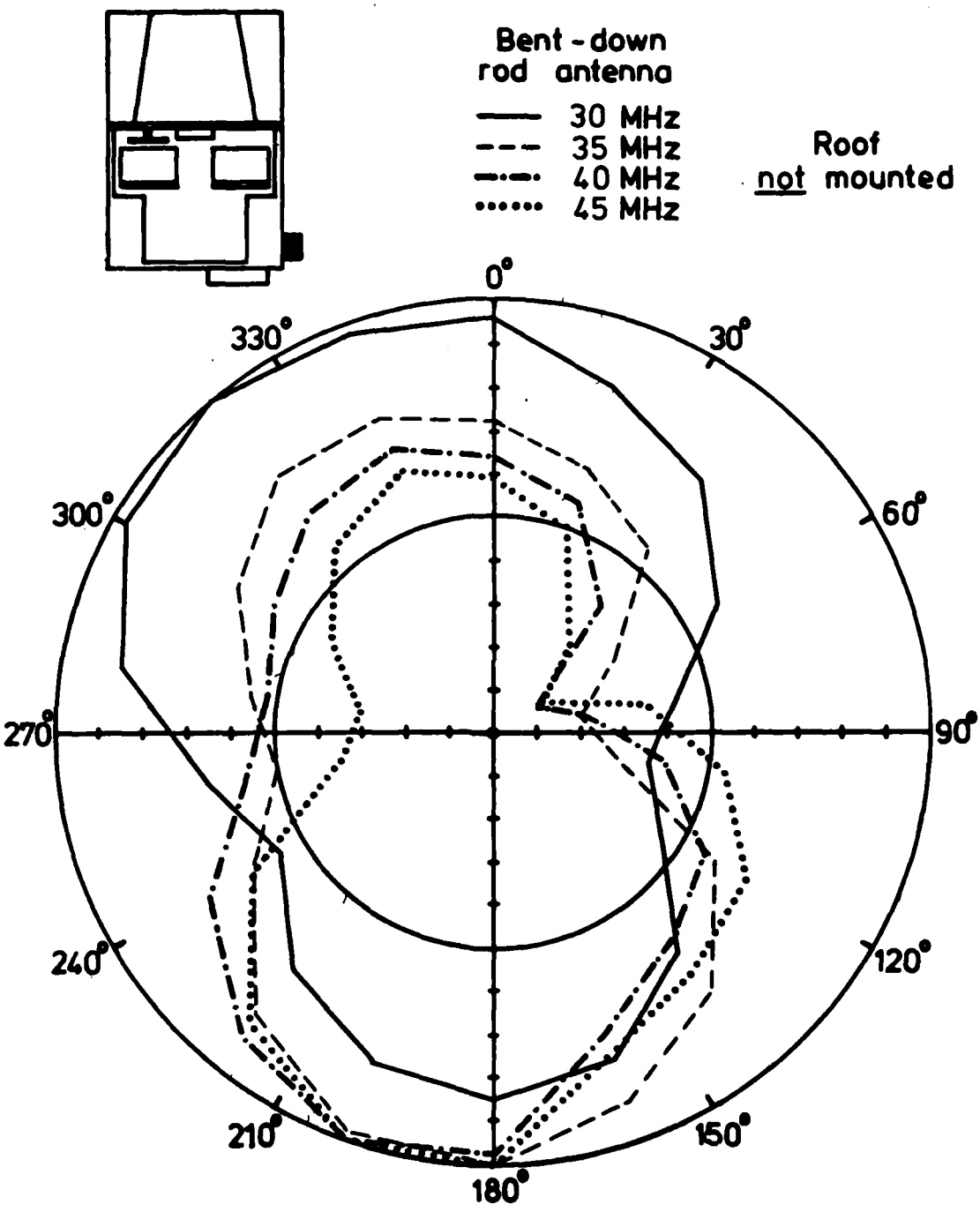

Fig. 56: Receiving pattern of a bent-down rod antenna.
f = 30/35/40/45 MHz.

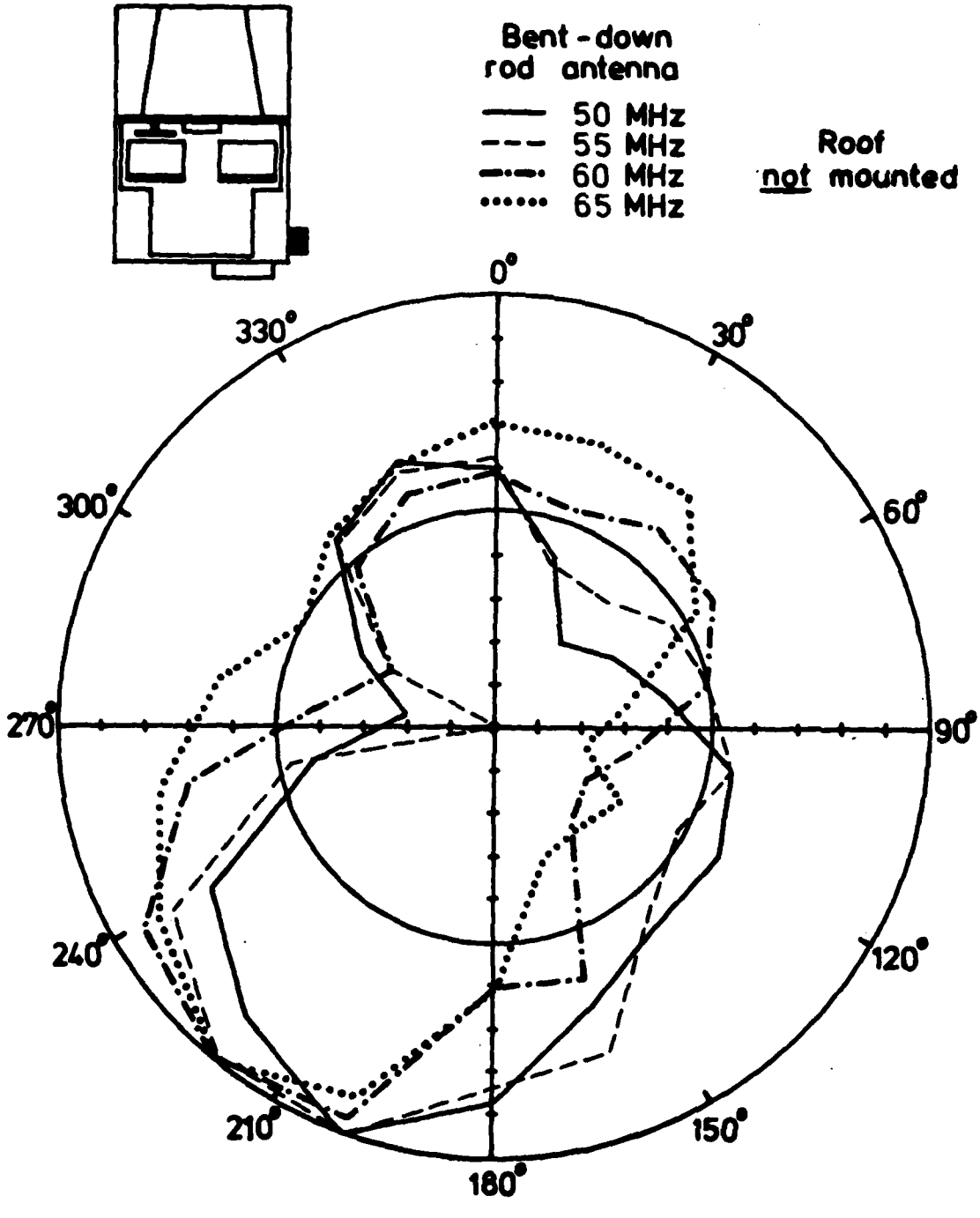

Fig. 57: Receiving pattern of a bent-down rod antenna.
f = 50/55/60/65 MHz.

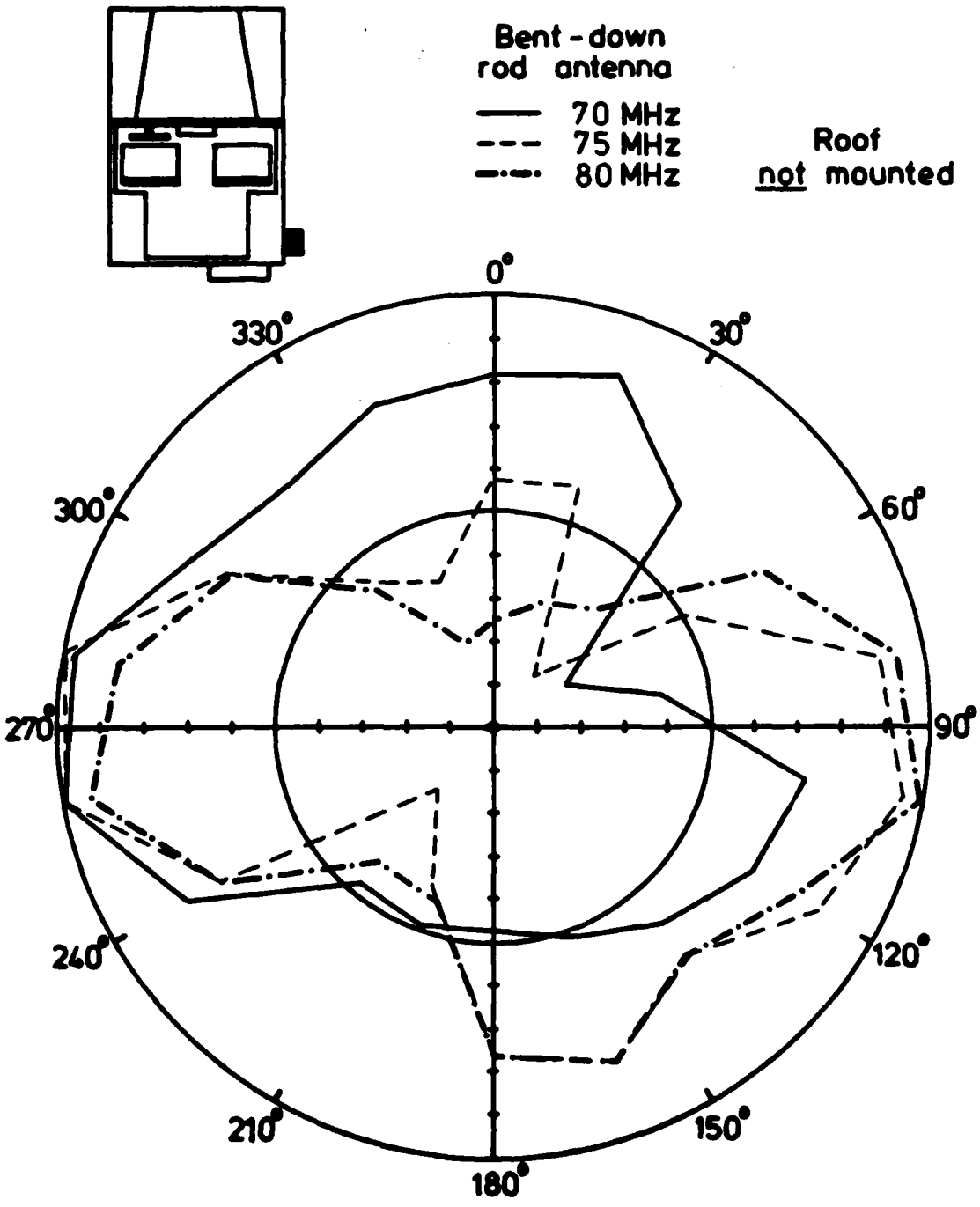

Fig. 58: Receiving pattern of a bent-down rod antenna.
f = 70/75/80 MHz.

Appendix 3

Normalized covariance function (correlation factor) of small active rod antennas at higher frequencies.

As a prospect to higher frequencies the correlation measurements of the two short rod antennas have been extended to the frequency range 80 through 300 MHz. Since the frequency range of the tall passive rod antennas used throughout this research work is restricted to 30 through 80 MHz, these antennas have not been considered during these measurements. To avoid interference effects caused from the passive antennas they have been removed from the truck during these measurements.

Fig. 59 gives a sketch of the antenna mounting and Fig. 60 the results for the correlation factor. The frequency increment has been chosen to be 5 MHz.

The correlation factors prove to be below .3 for this frequency range. It promises advantageous use of a diversity system, too, as already could be extrapolated from the measurements within the lower VHF-range.

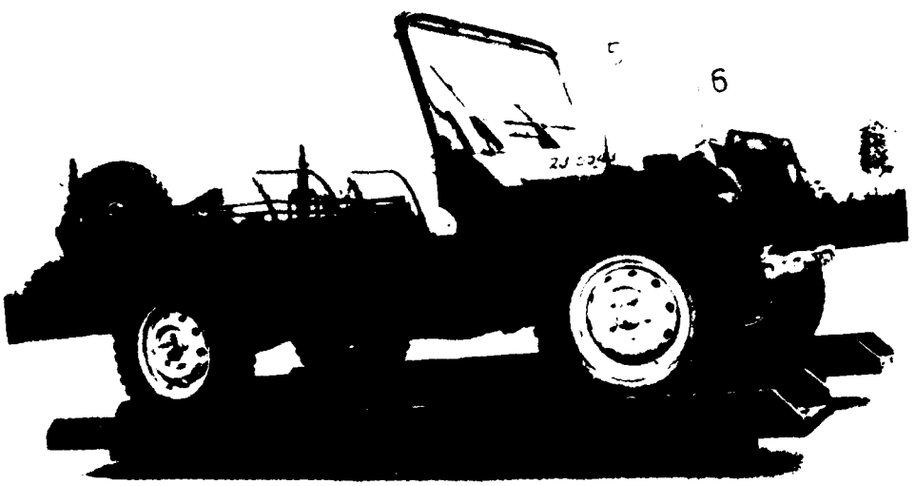

Fig. 59: Configuration of an active antenna pair for the frequency range 80 through 300 MHz.